



Amanda María Henríquez Coro

**A Comparative Study of Soil
Properties in South-Eastern
Norway and Coastal
Western India: A
Collaboration between USN
and SPPU**

Master's Thesis

4317

2024

Faculty of
Technology, Natural Sciences
and Maritime Sciences

Institute of
Natural Sciences and
Environmental Health

University of South-Eastern Norway

Faculty of Technology, Natural Sciences and Maritime Sciences

Institute of Natural Sciences and Environmental Health

3800

<http://www.usn.no>

© 2024 Amanda María Henríquez Coro

This thesis is worth 60 study points

Summary

This work presents a comparative analysis of inorganic soil properties across two distinct climate regions: South-Eastern Norway and Coastal Western India. Through a collaborative effort between University of South-Eastern Norway (USN) and Savitribai Phule Pune University (SPPU), the study aims to understand how climate conditions have influenced soil formation processes and altered the base rock in each region. While previous research has explored and documented this relationship, we present a distinctive methodology. Sampling locations were chosen based on similar land use patterns across the two study areas and various techniques to study the texture and chemical composition of the soils were employed, contributing to understanding how differently the base rock has been altered across the two different regions.

Our findings on the Indian samples help fill the knowledge gap in soil science of the study area, laying the groundwork for future investigations, whereas results from the Norwegian analysis aligns with the existing body of work already produced. The preservation of unique landscapes and soil resources found in both areas is also advocated in this study.

Overall, this thesis offers an exploration of soil properties, contributing to our understanding of the complex interactions between climate, geology, and soil formation.

Table of contents

Summary	2
Foreword	5
1 Introduction	6
2 Norwegian Study Area	8
3 Indian Study Area	16
4 Contrasting the two study areas	21
5 Methodology	25
Norwegian Study sites	26
Indian Study Sites	28
Soil texture classification	31
Sieve analysis	31
Scanning electron microscopy analysis	33
X-Ray analysis	36
Soil chemistry	37
6 Results	39
Sieve Analysis	39
Norway	39
India	42
Scanning electron microscopy analysis	45
Norway	45
India	48
X- Ray analysis	51

Soil chemistry	53
7 Discussion	58
Norway	58
India	60
Comparing the two study areas	60
8 Conclusion	63
References	64
List of tables and charts	73

Foreword

I would like to deeply thank all the people involved in this work, who have made of this project not only an academic learning journey, but also a humane learning experience, reminding me of the importance of being kind, open, compassionate, and understanding towards each other and oneself during the challenges that science can bring. To my supervisors, professors Johanna Anjar and Raymond Duraiswami, not only for their guidance but also for their patience and care, which I receive as a breath of fresh air in a sometimes very hostile academic environment.

I am also deeply thankful for the company and support received by Hemant B. Pednekar, whose willingness to help me unconditionally has been key for me to feel at ease during my stay in India. Vrishali Thorwat's warmly welcomed me in Goa, I'm very thankful for her time, dedication and knowledge provided of the Goan study area which was invaluable for conducting the fieldwork. Thanks to Professor Mona Sæbø for organizing and making this collaboration possible, and to Professor Makarand Ganesh Kale for his guidance during the interpretation of the scanning electron microscopy images.

I extend my gratitude to the institutions assisting this research, including Vasantdada Sugar Institute (VSI) and the central instrumentation facility at Savitribai Phule Pune University (SPPU).

14/05/2024

Amanda María Henríquez Coro

1 Introduction

Soil is a vital component of the Earth's ecosystem, it is a complex ecosystem in itself, that changes over time and responds to its environment, playing a crucial role in supporting life and influencing various environmental processes, leading to some authors stating it as being “a living organism”. With the current understanding of soil properties, it is evident that soil holds immense importance for agriculture, food production, and climate change mitigation.

The significance of soil for agriculture and food production lies in its role as a medium for plant growth, providing essential nutrients, water, and support for root systems. The physico-chemical properties of soil, such as pH, moisture, and nutrient content, directly impacts the quality and quantity of food production (Patel et al., 2022).

Beyond its agricultural importance, soil also plays a vital role in mitigating climate change, through carbon sequestration and reducing greenhouse gas emissions (Tripathi et al., 2021). Soil plays this role by storing carbon in a stable solid form through fixation in the soil, which can significantly reduce CO₂ concentration in the atmosphere (Kavya et al., 2023). Different management practices, such as reduced use of tillage, application of organic amendments, cover crops, and biochar application, can contribute to soil carbon sequestration and improve carbon stabilization (Anand et al., 2022; Moura et al., 2016; T.M. et al., 2023).

However, climatic variables influence the dynamics of soils, shaping its pedogenic or formation processes and properties. Soil formation involves a complex interplay of physical, chemical, and biological transformations that occur over time. It involves the weathering of parent material, leading to the development of different layers or strata of soil known as soil horizons (Chiapini et al., 2023). Soil biota, including microorganisms, soil animals, and plants, play a crucial role in pedogenesis by regulating biogeochemical transformations and functions such as nutrient cycling, organic matter turnover, and improvement of soil structure (Okon & Antia, 2022).

From the polar regions to the tropical latitudes, climatic variations exert profound effects on soil formation, composition, and fertility. The unique combination of temperature, precipitation, and vegetation in different climatic zones creates diverse soil types and profiles, each with its distinct features and taxonomy.

Soils from colder regions, such as those found in boreal climates, exhibit general characteristics such as high organic material, explained by the cold temperatures inhibiting microbial activity and organic matter decomposition rates, leading to the accumulation of organic material in the superficial soil layers (Kerfahi et al., 2019), this results in distinct soil

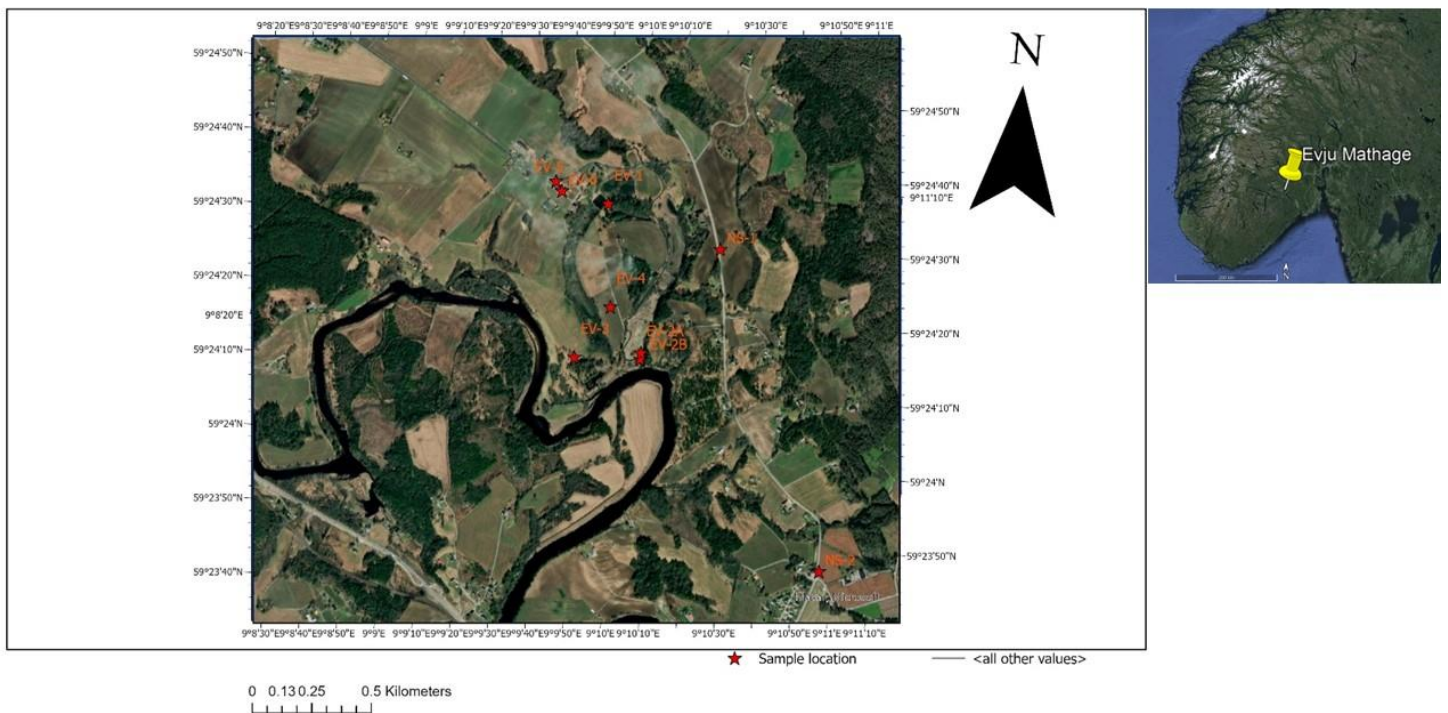
horizons, with layers of undecomposed organic matter known as "peat" or "peaty" layers (Okon & Antia, 2022). In addition, cold climates often result in acidic soil conditions due to slow weathering rates and limited leaching of basic cations, low pH levels can affect nutrient availability and microbial activity in the soil (Okon & Antia, 2022; Patel et al., 2022). When moving towards the equator, soils show more depth, higher microbial activity and abundant iron and aluminium oxides resulting in archetypical red coloured soils (Babu et al., 2021; Pal et al., 2009).

Therefore, soils from different climatic regions exhibit diverse properties and respond differently to environmental stressors such as drought, extreme precipitation events, and temperature fluctuations (Kerfahi et al., 2019; Tripathi et al., 2021), which can give insights about the characteristics making soils more vulnerable or resilient to these stressors.

After examining these considerations, this thesis embarks on a comparative study of soil properties to investigate the influence of climate on the inorganic factors driving soil formation processes across two different climatic regions.

2 Norwegian Study Area

The study area (SA) as seen in Map 1, is situated in Bø, in Midt-Telemark Municipality, located in continental southeastern Norway at 59 degrees latitude and a height above mean sea level of 105 m. An area surrounding Evju Mathage farm was selected as our study site, encompassing 1.13 square kilometres, with a perimeter of 4.62 kilometres.



Map 1. Location map around Evju Mathage farm, where the sampling locations are marked in red. Samples EV-5 and EV-6, were selected for soil microbiome investigations, therefore excluded from this study. Generated in ArcGis Pro Version (3.1.0)

Starting with the geology description of the study area, we aim to comprehend the soil-geology relationship and its connection to soil quality and nutrient availability. We present the lithological composition and mineralogy of the rocks which is related to the chemical elements that are released into the soil through weathering action, shedding light on the role of parent material in shaping soil properties (Chris-Emenyonu et al., 2020).

Furthermore, we first delve into the geological history of Norway that has shaped the current landscape, rock, and soil composition of the study area. This understanding sets a

foundational knowledge, providing the basis from which we can then develop a better understanding of the soils under examination.

Under the layer of superficial sediments, the main rock types present in southeast Norway are gneiss, granite, sandstone and limestone (Beylich, 2021).

Specifically in our study area, we are under the tectonic division of Telemark lithotectonic unit, where granitic gneiss predominates as indicated in the National Bedrock Database (1:250 000) of the Geological Survey of Norway (NGU). This granitic gneiss is of very ancient origin, dating back from the Mesoproterozoic era (1250-1200 Ma), when the region that is now Norway was located near the equator as part of the ancient supercontinent Rodinia (Ramberg, 2008, pp. 62–120). A picture of this granite can be seen in Figure 1.

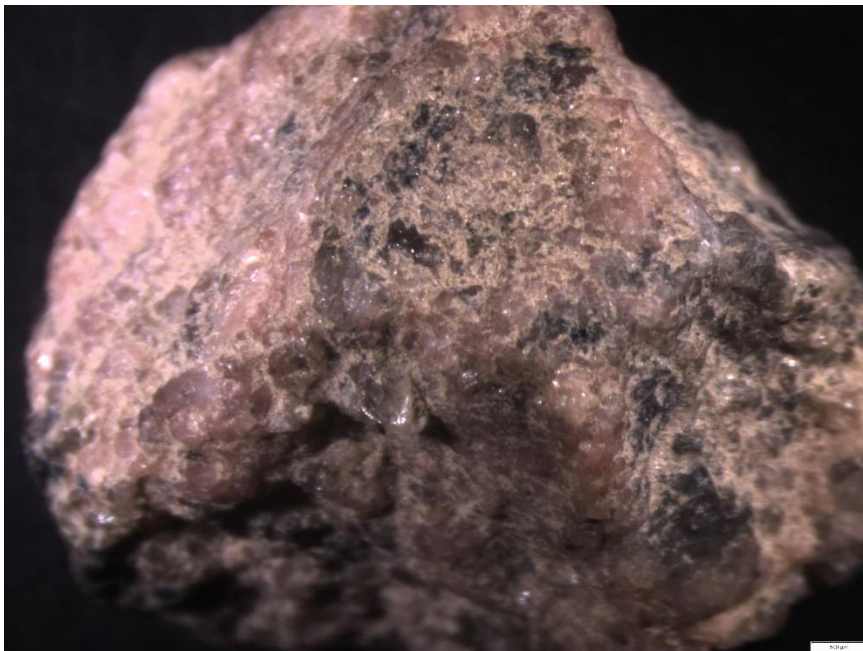


Figure 1 Picture of a grain of granite from Norwegian SA taken with a binocular microscope, showing pink coloured feldspars and black micas.

Advancing in time to the Paleozoic era, the collision between the Baltica and Laurentia plates took place, during what is known as the Caledonian orogeny. This collision formed the Scandinavian mountains and generated volcanic activity. It involved deep burial cycles, metamorphism, deformation events, continental subduction and the exhumation of mantle rocks from depths exceeding 185 km (Butler et al., 2015; Liu & Massonne, 2019; Roberts et al., 2006; Van Roermund & Drury, 1998).

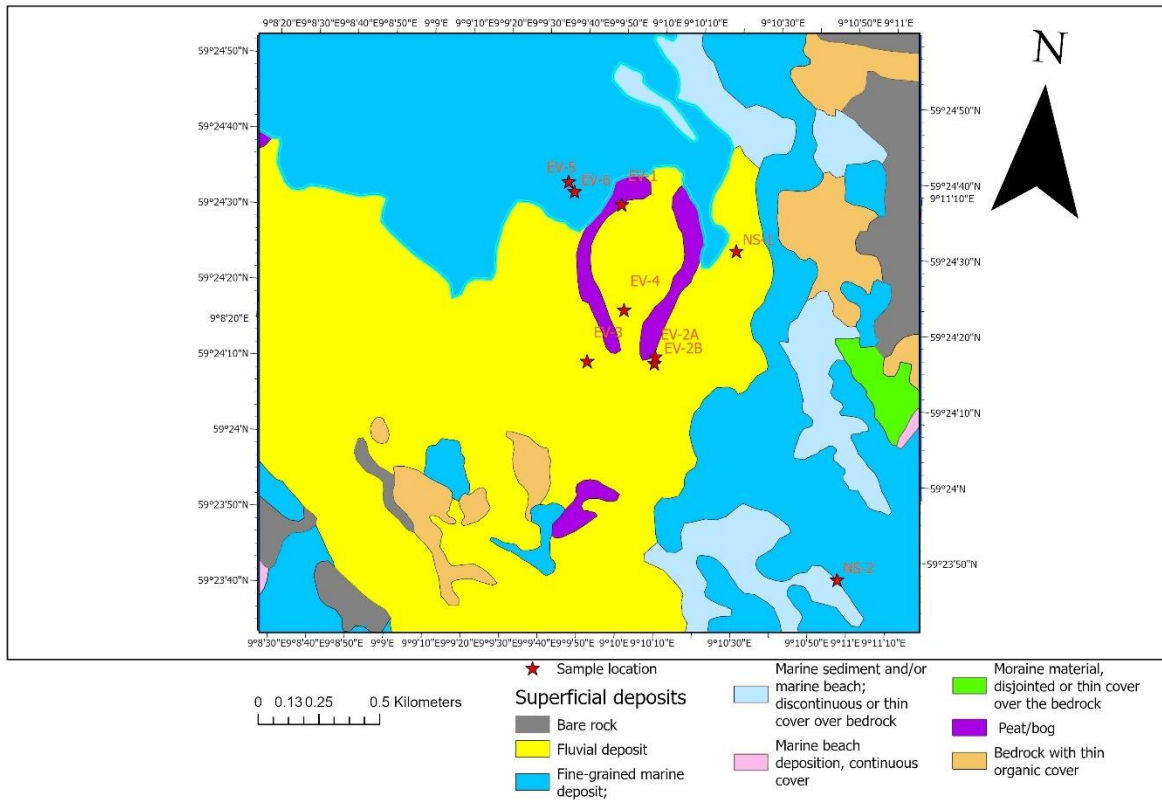
Moving to the Quaternary geology of Norway, where the last glacial period, also known as the Late Glacial Maximum (LGM) took place. It was a geological time characterized by extensive ice sheet coverage and climatic fluctuations (Bradley & Bradley, 1999; *Quaternary Geology of Norway*, 2013). The Eurasian ice sheet complex, which included the Scandinavian ice sheet, reached its maximum extent of approximately 5.5 million square kilometres and a volume of about 24 meters of sea level equivalent around 21,000 years ago (Hughes et al., 2016), covering the present-day Scandinavian peninsula as well as parts of northern Europe, including Russia and the Baltic States. This geological event shaped the topography of northern Europe, the weight of the ice sheet depressed the Earth's crust, creating deep basins, it sculpted fjords, valleys, lakes, moraines, and other glacial landforms with its advance and retreat movements.

The present-day geological and lithological characteristics of southeastern Norway is therefore linked to these tectonic and glacial events. In Midt-Telemark the presence of moraine ridges, ice-marginal deposits, and submarine features shapes the region's geomorphological features as indicated by previous studies on the last Eurasian ice sheets (Bergstrøm, 1999; Hughes et al., 2016; Wraa, 2020, pp. 4–8).

As temperatures warmed and the climate shifted to a more interglacial phase, our study area transitioned to a deglaciation period, during which the ice retreat causes isostatic depression, and subsequent isostatic uplift (Hughes et al., 2016).

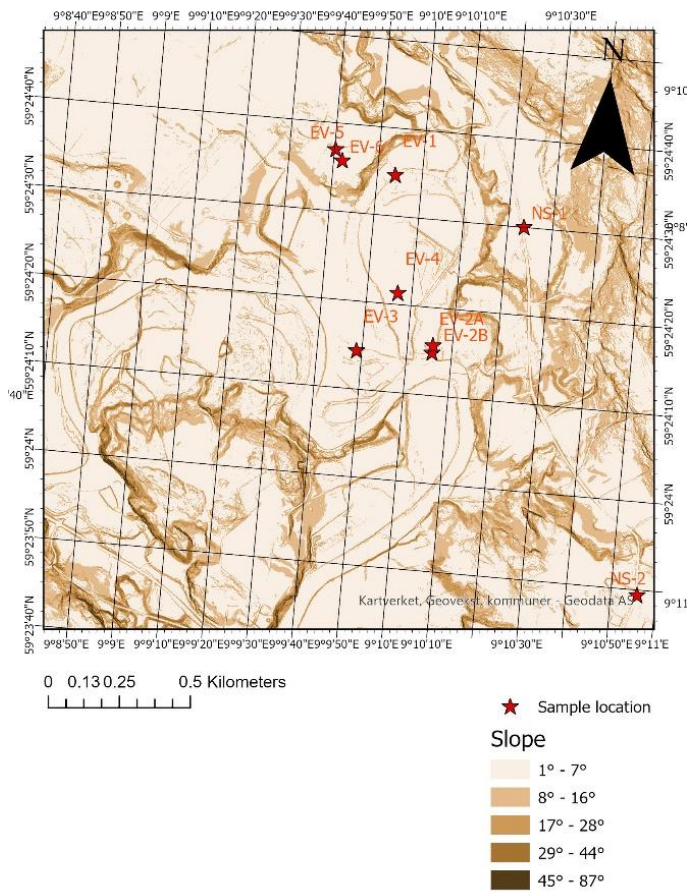
As the ice retreated, the isostatic rebound, a process of land rebounding after the removal of the immense weight of glacial ice, was a gradual process, leading to remnant isostatic depression. This depression led to the inundation of valleys by the sea, resulting in the deposition of marine sediments that we can see, represented in blue colour, in the superficial deposits map shown in Map 2. This marine sediments are the result of the detritus deposited at the oceanic bottom, where organic matter and calcium carbonate is accumulated, this sediments were then affected by diagenesis, which is controlled by the quality of the deposited material and the redox conditions of the sedimentary environment (Bianchi, 2007, 2007; Schüllli-Maurer et al., n.d.). Therefore, marine sediments provide important nutrients to present-day soils, playing a crucial role in the region's agriculture (Bianchi, 2007; Elvenes et al., 2019; Schüllli-Maurer et al., n.d.).

The subsequent isostatic uplift, caused regression, leading to the retreat of the sea (Stratford et al., 2008; Wraa, 2020, pp. 4–8). This process facilitated the formation of the meandering river in the valley seen in Map 1, leading to the sedimentation of the fluvial sediments as represented in yellow colour in Map 2.



Map 2. Superficial deposits map, the marine deposits are represented by blue colours. After the retreat of the sea, a river was formed leaving fluvial deposits, depicted in yellow colour. Extracted from Norges Geologiske Undersøkelse, n.d. ArcGIS Pro (Version 3.1).

Overall, the landscape of the SA has been shaped by glacial activity during Quaternary glaciations, which formed glacial landforms such as U-shaped valleys, fjords, and alpine relief. Subsequently, as the glacier retreated, the marine sea penetrated the area, depositing marine sediments (Beylich, 2021). The next phenomenon shaping the land was river erosion, further sculpting the terrain and creating more elevation contrast. This contrast in elevation makes possible to divide the SA in two categories, the plateau, characterized by higher altitudes with a maximum elevation of 55 metres, and the lower altitude basin with a minimum of 16 metres. This elevation distinction can be seen on the elevation profile in Figure 2 and the slope map in Map 3.



Map 3. Slope map of the Norwegian SA. The boundary between the plateau and the basin area is demarked by the darker brown lines representing steeper terrain. Data retrieved from Geonorge.no. ArcGIS Pro (Version 3.1).

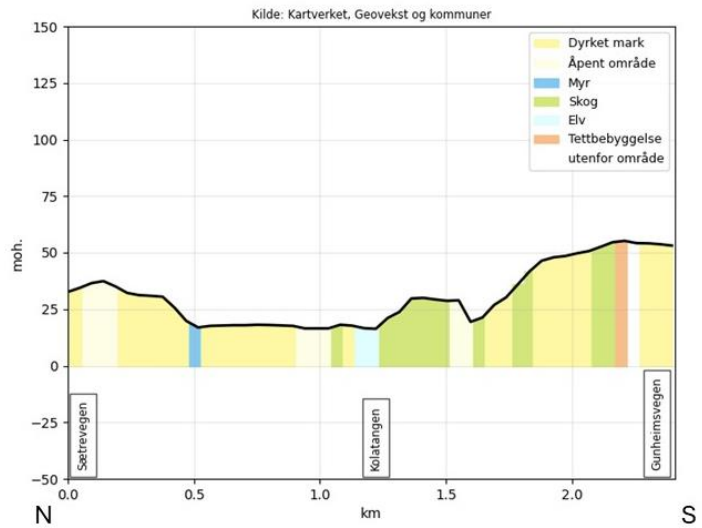


Figure 2. Elevation profile of the study area, representing various land uses in different colours in the legend. In dark blue is represented the bog, light blue indicates the river, green represents the forest, yellow depicts the crop land, and red marks housing area. Data retrieved from Kartverket.no.

The primary water body crossing the SA, is a tributary river named Kisebekken, that feeds into the main river of Bø, known as Bøelva. Situated within a valley, the river meanders as a result of the lower slope of the terrain.

Delving into the climatic characteristics of the area, it shows a temperate oceanic climate with cool summers and mild winters (*Observasjoner Og Værstatistikk - Seklima*, n.d.).

The Köppen climate classification system is widely used to categorize climate zones based on vegetation types, temperature, and moisture indices (Wang et al., 2021). The Köppen system can be also used to assess climate change impacts, such as shifts in climate zones and the spatio-temporal variation of climatic variables (Wu et al., 2021; Yılmaz & Çiçek, 2018), making it a valuable tool for understanding climate change (Carlson, 2021). In the case of Midt-Telemark in Norway, the climate zone falls under the Köppen-Geiger classification system. This region is in the mid-latitudes (35° to 55°N) and is characterized by its harsh winters (Straumfors et al., 2021). According to the Köppen classification, Midt-Telemark falls within the Dfc zone, which corresponds to the continental subarctic climate.

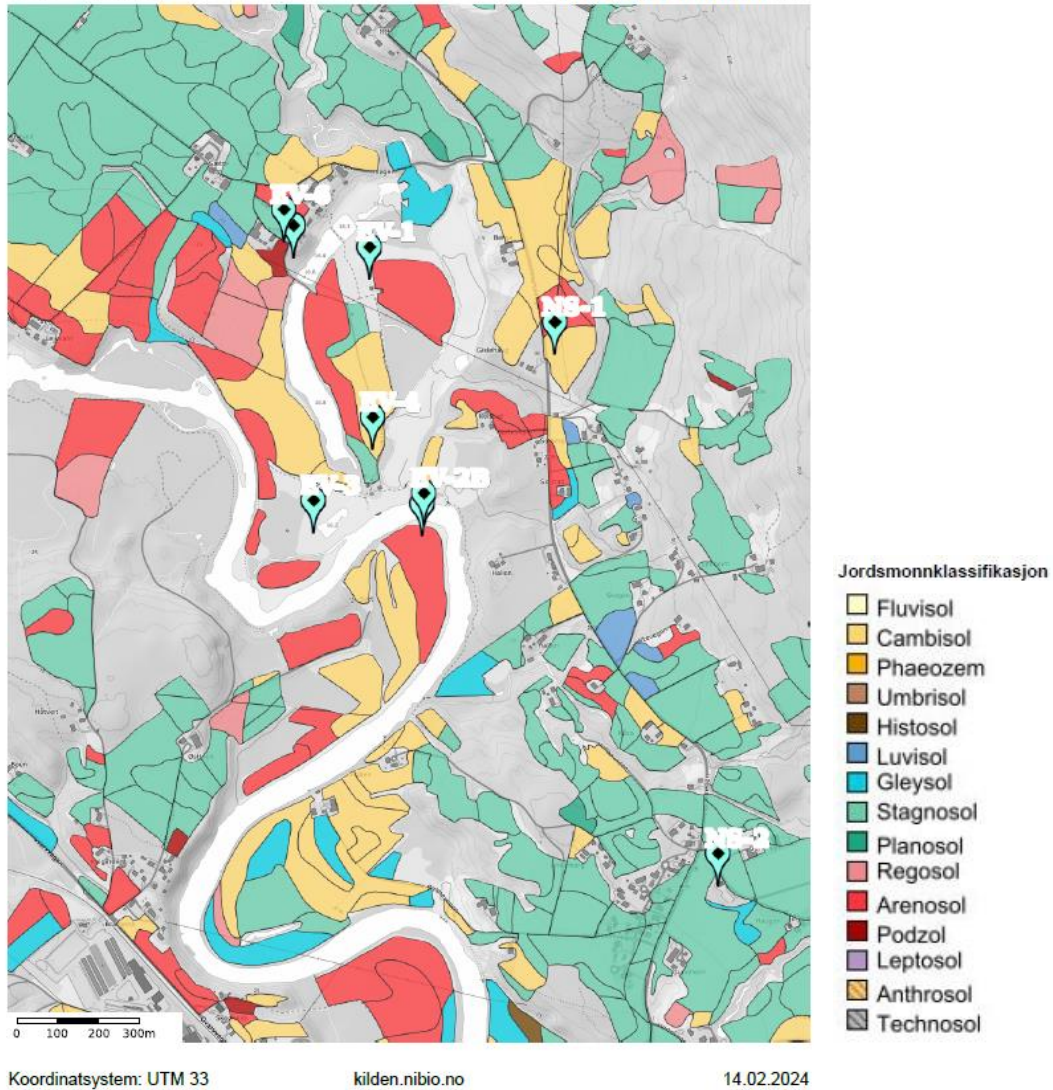
The Dfc climate zone is associated with a boreal climate, featuring relatively short and cool summers and no dry season, with cold, snowy winters, making it suitable for coniferous forests and cold-resistant vegetation (Błażejczyk & Skrynyk, 2019). Therefore, the SA exhibits distinct seasonal variations, with lush greenery in the summer months and snow-covered landscapes in winter.

Additionally, the terrain around the SA is characterized by rolling hills and forests, which can influence local weather patterns and microclimates.

Having described variables such as base rock, topography, and climate, we can now examine how these factors contribute to the pedogenesis of the soils found in the SA. The base rock, composed of granitic gneiss, provides minerals such as quartz, feldspar, and mica. This mineralogical composition influences soil texture, pH, porosity, and moisture content, nutrient cycling, and fertility. For example, feldspar can contribute to alkaline soil conditions when weathered, while certain mica minerals may release acidic compounds, affecting soil pH accordingly (Cardelli et al., 2017). As indicated in other studies, soils developed from granitic rocks tend to have low cation exchange capacity (CEC) and are generally poor in mineralizable nitrogen (MinN), potassium (K), calcium (Ca), magnesium (Mg) and sulfur (S) (Cardelli et al., 2017; Moore et al., 2022).

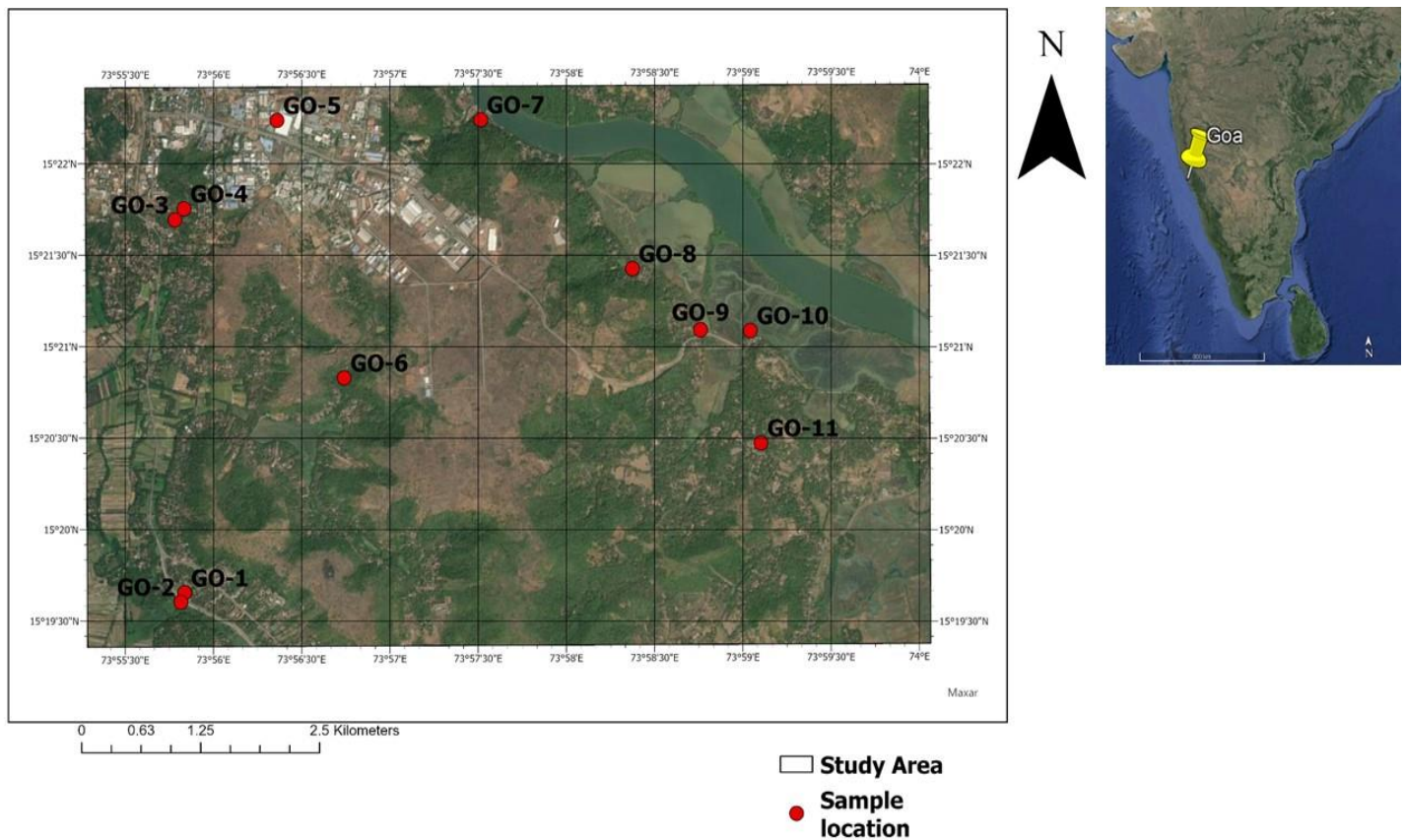
Therefore, the climate present in the region introduces significant challenges for pedogenesis. The cold temperatures during the winter limits microbial activity and decomposition rates, hindering dissolution rates, bioturbation and breakdown of rock materials (Kerfahi et al., 2019). The short cool summers translates into short growing season, meaning less vegetation cover and limited organic matter input. Additionally, the freeze-thaw cycles changes soil volume, disrupting soil structure, mixing soil horizons, increasing erosion and inhibiting its further development (Miranda-Vélez et al., 2023; Sun et al., 2021). All these factors resulting in the predominance of relatively immature soil classes.

Based on the soil classification map provided in Map 4 (NIBIO, *Jordsmonnkart*), our SA presents three main soil classes: Stagnosol, Arenosol and Cambisol. Among these, only Cambisol shows structure and development of horizons. Stagnosols, present only in the control sample NS-2, is characterized for their periodic waterlogging by surface water (NIBIO, *Jordsmonnkart*, n.d.; Solbakken, n.d.). Meanwhile, Arenosols are characterized by uniform sand and low gravel content, with poor organic material, resulting in low nutrient content and water retention capacity (Solbakken, n.d.). In terms of agricultural suitability, Cambisols are of better quality, according to the soil quality map available in Norsk institutt for bioøkonomi (NIBIO).



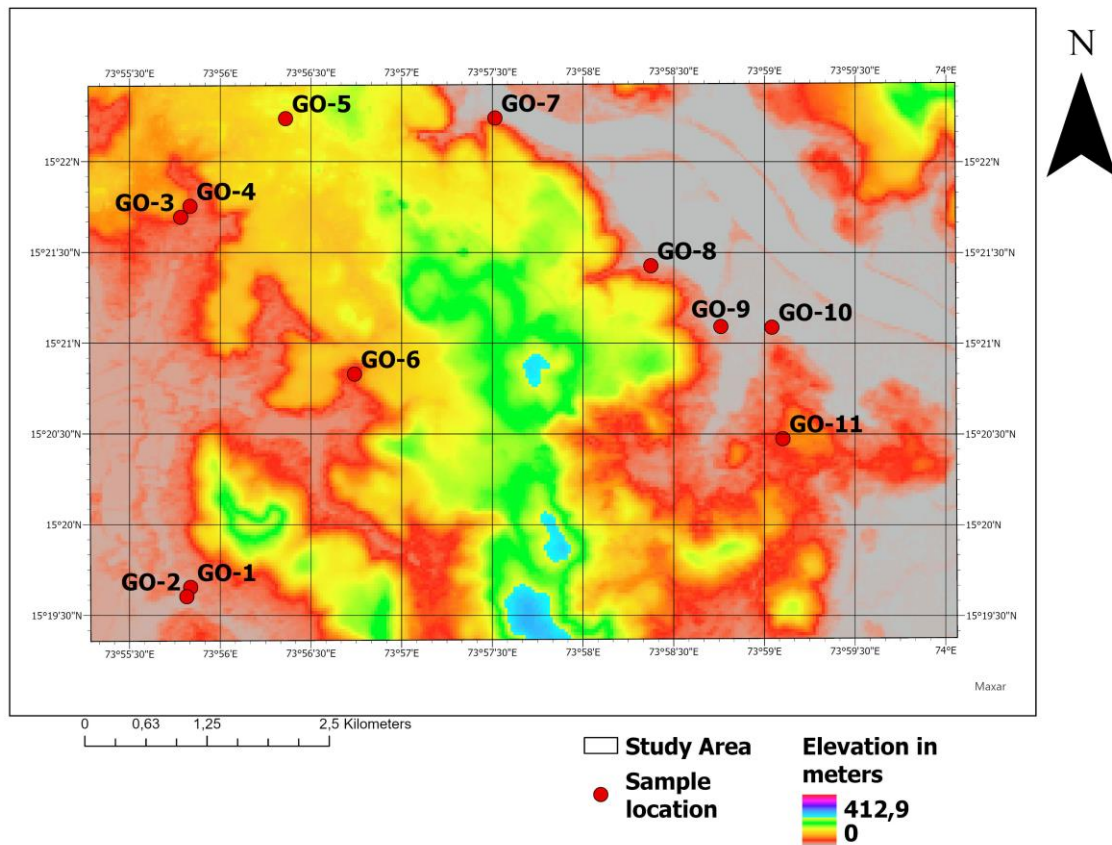
Map 4. Soil classification classes extracted from Norsk institutt for bioøkonomi (NIBIO, Jordsmonnkart).

3 Indian Study Area



Goa is a state lying on the West Coast of India with a long coastline of 110 km. The landscape of Goa can be divided into three areas, in the east we find the Western Ghats, a mountainous region with altitudes above 600 meters. Moving to the interior the topography softens to a maximum of 200 meters while we approach the mid-land plateaus, lastly, we find the low-lying river basins and the coastal plains with altitudes below 50 meters above mean sea level (Sawant, 2022).

Our Study Area in Goa is located in the state's midland region, where the mid-land plateaus follows the low-lying river basins (Map 5 and Map 6), specifically at the northern limits of the administrative division of Salcete, bordering Morugoa to the north.

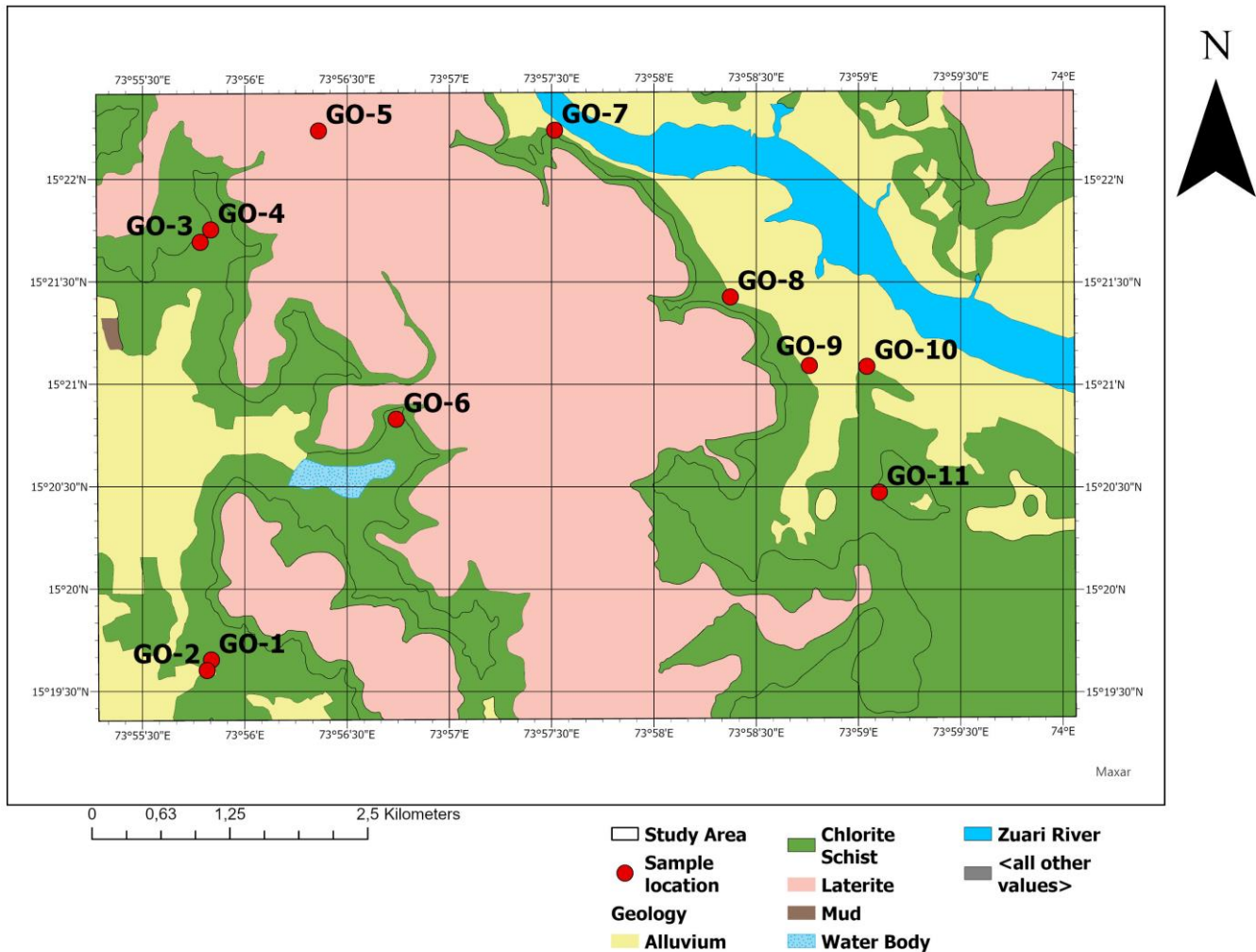


Map 6. Digital Elevation Model (DEM) of the Indian study area. Extrated from (OpenTopography, 2021).

The geological history of India is characterized by its movement and collision with other landmasses. The collision with Asia is an event described in depth in other works such as Van Hinsbergen et al. (2012), we will not delve into details of these geological processes. Instead, our focus is on describing the geological background of our study area. This part of peninsular India belongs to the Basaltic Deccan Plateau (Sawant, 2022) , a large igneous region in India composed of basaltic lava flows erupted during the Late Cretaceous period, approximately 66 million years ago (Valdiya, 2016, pp. 447–462).

Several key factors shape the geology we see today. Firstly, its coastal location contributes to coastal erosion and deposition processes. Also, fluvial action plays a crucial role, with six rivers that receive their water from the monsoon, transporting sediments from the Western Ghats into floodplains, estuaries, and coastal areas, creating alluvial plains and coastal deltas (Sawant, 2022; Sonak, 2014b). The tropical climate and monsoon season further accelerates chemical weathering as commonly observed in tropical climates (Babu et al., 2021; Pal et al., 2009).

The lithology found in Goa is composed of rocks of the Archaean-Proterozoic Dharwad group, including laterite, granite, chlorite schist, gneiss, conglomerate, and limestone (Sawant, 2022). Inside the boundaries of our SA specifically, we find alluvium, chlorite schist and laterite, as can be seen in the geological map provided in Map 7.



Map 7. Geological map depicting the rock types present in the Indian SA. Generated in ArcGis Pro with data provided by Vrishali Thorwat, research scholar, SPPU.

Goa is a state known for its mineral resources and exploitation of iron ore, manganese, bauxite, and limestone (Sonak, 2014b). Specifically in our SA, we find laterite plateaus that have undergone various degrees of leaching of soluble minerals and concentration of insoluble iron and aluminium oxides, known as laterization, resulting in iron-rich soils with magenta colour, characteristic of chemical weathering in tropical climates as seen in Figure 3.



Figure 3. Lateritic rocks showing red goethite, yellow limonite, and cream gibbsite/bauxite, next to GO-4.

We delve into more detail about these weathering features on the SEM chapter of the Indian samples, where we can see on the grains surface the marks left by these processes.

The presence of the Western Ghats mountain range acts as a major water divide due to which the Konkan coast receives 2500mm of annual rainfall and the Deccan Plateau towards the west receives less than 500mm of annual rainfall. In our SA, these mountains causes orographic rainfall as moist winds from the Arabian Sea are forced to ascend, leading to heavy precipitation along the slopes. This causes a gradient in rainfall and temperature as we move to the sea (Sawant, 2022). Although the mean temperature is between 24°-32°C with little variation throughout the year, the average rainfall falls between 350-400 cms showing skewness towards the monsoon season from June to September (Sawant, 2022). The proximity to the sea contributes to high humidity, reaching up to 90% during the monsoon (Sarkar et al., 2023). Köppen's classification categorizes Goa under the Amw climatic type, indicating a tropical monsoon climate (Sawant, 2022).

The Zuari River, crossing our research zone, draws a perpendicular line to the coast and it ends its path into the Arabian sea. The river shows a meandering course with expansive valleys at its sides. It serves a vital function by depositing nutrient-rich alluvial sediments sourced from the Western Ghats, supporting fish populations, and sustaining the livelihoods of local fishermen. Also, a tributary originating from the Sal River, running parallel to the coastline, enters our study area next to sample site GO-2.

Therefore, pedogenesis in Goa plays under tropical conditions, which promotes mineral breakdown and the development of specific soil profiles. Intense pedogenic transformations, indicated by feralization and rubefaction (Ghosh & Guchhait, 2020, pp. 83–94), are observed in these soils (Pal et al., 2009). Within our SA, we encounter lateritic soils, alluvial soils, and saline soils, with the latter being particularly fertile and utilized for cultivation after the monsoon season (Sawant, 2022; Pal et al., 2009).



Figure 4. Khazan lands

In our SA, specifically in samples GO-9 and GO-10, we find the Khazan lands (Figure 4), these wetlands are coastal agricultural systems managed by local villagers, where sustainable agricultural practices mainly of salt-tolerant rice varieties, have been crucial to the livelihoods of the local communities (Pombo, 2019; Sawaiker et al., 2022). Khazan lands are subject to periodic inundation by saline water during high tides, during the dry season they are utilized for salt extraction (Sawant, 2022), making this lands under the saline soils classification, mentioned previously.

4 Contrasting the two study areas

After describing in detail the two study areas, it is important to make connections between them since this work aims to provide a comparison of soil properties across different climatic regions.

Norway and India have different tectonic setting and evolutionary pathways, nevertheless, both are affected by geological processes operating on a global scale like plate tectonics, mountain building events and the formation of sedimentary basins. Norway was formed from the collision between the Baltica and Laurentia plates during the assembly of the supercontinent Rodinia, also known as the Caledonian orogeny (Beylich, 2021).

India, on the other hand, was part of the supercontinent Gondwana. As India moved towards the Eurasian Plate, it generated intense volcanism that developed the granitic and gneissic complexes we find in our Indian SA (Valdiya, 2016).

Moving on to the variables affecting pedogenesis, which are as expressed in the soil formation formula in equation 1, we delve into a comparison between the two regions, which is synthesized in Table 1.

$$S = f (Cl, O, R, P, T \dots)$$

Equation 1. Soil development is a function of Climate, Organisms, Relief/Topography, Parent material and Time.

Addressing first the climatic factor, it is known that most of the differences in the velocity of soil development can be explained by different climate and parent material (Schüllli-Maurer et al., n.d.). In higher latitudes such as the 59 degrees north where our Norwegian study area is situated, we find a temperate oceanic climate, contrasting sharply with Goa's tropical monsoonal climate. The tropical conditions foster more intense rates of chemical weathering of the rocks, in contrast with Norway's colder environment. Also, the parent material in the Norwegian SA, granitic gneiss, and Goa's chlorite schist sets a different mineralogical context.

One significant distinction between soils from tropical and temperate areas lies in the dynamics of soil organic matter. In tropical soils, the formation of organo-mineral complexes

contributes to soil structure and fertility (Moura et al., 2016; Ouattara et al., 2017), whereas in temperate soils, microbial activity is lower due to colder temperature conditions.

Soil pH values in the Norwegian SA ranges from alkaline to slightly acidic values, pH test was not performed for the Indian soils, nevertheless we expect the Goan soil to show similar values according to the established knowledge about tropical soils pH values (Barman et al., 2018). Norway's SA elevation remains relatively low, in the Goan SA the maximum elevation goes to 180 metres with steeper terrain.

Moving to the soil types present across the study areas, the Norwegian SA has been surveyed previously providing detailed soil classes of easy online access, in contrast with the Goan study area, where there is a need for such extensive work to be done. The soil class provided for the Indian SA are extracted from state-scale soil type maps, which may overlook interesting particularities of the soils in our SA.

Table 1. Comparison table of factors influencing soil development in Norway and India.

Factors	Norway	India
Climate	Temperate 59° Latitude	Tropical monsoonal climate 14° Latitude
Organisms	Low microbial activity and organic matter decomposition rates	Higher microbial biomass and activity
pH	Acidic to neutral	Slightly acidic to neutral
Weathering	Heavily influenced by mechanical glacial dynamics	Driven by chemical alteration Higher chemical weathering rates
Relief/Topography	55m of maximum elevation above mean sea level	180m
Parent Material	Granitic gneiss	Chlorite schist
Soil classification	Arenosol, Cambisol, Stagnosol	Lateritic soil, Saline soil

The horizons normally found in soils from higher latitudes are the result of a process called podzolization characterized by the leaching of iron, aluminium, and organic compounds from the surface horizon (A horizon) to lower horizons (B horizon). This process results in the formation of distinctive soil profiles with an ash-colored E horizon and an a B horizon

enriched in iron and aluminum oxides (Kerfahi et al., 2019). Whereas in tropical latitudes a common soil-formation process is laterization, as previously described.

Focusing on the agricultural context of our study areas (Table 2), both the selected study areas rank among the most agriculturally productive regions in their respective countries due to their specific soil properties. In Norway, crop lands are commonly used for wheat cultivation, whereas the Khazan land are used for rice cultivation. However, both agricultural lands are subjected to degradation risks.

Specifically in Goa, traditional practices are at risk of disappearing in Khazan lands, the integration of aquaculture with rice cultivation, creating a mutually beneficial ecosystem where fish waste fertilizes the rice paddies and rice plants provide of shelter for the fish (Pombo, 2019; Sawaiker et al., 2022). In addition, the use of composting, crops rotation and minimal tillage are common practices in Khazan lands (Sonak, 2014b). These practices are at risk due to the transformation of these lands for tourism needs (Noronha et al., 2002; Sonak, 2014b). These comparative studies also facilitate the exchange of good agricultural practices, allowing one country to benefit from the practices of another.

Table 2. Comparative table of the agricultural context of the study areas and their degradation risks. Khazan lands refers to the endemic and heritage ecosystem of Goa where low-lying coastal wetlands are used for salt tolerant rice species and aquaculture.

	Norway	India
Agricultural land use	Fluvial and marine sediments	Khazan lands as paddy fields
Crop type	Wheat	Rice
Degradation risks	Loss of topsoil by road projects, construction, intensive agriculture. Marine sediments as non-renewable resource key for food security	Construction projects Loss of traditional practices

By implementing standardized methods and analysis procedures across both regions, we seek to evaluate the impact of these regional differences on pedogenesis.

5 Methodology

The methodology employed for both study areas in Norway and India is the same, the sample locations were selected considering the subsequent analysis, which needs variation in the samples. The methodology followed for sampling involves two phases: the initial phase conducted in Norway and the following phase carried out in India. In the Norwegian study area, soil samples were collected from various land uses, including agricultural, forested, and water bodies. In the Indian study, the area was chosen to replicate the land use patterns observed in the Norwegian counterpart. This study design was selected to provide data variability to the subsequent statistical procedures.

As this study focuses on inorganic analysis, we eliminate excess organic material in situ, such as wood sticks and vegetation from our samples. Each sample involved digging a hole of approximately 15 centimetres deep, followed by mixing of the soil following the quartering methodology, before placing it into a plastic bag.

As for the rest of experimental techniques employed, the motivation for selecting these experiments is depicted in the diagram seen in Figure 5. Each to satisfy the objective of the study, which is to to evaluate the impact of regional differences on pedogenesis.

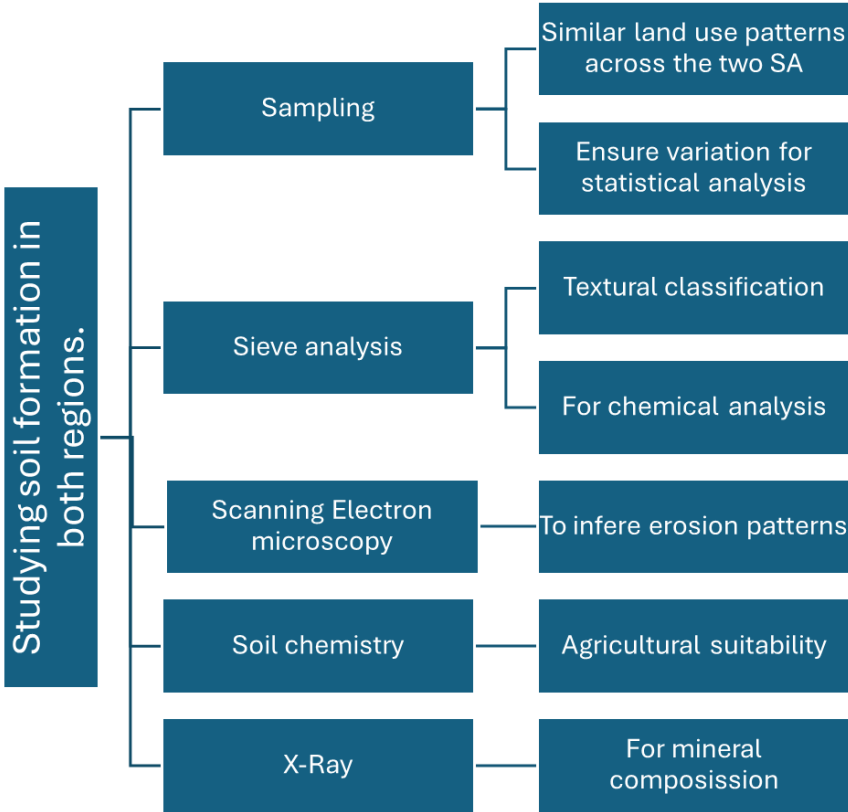


Figure 5. Study design.

Norwegian Study sites

The initial phase of this study involves sampling in Norway, within the Evju Mathage farmland. The area's geomorphology features an oxbow lake (Figure 7) and fluvial terraces, with land use predominantly consisting of wheat crops and forested areas. The sampling was conducted during late summer, following the harvesting season.

We can group the samples in two categories following differences in geomorphological features, for instance, EV1, EV2A, EV2B and EV3 fall into the bog environment category, where the elevation is lower and the river is influencing chemical conditions like pH. EV4 falls into farm land use, NS1 and NS2 are located on top of the plateau with higher altitude.

The sampling sites details can be found in Table 5.

The following observations were made during the fieldwork for the Norwegian sampling session. Starting with NS-2, on the highest elevation point, this sample served as the control sample, located furthest from the study area. NS-1 followed located next to a road path. From here, we leave the plateau area and move into a more depressive topography, arriving in the bog environment we sample EV-1, positioned in an oxbow lake seen in figure 9, surrounded by wetland vegetation such as reeds, a first visual examination we see a sediment rich in organic materia, sand and silt. EV-2A was collected from shallow waters near the river shore, these river sediments were carefully taken introducing a plastic tube in the river bed. EV-2B falls also into wetlands where we observe aquatic vegetation species, an environment similar to EV-1. Following the river meander to the west, we find an ancient preserved fluvial flood terrace formation, characterized by dense grass and pine trees, exhibiting darker brown soil with increased air, roots, and decreased humidity compared to the previous water-embeded samples. Finally, to include in our study an agricultural land use pattern, we move to a central location withing a wheat crop field seen in Figure 6, EV-4 was sampled following the coning and quartering sampling methodology to ensure sample representativeness.



Figure 7. Oxbow lake



Figure 6. Sample EV1 on the left, highlighted in red is the specific spot where the sample was collected. On the right is EV4, located on the crop field.

Indian Study Sites

The methodology employed and the criteria for designing the sampling locations were consistent with those used during the Norwegian sampling session, as previously described in this methodology chapter. Sampling in India took place after the monsoon season, during ongoing harvesting activities.

The Samples can be categorized based on the Goan DEM (Map 4). The floodplain and Khazan lands fall under grey areas, while the plateau is represented in varying shades of red, yellow, green and blue. Samples from GO1 to GO-4 and GO7 to GO10 are located on the first category in lower altitude areas, while samples GO-5, GO-6, GO-11 are situated on the plateau.



Figure 8. GO-5, Lateritic soil.

In this section, we provide a description of the observations made during the fieldwork session in the Indian SA. Most samples exhibited a high porosity and reddish colour due to granular weathering and oxidation (Sawant, 2022), as seen in Figure 8.



Figure 9. GO-2 sample, Construction site at the left with blue arrow denoting the tributary river location, to the right we can distinguish in a first visual examination three horizons in this alluvial soil type.

Starting from the south and moving northward, we collected sample GO-1, which showed high porosity and sandy characteristics. Moving next to a tributary river originating from the Sal River, where construction work was ongoing, we observed visible differentiation of soil horizons, falling under the laterite plateau (Figure 9).

Continuing northward, sample GO-4 was obtained from a road cut excavation site, displaying signs of heavy laterization and iron oxide (Figure 10). On the highest elevation position of our study area, we sample GO-5 next to the road, observing gravel-size pebbles compared to previous samples with smaller grain sizes. Descending, sample GO-6 exhibited an orange to reddish colour and sandy texture. On the eastern side of the plateau, we collected GO-7 in an area classified as alluvium rock type. Further down in elevation, we reached the low-lying river basins.

To parallel the land class of samples collected in a riverbed in Norway, we sample in a stream bed influenced by tidal waters for GO-8. Both GO-9 and 10 were taken from paddy fields used for cultivation located in the Khazan lands, with sediments exhibiting a heavy clay consistency.

Finally, GO-11 was sampled under the chlorite schist area, this rock type comes from the alteration of pre-existing rocks like basalt under specific temperature and pressure conditions resulting in chlorite, a green mineral of low-grade metamorphism (Babu et al., 2021). The alternation between wet and dry conditions typical of monsoonal climates has led to the alteration of chlorite schist, resulting in the laterization process and high concentrations of aluminium.



Figure 10. Laterite profile exposed on the plateau slope.

Soil texture classification

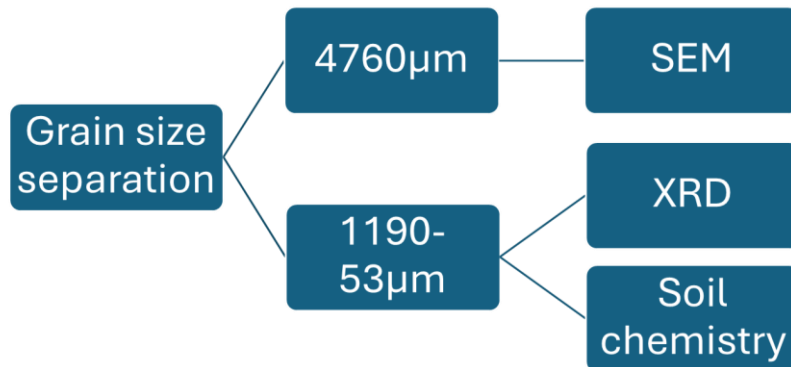


Figure 11. Grain size selection for each experiment.

To prepare the samples for laboratory experiments, we dry them in a hot air oven at a temperature not higher than 60°C, to ensure that the structure of clay particles remains unchanged.

Following drying, we conduct sieve analysis to separate grains of varying sizes for laboratory experiments and classify their texture following the Wentworth grain size classes (Figure 11).

Sieve analysis

The sediment grain size distribution (GSD) and textural characteristics (TC) play important roles in fields such as Sedimentology, Geomorphology, and Soil Sciences. In the case at hand, the sieving analysis is important to determine the fractions selected for chemistry analysis and for the study of GSD and TC, which can give insights about deposition

environment, water retention properties of soils, pore-space available for biological activity and other parameters important for agriculture.

The methodology is as followed; The sieves are stacked from coarser on the top to finer on the bottom, the dried samples are poured onto the top and then the sample will be separated in each different grain size. We use a shaker machine for 20 minutes, and medium to high intensity, to separate the particles according to its size (Figure 12).

The material trapped in each mesh size is then removed from each sieve and weighted in an analytical balance, the result is recorded in an excel sheet where the Statistics Package GRADISTAT Version 4.0 is employed to calculate the percentage of material retained on each sieve with respect to the total initial sample weight, and generate grain size distribution curves and ternary diagrams.

Figure 12. During the sieve analysis, we employed mesh sizes from 4 to 240 on the ASTM U.S. Standard scale representing 4760 to 53µm, and a sieve shaker to speed up the process.



Grain size distribution (GSD) is displayed with distribution histograms, giving information about the percentage of material retained on each sieve with respect to the total initial weight. Following the common practice in sediment research, grain size or particle diameter is plotted on the horizontal axis, both in phi (ϕ) intervals and microns, while the percentage is displayed on the vertical axis. The coarsest grain sizes fall on the right side of the graph and the finest on the left. Phi units are obtained after calculating the negative logarithm of the diameter in millimetres, following the conversion expression in Equation 2. This conversion is done to simplify statistical computations and graphic representations (Ruiz-Martínez et al., 2016).

Equation 2. Phi conversion formula

$$\text{Phi } (\phi) = -\log_2 S$$

Scanning electron microscopy analysis

The scanning electron microscope (SEM) is a type of electron microscope that generates high resolution images of the surface of solid samples based on light optics principles (Mohammed & Abdullah, n.d.). The instrument incidents a beam of high energy or accelerated electrons that scans the sample surface and stimulates emissions (Mohammed & Abdullah, n.d.). Detectors receive these emissions, convert them into a light signal, and produce an image of the material on a computer screen, as seen in Figure 13.



Figure 13. SEM equipment on the left side. On the right side, the Studs with the grains spread ready to be introduced into the SEM machinery.

These emissions can be X-Rays, Auger electrons, primary backscattered electrons and secondary electrons. Each of these type of electrons gives different information about the sample, depending on the atomic structure of the sample material, its atoms will interact differently to the incident beam from the instrument. The electrons from the instrument beam are called primary electrons (Holly A. Ewing & Edward A. Nater, 2003; Mohammed & Abdullah, n.d.).

Secondary electrons give information about the surface topography of the sample because they are the product of the interaction between the primary electrons from the SEM beam and the electrons from the outer layer of the sample's atoms. Backscattered electrons are generated more commonly by high atomic number atoms, they are also called reflected electrons. The emission is of high energy and generates a distinct contrast compared to other signals, therefore these electrons can help contrasting different materials in the sample. Overall, depending on these emissions the image generated will be of different quality (Holly A. Ewing & Edward A. Nater, 2003; Mohammed & Abdullah, n.d.).

The sample must be prepared for the SEM analysis to obtain clean and quality images for an easier interpretation. Another element that affects the image quality is the charging of the sample surface, charging effects are caused by the sample accumulating electronical signals, which generates very bright images of difficult interpretation. To avoid this phenomenon, a thin layer of conductive material is placed on the sample surface, our sample is coated with gold. This enables the charged electrons to be dissipated through the conductive coating material, reducing image brightness and distortion.

In this study, the portions selected for SEM are the coarse fraction derived from the sieve analysis of each sample, which consist of pebbles from the mesh number 4 with an aperture of 4.76 mm of space between the mesh openings.

Our interest is to observe surface features on the pebbles, therefore it's important to clean the samples from organic and clay particles attached on the grains surface. The samples are first washed with distilled water to decant suspension matter, secondly, we implement 69% concentrated hydrochloric acid (HCl) diluted in 10ml of distilled water to further eliminate organic material. To remove clay from our grains, 69% concentrated nitric acid (HNO₃) diluted solution is used. These acids are commonly used for clay dispersion based on ion exchange interactions.

By examining the surface features of Norwegian sample grains, we aim to identify micro-texture indicators that can provide insights into the historical processes and environmental changes experienced by the landscape. The research is particularly focused on identifying glacial features on grain-sized particles to confirm previous knowledge about the deposition environment. To achieve this, we received the guidance of Professor Makarand Ganesh Kale from the Department of Geology (SPPU) and we followed the principles outlined in the "Atlas of Quartz Sand Surface Textures" by David H. Krinsley and John C. Doornkamp (Krinsley et al., 2011) (Table 6).

According to Krinsley et al, typical micro-texture features associated with glacial erosional features are subconchoidal fractures, Arc-shaped semiparallel steps, Striations and polished

surfaces. An area subjected to glacial activity leaves specific erosive and transportation patterns on its surface and landforms. The sediments a glacial carry on its bottom layer scratches and grinds the surface of the base rock beneath it, leaving a set of recognisable marks such as; striations, parallel lines with consistent orientation and direction, in relation to the movement of the glacier flow. Another distinctive feature is the polished surface resulted from glacial ice scraping and smoothing the rocks surface. Semiparallel arc-shapes and subconchoidal fractures are typical from quartz grains subjected to cracking from ice pressure.

Weathering leaves marks on the surface of the Norwegian grains, with specific features like triangular pits, dissolution, Hacksaw terminations, V-shaped indentations and pitted surface. Hacksaw terminations, also known as denticulated margins, are indicative of low-temperature aqueous corrosion origin in silicate minerals (Velbel & Losiak, 2010).

Pitted surfaces are related to the time the rock has been exposed, reflecting the extension of the weathering conditions over time, with pit depth increasing with exposure age (Hall & Phillips, 2006).

Dissolution rates of rocks serve as an important indicator of diagenetic conditions, factors such as mineral structures, chemical compositions, and the presence of secondary minerals influence dissolution rates, impacting the overall chemical degradation and weathering of rocks (Lo et al., 2017)..

X-Ray analysis

To study the mineralogical composition of our samples, we perform X-Ray diffraction analysis (XRD). XRD is a widely used technique used for crystallographic and material characterization (Jenkins & Snyder, 1996). In the case at hand, XRD results can give light on the different mineral genesis and metamorphism that the rocks experimented in such different geological and climatic environments. Under different temperature, pressure, pH or humidity conditions, the structure of certain minerals have different stability which then determines its crystal structure or mineral phases (Singh, 2023).

This technique is based on the Bragg's Law expressed in Equation 3 , which determines the angle at which X-rays are diffracted by the crystal lattice of a mineral, different minerals will display a characteristic reflected angle of the X-rays with respect to their specific atomic structure, allowing for their identification (Jenkins & Snyder, 1996; Singh, 2023).

$$n\lambda = 2d\sin(\theta)$$

Equation 3. Where, (n) represents the diffraction peak's order, (λ , lambda) is the X-ray wavelength, (d) is the distance between crystal lattice planes, and (θ , theta) stands for the angle of incidence relative to the crystal lattice planes.

We selected two samples from each study area. For the Norwegian study area EV1 and EV4 were selected under the following criteria: EV4 is utilized for agricultural purposes, showing higher mud concentration than EV1 and, EV1 is interesting to explore the mineralogical composition under the bog environment. For the India study area, we choose GO9 and GO10 to investigate into the mineralogical composition of the clays in Khazan lands.

The portions from the mesh sizes 16-240/ 1190-53 μ m are mixed for each sample and were prepared them for the analysis by grinding into a powder using an automatic Agate mortar, to achieve a consistent particle size distribution.

The powdered sample is then placed onto a sample holder designed for XRD analysis and evenly spread to ensure a flat surface. Once the sample is in the XRD instrument, the sample will be exposed to X-rays and scattered waves will be reflected at a specific angle known as the 2θ angle, representing the angle between the incident and scattered beams. After applying Bragg's Law and interpreting the peaks on the graphs generated, we can determine mineral phases present in the sample and their crystalline structure.

Soil chemistry

The Norwegian samples were sent to Vasantdada Sugar Institute (VSI) to be analysed following the standard laboratory methodology for each experiment. Test were performed for the following parameters, pH, Organic carbon, Organic matter, Electrical conductivity, Available Nitrogen, Phosphorus and Potassium or NPK test.

We then perform with the data generated, a multiple regression model using the Python programming language with a software library called Pandas (McKinney, 2010). This method allows us to investigate the research question of whether the elevation and terrain characteristics may influence or not the distribution of these chemical variables across the landscape.

Due to time and resource limitations, this analysis was performed only on the Norwegian samples.

We've strategically placed our sampling sites along the X axis, according to their location from west to east and north to south, following the convex shape that the elevation profile shows (Figure 2).

By aligning the sampling sites with the elevation profile, we can begin to explore the potential correlation between topography and the various chemical variables presented in this chapter. The study design is graphically summarized in Figure 14.

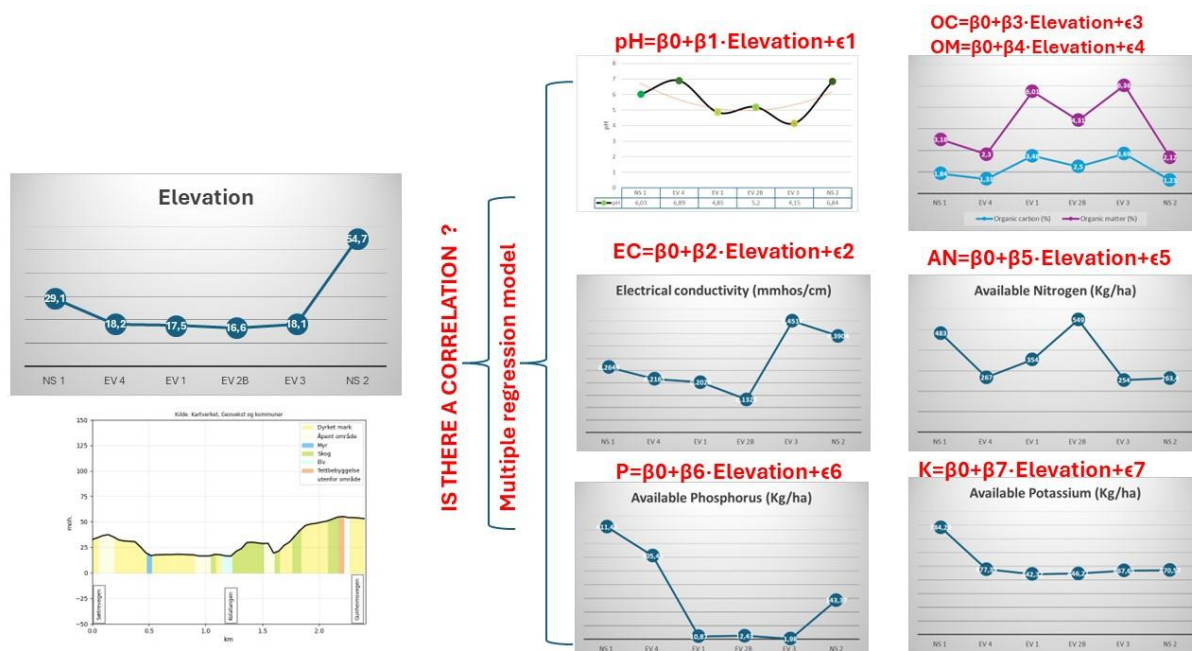


Figure 14. Diagram synthesizing the study hypothesis. Using a multiple regression model, we explore whether terrain characteristics affect the distribution of these variables across the landscape.

It is important to consider the limitations of multiple regression testing on a small sample size ($n < 10$) which is associated with low confidence estimations, leading to unreliable and inaccurate conclusions (Armstrong, 2019). This study consists of a small pool of six samples per variable, for further studies is recommended to amplify the sample size, in addition, other authors have suggested alternative techniques like Jackknife and Bootstrap to be better suitable for small sample sizes (John Michael , 2019).

6 Results

Sieve Analysis

Norway

As a result of the sieving analysis of the Norwegian samples, we generate ternary diagrams to study the textural characteristics (TC) of the sediments, a selection can be seen at Figure 15 and the rest at Table 9. Ternary diagram of the soil textural groups for the Norwegian samples. We found that the TC all are of sandy texture ranging from gravelly muddy to muddy sandy gravel as can be seen represented on the study area on Map 8. These results are congruent with the soil classification provided on Map 4 where our samples fall under Arenosol soil class like NS1 or Cambisol like EV4, both soil groups having high sand content.

The interpretation of the Grain Size Distribution (GSD) histograms (Figure 16) show that our samples are polymodal, bimodal and trimodal, varying from moderately sorted to very poorly sorted. All GSD diagrams for the rest of the samples can be seen in Table 8.

Sample EV-1 exhibits a polymodal grain size distribution and very poorly sorted, with gravel composition of 11.8%, sand 68.5%, and mud 19.7%. In contrast, sample EV2A displays a bimodal distribution with moderate sorting, showing compositions of gravel at 1.5%, sand at 92.9%, and mud at 5.6%. Similarly, sample EV-4 also shows bimodal distribution, however with very poorly sorted conditions, with gravel representing 0,1%, sand 59.9%, and mud 40.0%. Lastly, sample NS-2 shows a polymodal distribution, with very poorly sorted conditions as well, comprising 32.9% gravel, 58.4% sand, and 8.7% mud.

These results highlight the variability in textural groups and grain size distributions across the studied samples.

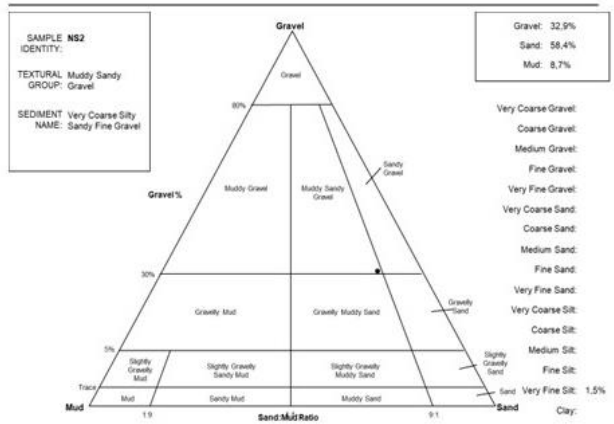
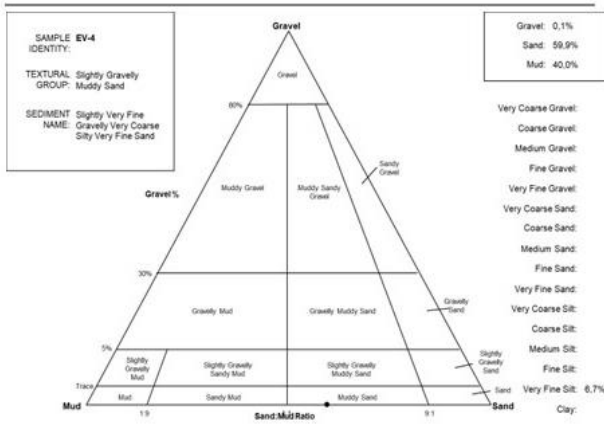
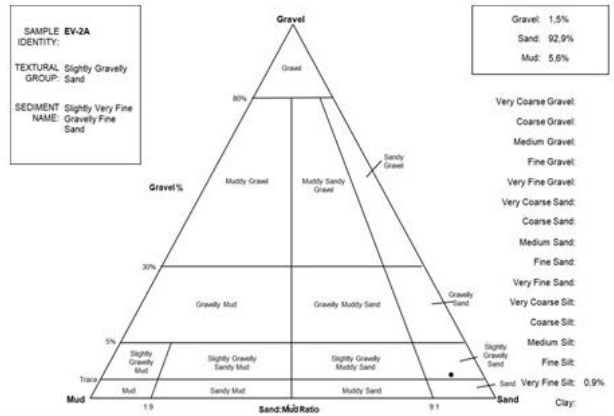
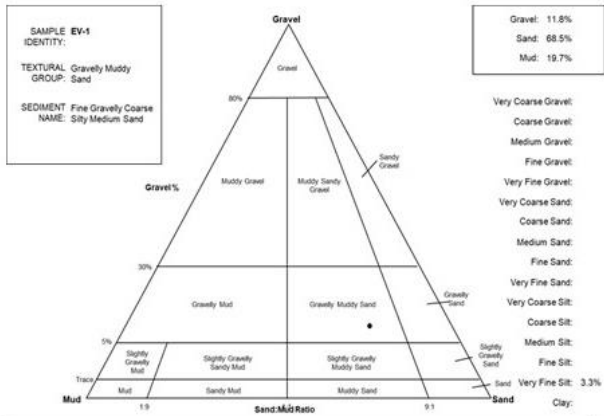


Figure 15 Ternary diagrams of the soil texture for samples EV1, EV2A, EV4 and NS2

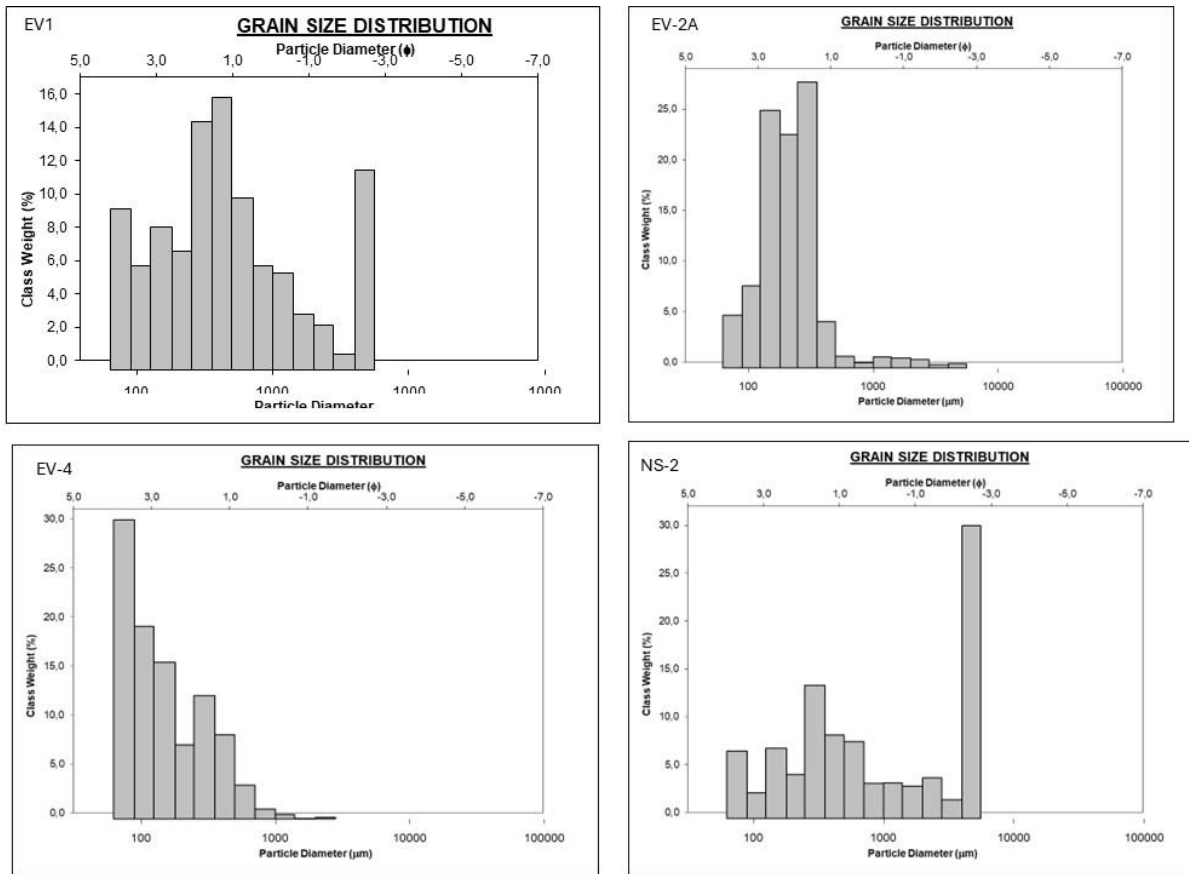
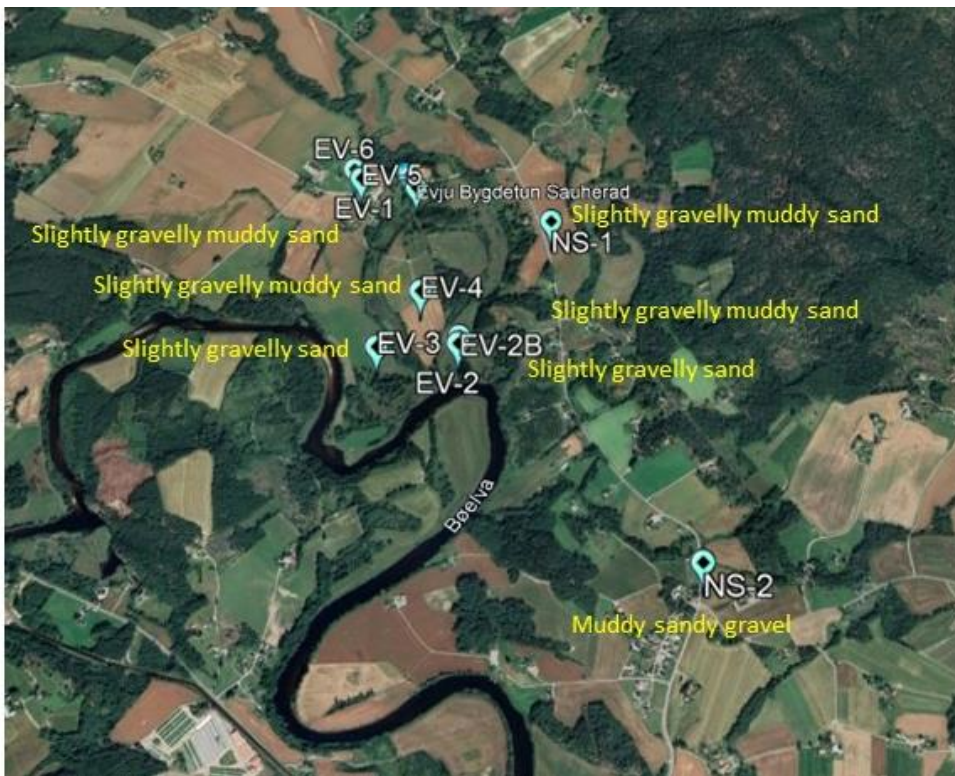


Figure 16. Grain size distribution illustrating Norwegian samples, showing the percentage of material versus particle size. From left to right: EV1 exhibits a polymodal distribution and is categorized as very poorly sorted ; EV-2A is moderately sorted and bimodal; EV-4 also is very poorly sorted and displays a bimodal distribution pattern. NS-2 shows bimodal coarse sand.



Map 8 . Textural groups in Evju study Area.

India

In our analysis of the texture classification of the Indian samples, we relied on the base rock map (Map 6) and soils classifications maps provided in previous works such as “Goa's Landscape Through Maps” by N. Sawant. Due to time limitations, we focused our analysis on samples from GO-1 to GO-5, which distribution across the study area can be seen in Map 9.



Map 9. Textural groups in Goa study area.

These samples exhibit different texture classification (TC) and grain size distribution (GSD) patterns depending on the nature of the parent material and depositional environment as explored in more detail in the discussion. TC and GSD for GO-1, not included in this chapter, can be seen in Table 10.

Sample GO-2 presents a bimodal grain size distribution, classified as poorly sorted, with gravel representing 4.5%, sand 95.5%, and no mud content. In contrast, Sample GO-3 displays a unimodal distribution but also poorly sorted, with significant gravel component of 71.2%, 28.8% of sand and no mud. GO-4 demonstrates a polymodal distribution and is poorly sorted, with a high content of 88.6% in sand, gravel comprising 11.4%, and no mud. Lastly, sample GO-5 shows a bimodal distribution, presenting a high gravel content of 71.6%, sand at 28.4%, and no mud.

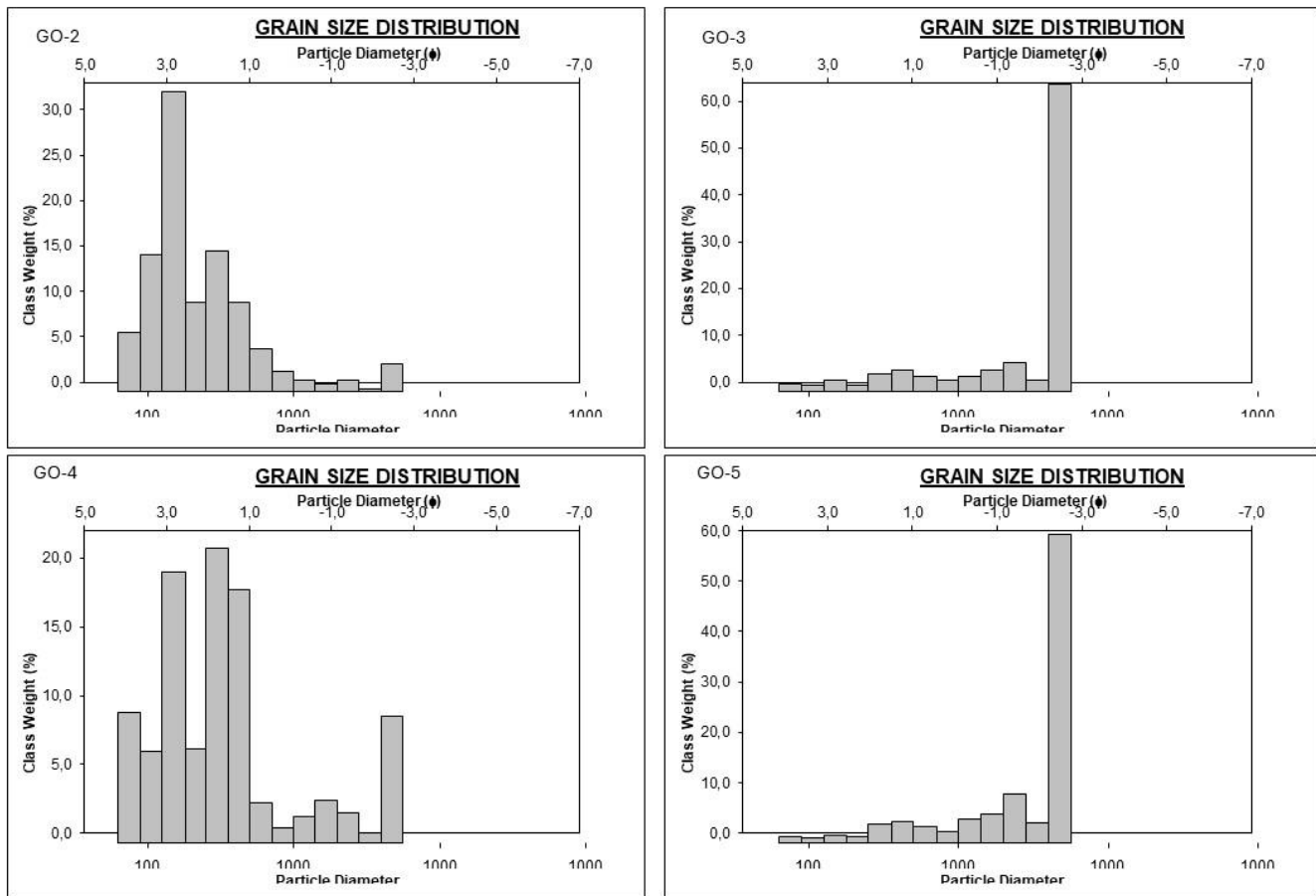


Figure 17. GO2 and GO5 are Bimodal, GO3: Unimodal, GO4: Polymodal, all being poorly sorted.

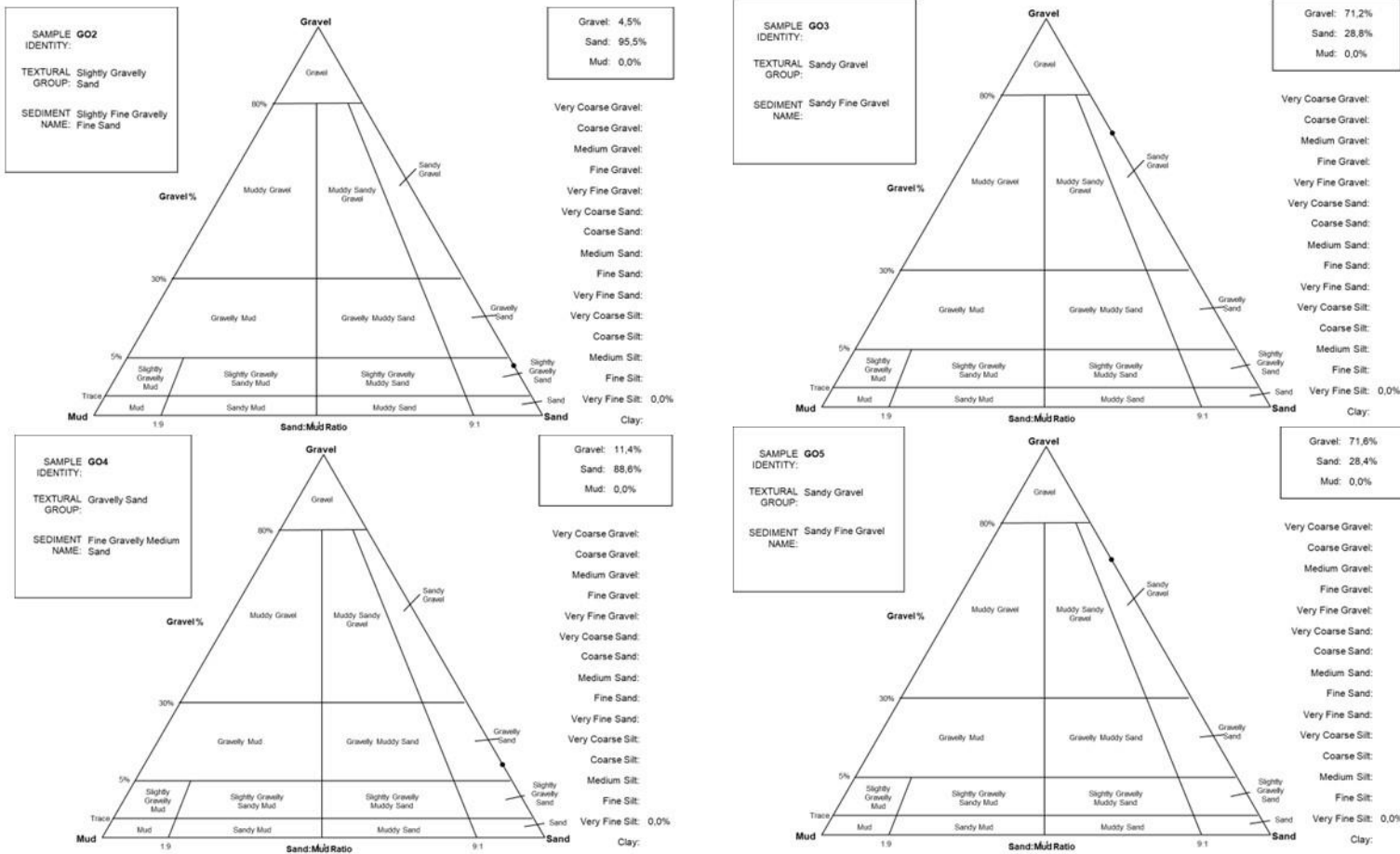


Figure 18. Ternary diagrams of the soil texture for the Goan samples.

Scanning electron microscopy analysis

Norway

The coarse fraction derived from the sieve analysis of all the Norwegian samples were selected for the SEM analysis in two sessions. The sediments showed micro-texture features such as subconchoidal fractures, arc-shaped semiparallel shapes, striations and polished surfaces depicted in Figure 19, more detailed description of these features is available in previous chapters.

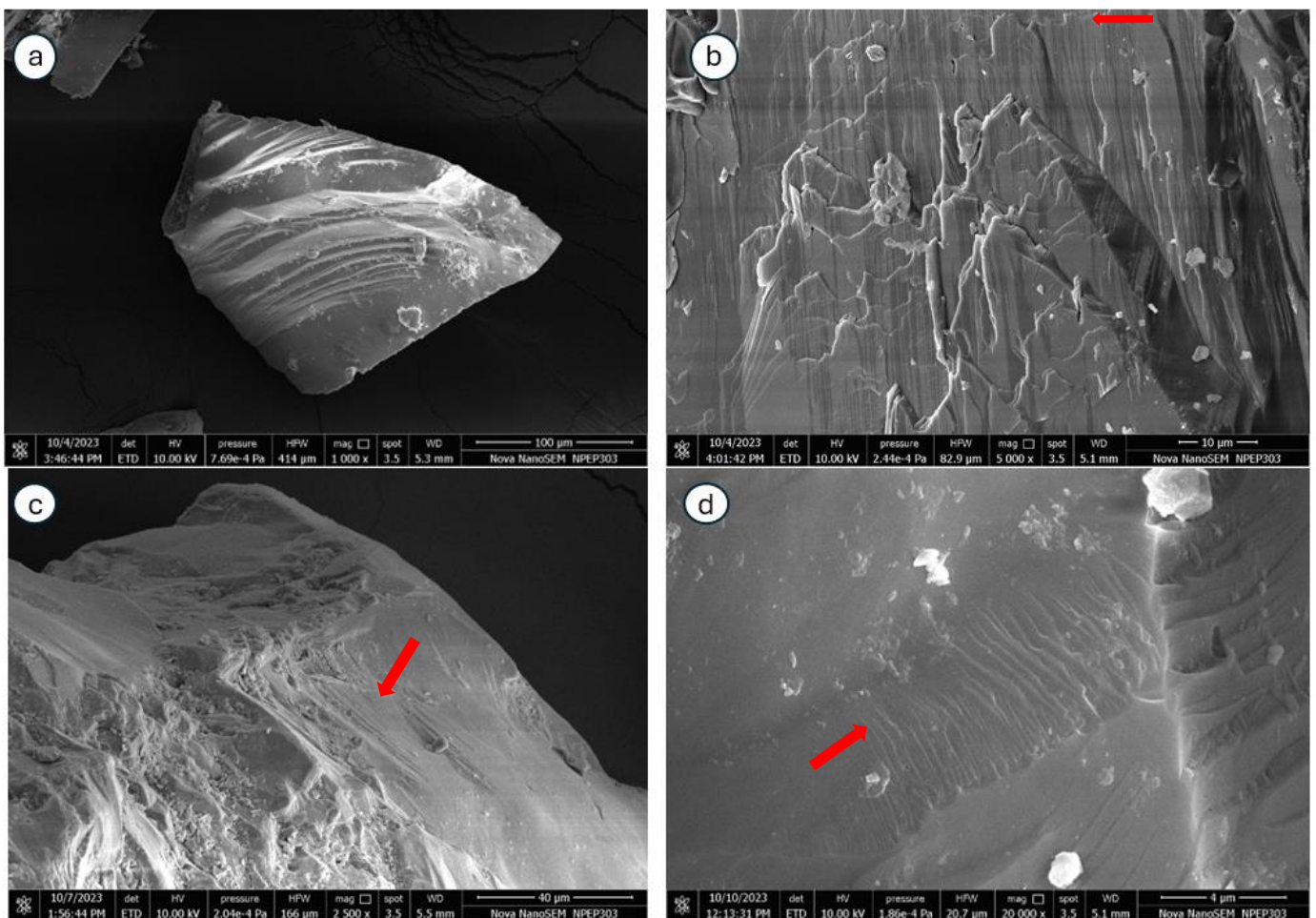


Figure 19. Picture a) Illustrates characteristic micro-texture features linked with glacial erosion patterns, including angular edges, polished surfaces, and arc-shaped semiparallel shapes. In Figure b), parallel striations are visible, with additional striations depicted in Figures c) and d), resulting from the abrasive action of moving glaciers against the bedrock surface.

Chemical weathering also left distinctive marks on the Norwegian grains surface that can be observed in Figure 20.

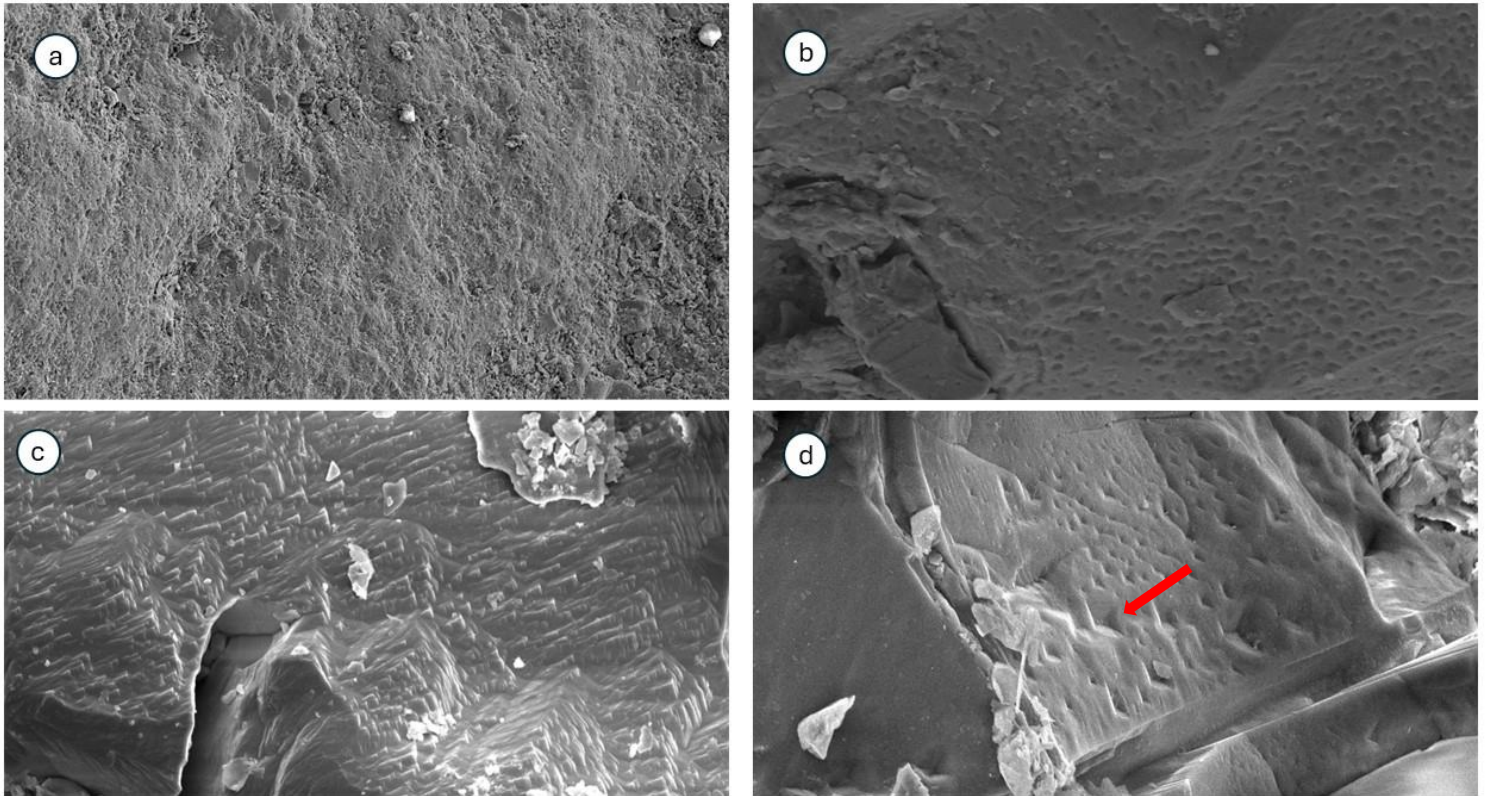


Figure 20. Series of images indicating various weathering processes. The first image (a) shows irregular depressions likely from acid dissolution, (b) displays a pitted surface indicating ongoing weathering, (c) exhibits hacksaw terminations along cleavage planes, indicating low-temperature aqueous alteration, and (d) reveals V-shaped indentations.

Following the acidic treatment undergone by the sample, the external walls, or frustules of some diatoms remained intact. As these walls are primarily composed of silica, various morphologies of diatom external walls are observable after the sample treatment.

A selection of some of the diatom's pictures generated during the SEM analysis is provided in Figure 21, the rest of the pictures can be accessed in Table 6.

This study is not focus on an extended diatom analysis nor in an advanced identification, however, we provide a simple note on the most noticeable species observed, we see two different species, one is *Fragilaria* species, falling into the family classification of Fragilariaceae, which includes diatoms characterized by elongated and straight frustules, the second species is *Navicula* sp, which belongs to the family of Naviculaceae, including diatoms with boat-shaped frustules. Both are classified under the class Bacillariophyceae, which includes diatoms with a wide range of morphological diversity (Wendy Guiry in Guiry, M.D. & Guiry, G.M., n.d.).

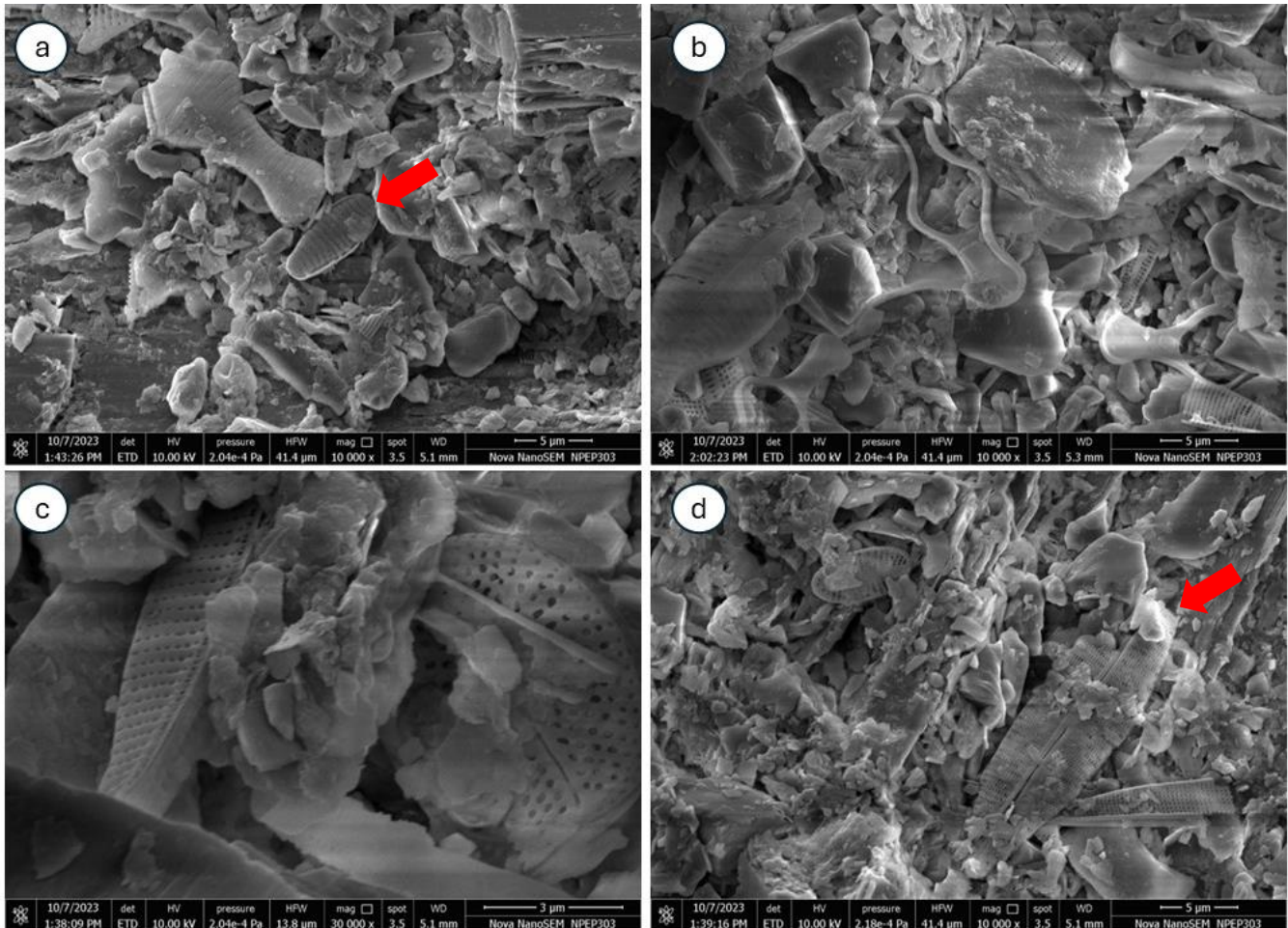


Figure 21. In image a), frustule corresponding to *Fragilaria* sp. is highlighted by the red arrow. In image d), *Navicula* sp. is observed at the right corner.

India

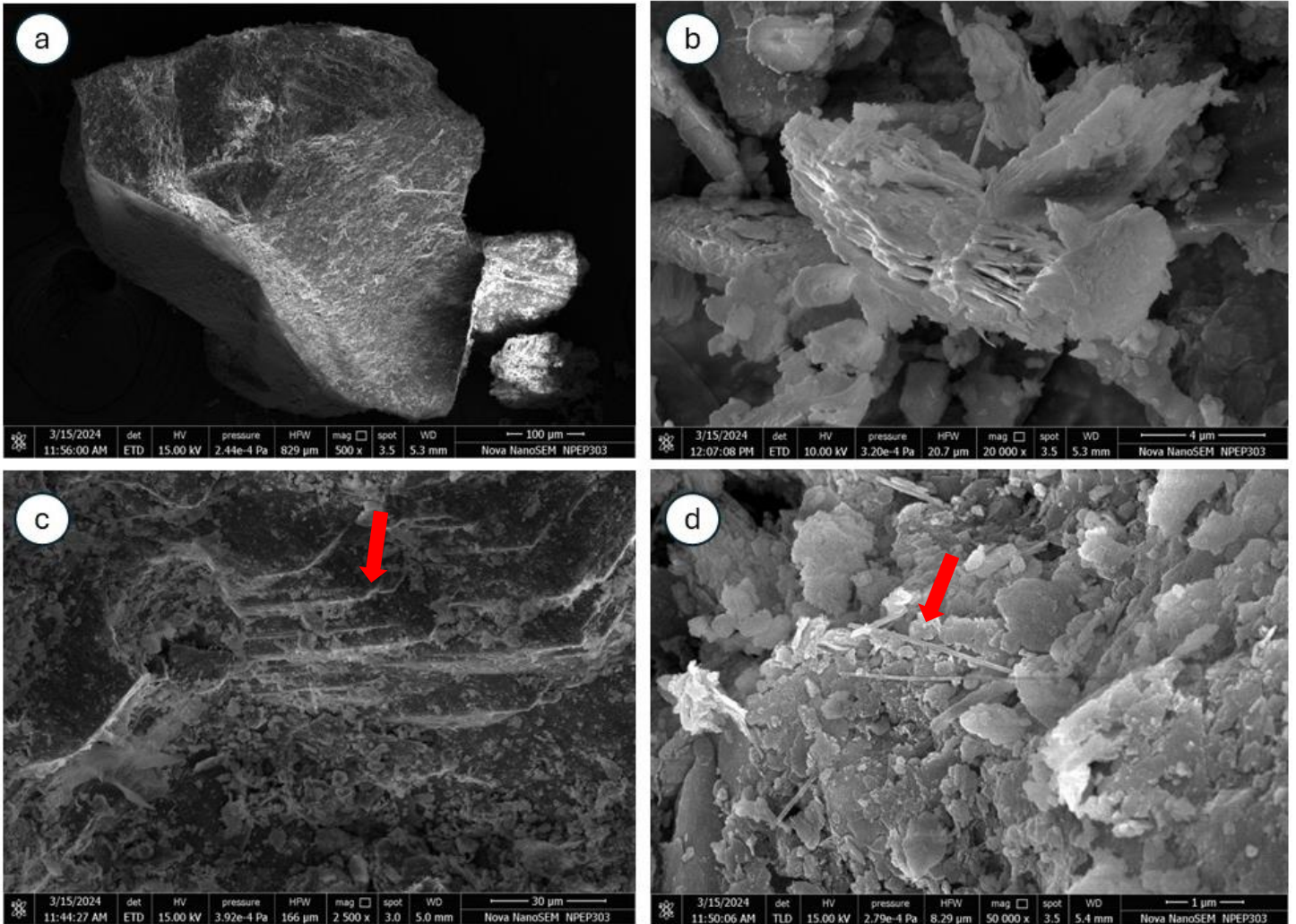


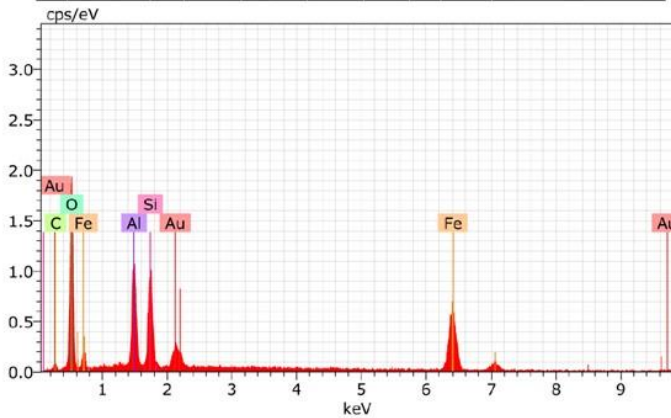
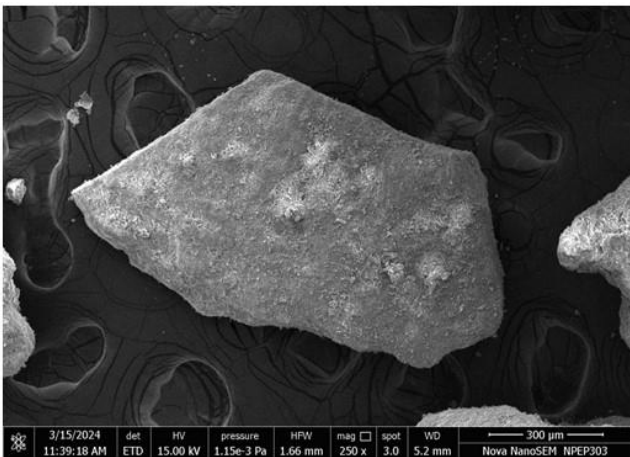
Figure 22. Micrographs showing diverse surface features observed on the Goan samples: On the first image a grain with precipitation marks on its surface, the darker areas are fractures. In picture c) by the red arrow we observe step-like cleavage of highly weathered chlorite, revealing the effects that weathering has on the mineral's aspect. The distinct platy and flaky crystalline morphology of gibbsite can be seen in pictures b) and d), in the last picture the red arrow points where we see fibrous minerals.

The selected grain sizes from samples GO-6 to GO-9 of the Goan samples were individually spread on the four studs within the SEM instrument in one session. Additional SEM pictures generated can be accessed in Table 7.

As a result, several key features are found in the pictures generated in Figure 22. These includes the crystallization of aluminium hydroxide ($\text{Al}(\text{OH})_3$), also known as gibbsite, the presence of highly porous clay surfaces, and the observation of cleavage planes and unidentified fibrous minerals.

Gibbsite, is a mineral commonly found in soils from tropical regions (Gasparini et al., 2022). Its physical characteristics typically show laminar shapes, as seen in picture b) from Figure 22. The genesis of gibbsite involves the alteration of primary aluminosilicate minerals by weathering elements like water and carbon dioxide, the aluminium ions dissolved by this action react with hydroxide ions (OH^-) present in the soil solution to precipitate as gibbsite (Gasparini et al., 2022).

GO-8



GO-9

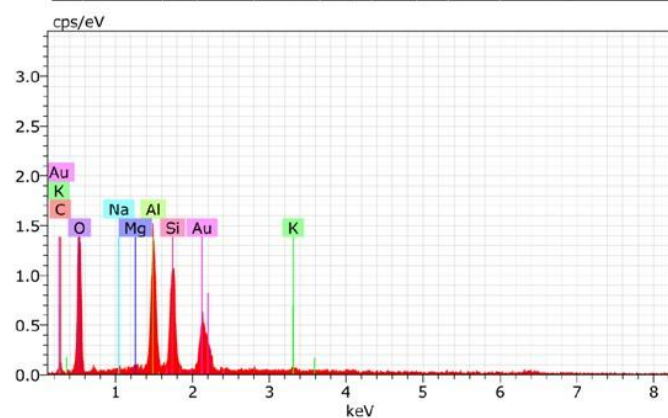
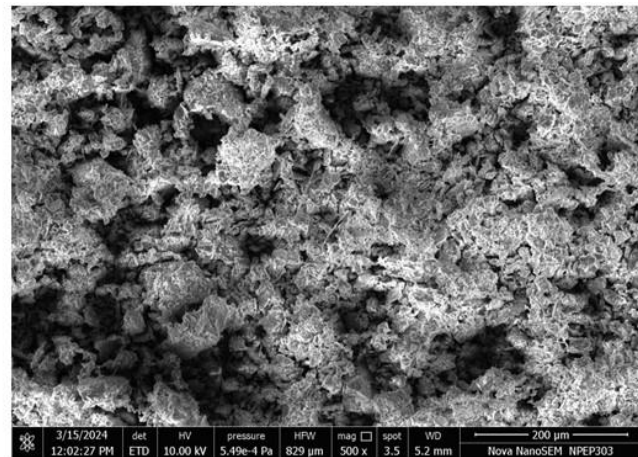


Figure 23. EDS reports for samples GO-8 confirms the high composition of Aluminium (Al) and Iron (Fe), characteristic of Laterite. Whereas the results for sample GO-9 aligns with clay, as expected. Gold (Au) values are due to this element being used for the coating material spread on top of the samples acting as a conducting surface for the SEM experiment.

To further confirm the lithological characterization and relative abundance of elements in the samples, we performed energy-dispersive X-ray spectroscopy (EDS) analysis. Due to budget limitations, we selected GO-8 taken from a stream shore as representative of the lateritic soil type samples, and GO-9 as representative for the samples falling in the Khazan lands, as we

expect the rest of the samples to have similar composition. The plots seen in Figure 23 show that the major elements composition for sample GO-9 are oxygen (O), silicon (Si) and aluminium (Al) with atomic abundance percentages of 54.4%, 17.7%, and 16.5 % respectively, aligning with the most abundant elements present in clay minerals. Other trace elements present in these clays are carbon, potassium, magnesium and sodium, providing insights of the specific type of clay and its environment.

In contrast, for GO-8 a composition of 21.1% iron (Fe) and 11.4% of Al was observed, as expected for lateritic samples. Notably, the oxygen abundance of 51.7% in GO-8 might be related to the weathering rate, the aquatic environment from which the sample was collected, or the microbiological activity involved (Amrutha et al., 2021; Coto Pérez et al., 2013; Ghosh & Guchhait, 2020; Roshan et al., 2022).

From these results, we can confirm the lateritic nature of sample GO-8 and clay composition of GO-9.

X- Ray analysis

The X-ray diffraction (XRD) results reveal notable differences between the samples from India and Norway. The X-ray diffraction plots for the Indian samples shows more complex spectra patterns, meaning more mineralogical diversity and weathering products (Figure 25).

In contrast, the Norwegian X-ray plots displays less mineral diversity, in Figure 24 we can see that the main mineral composition of both the samples EV1 and EV4 is Kaolinite. However, in sample EV4 there is six orders of magnitude higher intensity of Kaolinite crystals than EV1. A trace amount of quartz crystals can be seen as the smaller peaks.

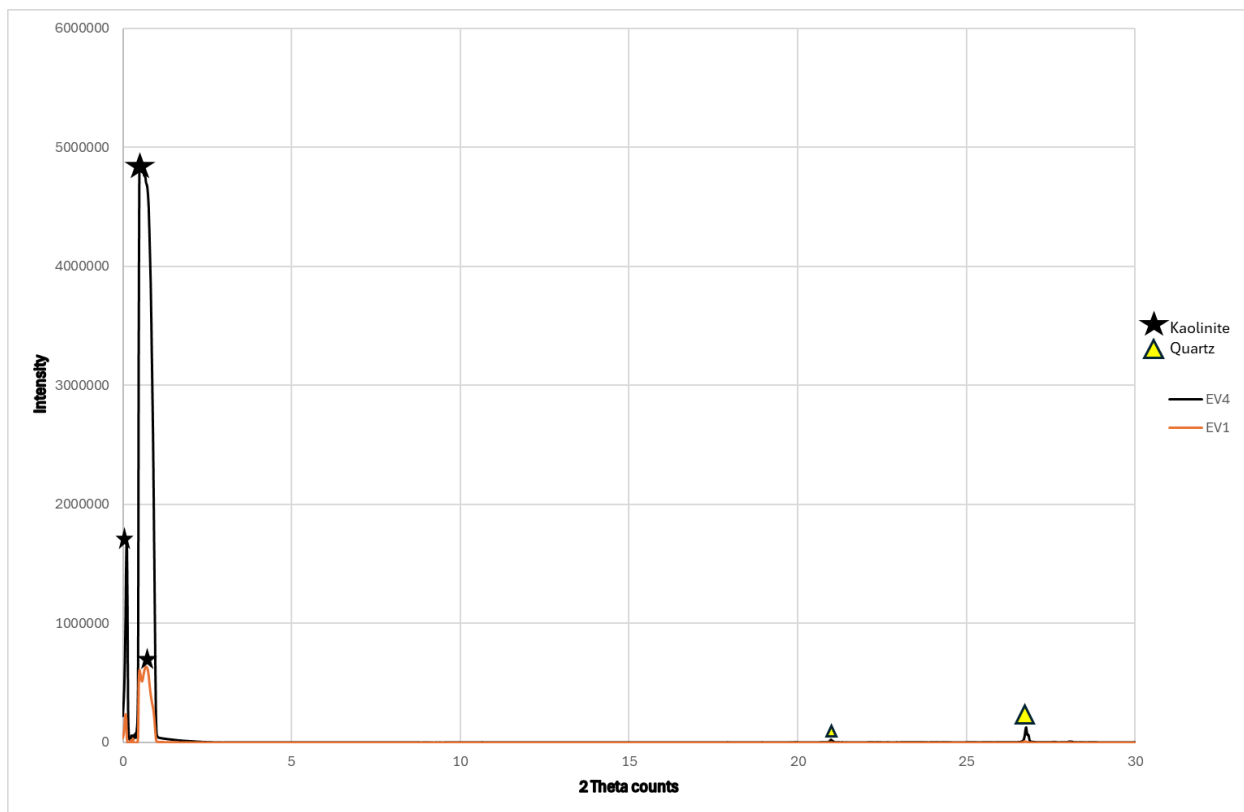


Figure 24. X-Ray diffraction plots for sample EV1 in orange colour, and sample EV4 in black, with EV4 exhibiting significantly higher intensity of Kaolinite crystals compared to EV1. Minor peaks corresponding to quartz crystals are also discernible in the spectra.

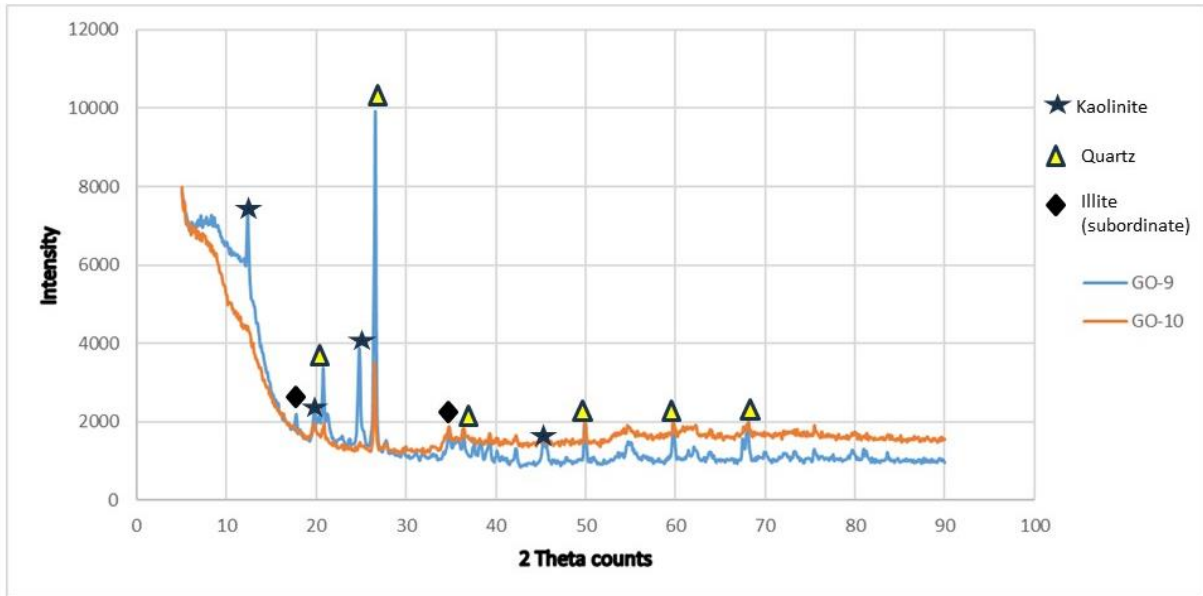


Figure 25. X-Ray diffraction plots for sample GO9 in blue colour, and sample GO10 in orange, revealing prominent peaks of quartz, minor kaolinite peaks and subordinate peaks of illite.

In Norway, the plagioclase present in the granitic gneiss from the base rock, transforms into kaolinite as a weathering product. Slower weathering rates due to the colder climate conditions can be related to the less mineral diversity found in the Norwegian samples. Conversely, in India the chlorite schist is exposed to tropical conditions and heavy rainfall, coupled with the rock porous texture, which can result in the formation of more complex weathering products.

Soil chemistry

As a result of the different laboratory experiments performed on the Norwegian soil samples, a table with the data generated is presented in Table 3.

Table 3. Soil chemistry values for Evju study area. Provided by Vasantdada Sugar Institute (VSI).

	pH	Organic carbon (%)	Organic matter (%)	Electrical conductivity (mmhos/cm)	Available Nitrogen (Kg/ha)	Available Phosphorus (Kg/ha)	Available Potassium (Kg/ha)
NS 1	6.03	1.84	3.18	0.2643	483	411.42	784.29
NS 2	6.84	1.23	2.12	0.3904	263.4	143.37	470.57
EV 1	4.85	3.48	6.01	0.2028	354	10.87	442.32
EV 2B	5.2	2.5	4.31	0.1329	549	12.43	446.21
EV 3	4.15	3.69	6.36	0.4517	254	1.98	467.65
EV 4	6.89	1.33	2.3	0.2161	267	305.45	477.39

The pH results (Figure 27 , a) show varied values across the different samples. Sample NS1 presents a pH of 6.03, indicating a slightly acidic to neutral soil environment, similarly, sample NS2 shows a value of 6.84. Samples EV1 and EV3 displayed lower pH values of 4.85 and 4.15, respectively, indicating a more acidic soil condition which can be related to the denser vegetation cover present in both samples and the possible higher microbial activity. Sample EV4, from the crop field, recorded a pH of 6.89, leaning towards a more alkaline to neutral soil environment. Sample EV2B falls within the acidic range with a value of 5.2 but closer to neutral compared to EV1 and EV3. These pH values, ranging from neutral to slightly acidic soils are considered of good suitability from the agricultural perspective (Barman et al., 2018).

Moving to the organic carbon (OC) and organic matter (OM) results (Figure 27, c), samples EV1, EV3, and EV2B shows relatively higher levels of both OC and OM compared to the other samples, this is related to the thicker vegetation cover on those sites. EV4 shows relatively low levels of OC and OM from an agricultural point of view (Bardalen et al., n.d., pp. 40–50), which might have an influence from its intensive agricultural use, this soil may benefit from organic amendments to improve fertility and soil health.

Regarding the electrical conductivity, samples NS2 and EV3 shows the highest values. Moving to the available nitrogen (Figure 26), of crucial importance for plant growth, we find that EV2B exhibits the highest value (549 Kg/ha) whereas EV4 has a nitrogen content of 267 Kg/ha. The available phosphorus, also important for agricultural productivity, shows big variations, NS1 and EV4 having high values of 411,42 Kg/ha and 305.45 Kg/ha respectively,

while EV3 has a content of 1.98 Kg/ha. Finally, available potassium, also important for plant growth, shows that NS1, NS2 and EV3 presents the highest concentrations of this crucial element, in significant higher levels for NS2.

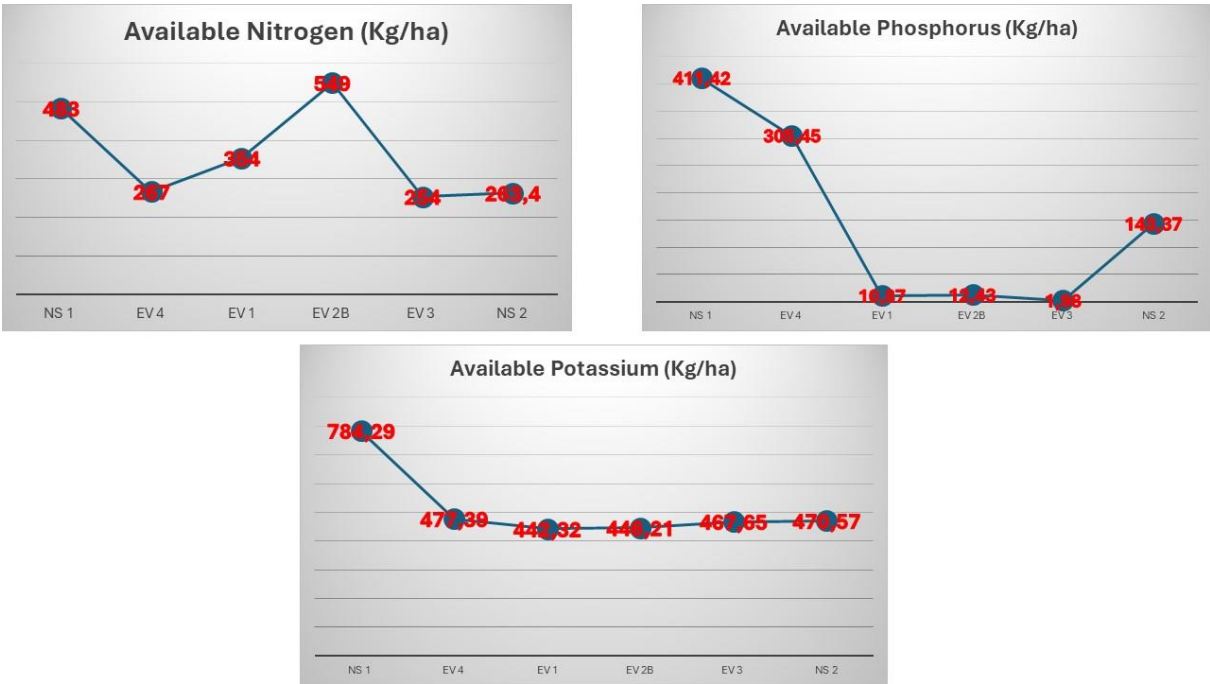


Figure 26. Graphical representation of the NPK results.

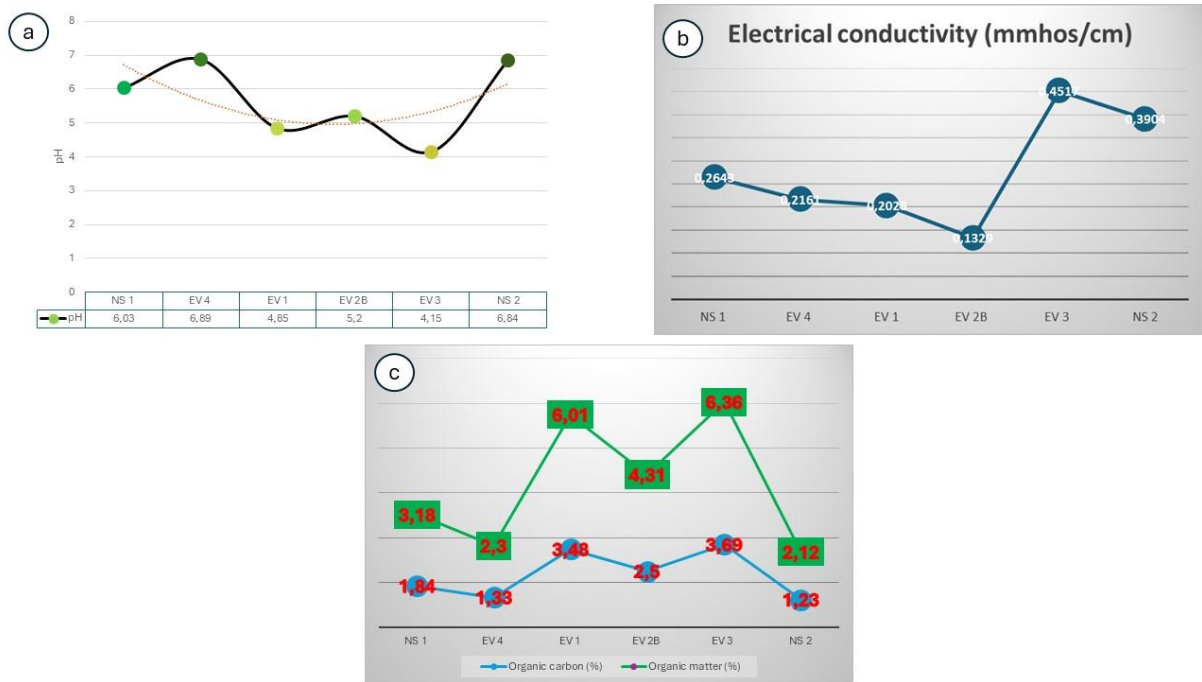


Figure 27. Plots representing; a) pH values, b) Electrical conductivity and c) organic matter values on the green line, and organic carbon on the blue line.

With the data provided, we generate a correlation matrix that can be seen in Figure 28. The results show that available Potassium (K), Phosphorus (P), Electrical conductivity (EC) and pH values might be correlated to the elevation of the terrain. Other variables showing correlations with values higher than 0.600 can be seen at Table 4.

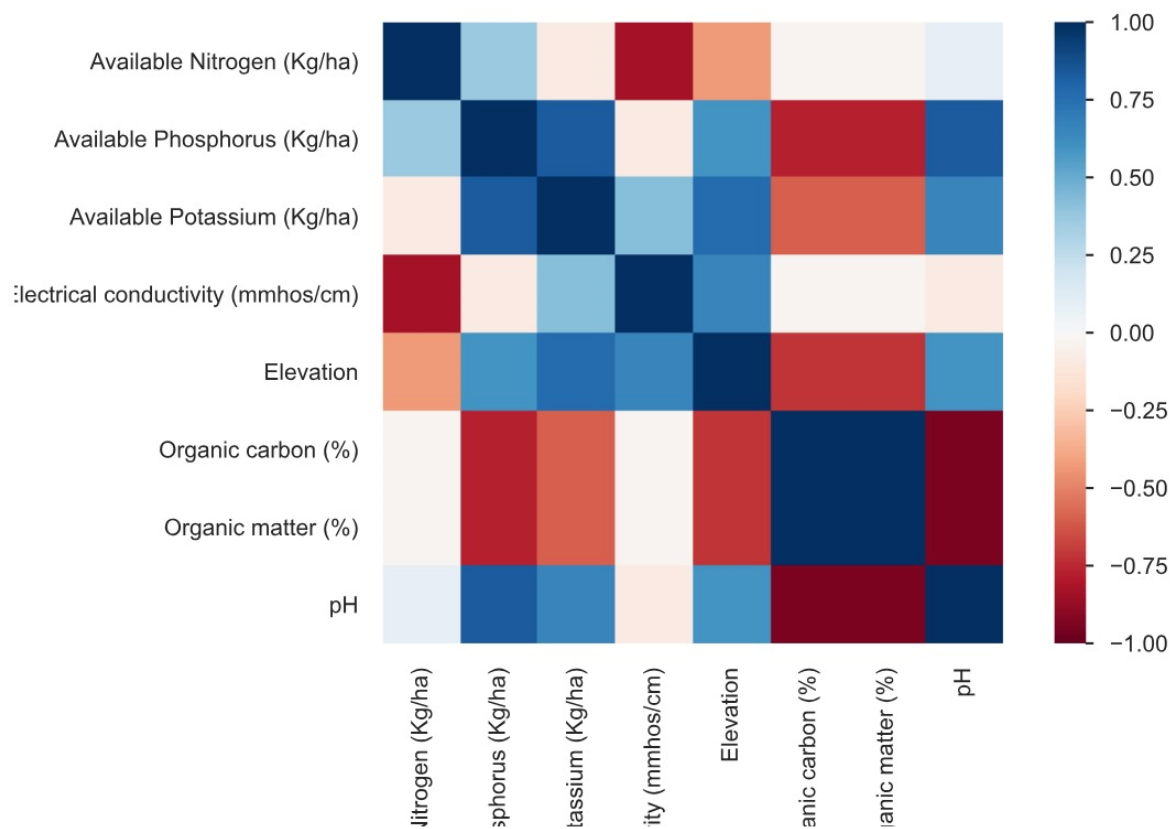


Figure 28. Correlogram or correlation matrix. Positive correlations are displayed in blue and negative correlations in red colour.

Table 4. Correlations with values higher than 0.600.

	Elevation	pH	Organic carbon (%)	Organic matter (%)	Electrical conductivity (mmhos/cm)	Available Nitrogen (Kg/ha)	Available Phosphorus (Kg/ha)	Available Potassium (Kg/ha)
Elevation	1	0.600			0.657		0.600	0.771
pH		1				0.086	0.829	0.657
Organic carbon (%)			1	1				
Organic matter (%)			1	1				
Electrical conductivity (mmhos/cm)	0.657				1			
Available Nitrogen (Kg/ha)						1		
Available Phosphorus (Kg/ha)	0.600	0.829					1	0.829
Available Potassium (Kg/ha)	0.771	0.657					0.829	1

7 Discussion

In this discussion chapter, we delve into the significant findings, discuss their implications and explore potentials for future research and soil management strategies in these different geographical settings.

Norway

Understanding the characteristics of fluvial and marine sediments is important when studying their textural classifications, fluvial and marine sediments have different grain size distribution (GSD) as a result of different mode of transportation, marine sediments usually have a lower sedimentation rate due to longer transport distances, being transported by currents and tides which can result in a wider range and mixing of grain sizes and less sorting (Kumar Maity & Maiti, 2018). In contrast, sedimentation rate in river is usually faster. In addition, fluvial sediments are influenced by hydraulic sorting due to particles being transported by the river flow and deposited according to its size, density and energy of the water flow (Kumar Maity & Maiti, 2018).

Typically, marine sediments show finer grain sizes than the fluvial sediments because of lower energy transport (Abdulkarim et al., 2021), our results show coarser marine sediments compared to the fluvial sediments, this can be related to the original location of the sediments within the marine environment, the shelf, slope or marine basin show different grain size distribution (Ohta et al., 2015), for instance, NS-2 being Muddy Sandy Gravel (Figure 15) can indicate these sediments were located under the sand-rich shelf or the basin floor where both sand-rich and mud-rich sediments can be found (Jia et al., 2020). These findings are congruent with the superficial sediments detail description available in Norges geologiske undersøkelse (NGU), where it is specified that the areas under light blue colour in the sediments map are of marine beach sediments. Additionally, in areas characterized by low-energy river flow like the meander and oxbow-lake found in our area, a low slope and widening of the channel means low river competence, meaning the maximum size of sediment particles that the river flow can transport will be smaller and lighter particles. There is growing concern regarding the loss of topsoil in Norway, where only three percent of the country's land is arable (*regjeringen.no*, 2017), scarce agricultural land is being discarded and used for road projects, industrial development, construction of railways and cottage fields (Stranden, 2024). Efforts should be done to preserve the marine sediments for its fertility and national food security importance, as they are a non-renewable resource from which food production relies heavily in this country.

It is worthy of mention the differences obtained in GSD and TC despite most of the samples having in common the fluvial sediments characterization, for instance, EV-4 has the highest proportion of mud (40.0%) among the samples, indicating a significant fine-grained component compared to EV-1 and EV-2A despite falling inside the same fluvial sediments category. Also, EV-2A is moderately sorted, with a more uniform distribution of particle sizes compared to the very poorly sorted distributions of EV-1 and EV-4 (Figure 16Figure 15).

It is also interesting to mention that we find two different soil classes developed on top of the same superficial sediments' classification. Arenosol and Cambisol are found on the fluvial sediments. The differences in soil class and texture within samples from the same superficial sediments might be driven by different factors such as; different proximity to the river, vegetation distribution, soil moisture, changes in the river dynamics, such as spatial variations in sediment deposition, erosion and floodplain formation can lead to differences in soil class and texture within a similar environment.

Regarding the SEM results, the observed micro-texture features on the SEM analysis are associated with glacial erosion patterns, which aligns with previous literature findings, suggesting ice sheet coverage from the Eurasian ice sheet (Hughes et al., 2016; Bergström, 1999). The chemical weathering rates observed between the two sample sites serves as a vehicle for understanding how climatic conditions can affect rocks differently. The images from the Goan samples reveal evidence of higher chemical weathering, characteristic of tropical climates compared to the chemical weathering rates observed on the Norwegian grains.

As EV-1 is the only sample in which diatoms frustules were observed, it may be related to the specific habitat of its collection. EV-1 was collected from the bog, characterized by sediments of organic origin and surrounded by typical wetland vegetation. As water from the oxbow lake is pumped to the surrounding agricultural lands, conducting further research regarding metagenomics can offer insights into the microdiversity present in both the water and soil samples from the oxbow lake habitat. This research can help elucidate the role of the oxbow lake when irrigating the Evju Mathage farm and other adjacent agricultural lands. This distinctive micro-habitat deserves preservation efforts for its ecosystem services and habitat importance.

Although this work is focused on inorganic variables, attention can be given in future studies to the relationship between grain size and soil microbiome diversity (Lin et al., 2023).

India

We now delve into the connections between tropical soil characteristics and their textural and geological setting for the Indian SA. Soils developed from laterite, are expected to present a coarse-grained texture, as indicated in previous studies (Amrutha et al., 2021; Roshan et al., 2022). In our case, samples GO-3 and GO-5 present the coarsest GSD as seen in Figure 17, where the histogram is skewed towards the right, with a textural classification of sandy gravel, with gravel composition of 71,6% as illustrated in Figure 18.

For soils developed from alluvium, TC and GSD vary depending on factors such as water flow velocity, carrying capacity, and topography (Kumar Maity & Maiti, 2018; Sharma et al., 2000). Sample GO-2 exhibits a bimodal GSD, suggesting a mixing of sediments of two distinct sizes, with 95,5% of gravel and 4,5% of sand. This might indicate the influence of multiple sedimentary processes, with periods of changing environmental conditions and the action of different sediment transport mechanisms (Kumar Maity & Maiti, 2018).

Sample GO-4 baserock is chlorite schist, showing a GS polymodal distribution, which may be a result of redeposition processes.

Chlorite schist is a metamorphic rock with fine-grained texture compared to laterite. This difference in TC between the two rock types can be explained by their different geological origins. Laterite undergoes laterization, which involves the breakdown of primary minerals and the concentration of iron and aluminum, this can lead to the formation of coarse-grained aggregates, such as concretions or nodules (Ghosh & Guchhait, 2020, 2020; Roshan et al., 2022) while the metamorphism of chlorite schist involves recrystallization of minerals that might result in smaller and compact minerals formed under intense pressure conditions (Babu et al., 2021).

Therefore, chlorite schist-derived soils may contain higher proportion of fine particles, consistent with our findings. For example, sample GO-4 only contains 11% of gravel, whereas GO-5, under lateritic parent material, has a composition of 70% of gravel.

Future research could focus on soil mapping at the specific scale in our study area, creating a soil classification dataset and map following the nomenclature system of the World Reference Base (WRB) for soil classification. This would contribute to the detailed understanding of the specific soil horizonation found in this area. In addition, we could better compare the Indian soil classes with the classification provided by the Norwegian Institute of Bioeconomy (NIBIO) for the Norwegian soils.

Comparing the two study areas

The chemical weathering rates observed between the two sample sites serves as a vehicle for understanding how climatic conditions can affect rocks differently, the environment affects rocks through both mechanical and chemical forces, such as ice movements and dissolution respectively. The SEM images from the Goan samples reveal evidence of higher chemical weathering, characteristic of tropical climates compared to the chemical weathering rates observed on the Norwegian grains.

In glacial environments low rate of alteration is influenced by the lower temperatures (Brown, 2010) where certain minerals may be more resistant to weathering and erosion due to the stability conferred by these conditions resulting in lower rates of mineral breakdown. In addition, lower biological activity also slows down reactivity, the alteration that does occurs is normally in subglacial settings, where acids dissolved in melted waters under ice sheets interacts with the underlying rock (Beylich, 2021).

In contrast, in tropical conditions, rocks are more exposed to the open atmosphere, higher temperatures and stronger precipitation leading to accelerated chemical reaction, a higher decomposition rates from microbial communities by producing organic acids (Kerfahi et al., 2019; Pal et al., 2009). In addition, a denser vegetation translates to stronger root penetration and bioturbation (Okon & Antia, 2022).

The Norwegian soils are mainly of sandy texture, which due to the high drainage tendency will need more irrigation during the growing season. Overall, Arenosols may not be ideally suitable for agricultural purposes, nevertheless, in less favourable climates, Arenosols are considered productive despite its limitations (Bardalen et al., n.d.). Whereas soils from Khazan lands in India are highly productive due to a combination of factors such as the organic matter and nitrogen provided by the alluvial and loamy soils (Sonak, 2014a, pp. 15–31) in addition to the sustainable traditional farming practices, the aquaculture practices and the salt-tolerant rice varieties used (Sawaiker et al., 2022; Sonak, 2014b).

Both agricultural lands of the study areas are under degradation risks, Norwegian fertile soil is at risk of erosion and permanent loss due to construction projects, while Khazan lands in Goa are often in conflict between the region's industrial and touristic development. Also, Laterites from Goa are a good medium for housing and other development projects, despite being declared as a Global Heritage Stone (2023). We suggest finding a win-win solution that both answers the demand for housing and economic dynamism while taking care of natural resources crucial for national and global food security.

As per climate change vulnerabilities, perturbation in the El Niño Southern Oscillation (ENSO) could potentially disrupt temperature and precipitation patterns in tropical India, posing risks to livelihoods (Iizumi et al., 2014). Whereas Norway's weather is vulnerable to perturbations of the North Atlantic Oscillation (NAO) (Tsanis & Tapoglou, 2019).

In contrast to the well-documented soil profiles and established research in Norwegian soil science, our study in India provides novel insights and data about the particular geology and soils of the study area. This can contribute to fill the knowledge gap in contrast to the abundant and easy access soil data and literature available in Norway.

Regarding the limitations of this piece of work, the initial objective was to study the factors driving the diverse soil formation processes despite similarities in parent material. However, during fieldwork in India we discovered that the base rock differs from the initial assumption. Therefore, for future research, it might be beneficial to focus on a common variable between the two study areas, amplifying the sample size and delving deeper into a single experiment, facilitating more robust comparisons and pattern identification.

On the other hand, there is potential to further study key drivers shaping soil formation across different climates when performing statistical analysis with a bigger sample size.

Overall, understanding soil properties and their variations across geographical regions is a step towards advancing sustainable agricultural practices and fostering interdisciplinary collaboration. This approach aligns with the concept of 'One Health,' as advocated by the World Health Organization (WHO), which works for an integrated approach to the health of people, animals, and the environment.

This research is the culmination of collaborative efforts between the University of South Eastern Norway (USN) and Savitribai Phule Pune University (SPPU), under the umbrella of the NIWASm project. The NIWASm project, focusing on the Norway-India Water-Soil Microbiome nexus, emphasizes blended mobility and interdisciplinary research. As a demonstration of its collaborative intentions, in this study participates different departments such as Environmental Science, Geology, and Statistics from SPPU, in conjunction with the Department of Natural Sciences and Environmental Health from USN.

Through this project, we hope to contribute to collaborative research methodologies to tackle global environmental challenges. By bringing together knowledge and expertise from multiple disciplines and geographical regions, we hope to fill knowledge gaps and contribute to study the intricate interactions between soil, geology, landscape, and human interactions to work towards sustainable land management practices.

8 Conclusion

In conclusion, this comparative study between Indian and Norwegian soils manifests the complexity of soil formation processes in diverse geographical settings. From all pedogenesis factors, this work has focused on the parent material and climate variability, with the purpose of describing how climate conditions have altered the base rock, setting the base ground from which pedogenic processes keeps developing.

The methodology employed has shown inherent limitations such as, the small sampling size. In addition, the different parent material found between the study areas represented a challenge to establish a common variable from which develop comparisons. The influence of climate on pedogenesis is already well studied and documented in previous works, however, the methodology employed in this study is unique. Also, our work in the Goan study area is a new contribution to the specific soil description of the area, serving as a foundation for future research.

Our findings from the Norwegian sieve analysis and SEM surface observations align with existing knowledge of the sediment's deposition environment, also confirming the congruence with previous soil surveys. We found variability in texture and soil class within the same category of fluvial sediments, suggesting localized influences, possibly driven by the different proximity to the river.

We also encourage the preservation of the oxbow lake habitat, given its distinctive characteristics and the ecosystem services it provides.

Moving to the Indian samples, a revision of the base rock of the area was done, specifically chlorite schist, which corrected previous identification efforts. The soil properties vary based on the geological setting, with laterite-derived soils displaying coarser textures compared to the chlorite schist-derived soils and alluvial soils presenting diverse grain size distributions.

Intense pedogenic transformations, such as laterization, are evident in Goan soils, contrasting with the less mature soils and weak horizon development observed in the Norwegian study area.

Ultimately, our work highlights the importance of understanding and preserving soil resources in both countries, in the face of ongoing environmental changes. We also emphasize the need for sustainable land management practices informed by interdisciplinary and collaborative research efforts. Also, it is important to support the implementation of sustainable soils practices where it is not developed such in Norway, or its preservation where it is already practiced and in danger of disappearing, like in Goa.

References

- Abdulkarim, M., Grema, H. M., Adamu, I. H., Mueller, D., Schulz, M., Ulbrich, M., Miocic, J. M., & Preusser, F. (2021). Effect of Using Different Chemical Dispersing Agents in Grain Size Analyses of Fluvial Sediments via Laser Diffraction Spectrometry. *Methods and Protocols*, 4(3), 44. <https://doi.org/10.3390/mps4030044>
- Amrutha, K., Warriar, A. K., Sandeep, K., Jyothinath, A., Ananthapadmanabha, A. L., & Shankar, R. (2021). Environmental Magnetic Properties of Lateritic Soils from Southwestern India. *Eurasian Soil Science*, 54(2), 238–248. <https://doi.org/10.1134/S1064229321020022>
- Anand, A., Kumar, V., & Kaushal, P. (2022). Biochar and its twin benefits: Crop residue management and climate change mitigation in India. *Renewable and Sustainable Energy Reviews*, 156, 111959. <https://doi.org/10.1016/j.rser.2021.111959>
- Armstrong, R. A. (2019). Is there a large sample size problem? *Ophthalmic and Physiological Optics*, 39(3), 129–130. <https://doi.org/10.1111/opo.12618>
- Babu, L., Mohan, S. V., Mohan, M., & Pradeepkumar, A. P. (2021). Highly mature sediments in the tropical monsoonal environment of southwestern India: An appraisal based on weathering indices. *Ecofeminism and Climate Change*, 2(2), 69–82. <https://doi.org/10.1108/EFCC-05-2020-0017>
- Bardalen, A., Aune-Lundberg, L., & Ulfeng, H. (n.d.). *Knowledge base for Norwegian soil conservation strategy*.
- Barman, U., Choudhury, R. D., Talukdar, N., Deka, P., Kalita, I., & Rahman, N. (2018). Predication of soil pH using HSI colour image processing and regression over Guwahati, Assam, India. *Journal of Applied and Natural Science*, 10(2), 805–809. <https://doi.org/10.31018/jans.v10i2.1701>
- Bergstrøm, B. (1999). Glacial geology, deglaciation chronology and sea-level changes in the southern Telemark and Vestfold counties, southeastern Norway. *Norges Geologiske Undersøkelse Bulletin*, 435, Article 435.
- Beylich, A. A. (Ed.). (2021). *Landscapes and Landforms of Norway*. Springer International Publishing. <https://doi.org/10.1007/978-3-030-52563-7>

- Bianchi, T. S. (2007). Geochemistry of Marine Sediments. *Eos, Transactions American Geophysical Union*, 88(47), 507–507. <https://doi.org/10.1029/2007EO470014>
- Bradley, R. S., & Bradley, R. S. (1999). *Paleoclimatology: Reconstructing climates of the Quaternary* (2nd ed). Academic Press.
- Brown, A. (2010). Reliable Mine Water Technology. *Mine Water and the Environment*, 29(2), 85–91. <https://doi.org/10.1007/s10230-010-0111-7>
- Butler, J. P., Beaumont, C., & Jamieson, R. A. (2015). Paradigm lost: Buoyancy thwarted by the strength of the Western Gneiss Region (ultra)high-pressure terrane, Norway. *Lithosphere*, 7(4), 379–407. <https://doi.org/10.1130/L426.1>
- Cardelli, V., Cocco, S., Agnelli, A., Nardi, S., Pizzeghello, D., Fernández-Sanjurjo, M., & Corti, G. (2017). Chemical and Biochemical Properties of Soils Developed from Different Lithologies in Northwestern Spain (Galicia). *Forests*, 8(4), 135. <https://doi.org/10.3390/f8040135>
- Chiapini, M., Schellekens, J., Oliveira Junior, J. C., Calegari, M. R., & Vidal-Torrado, P. (2023). Pedogenesis in very deep autochthonous Ferralsols of the Paraná Igneous Province (Brazil). *CATENA*, 224, 106981. <https://doi.org/10.1016/j.catena.2023.106981>
- Chris-Emenyonu, C. M., Onweremadu, E. U., Njoku, J. D., Ahukaemere, C. M., & Aririguzo, B. N. (2020). Soil Carbon Sequestrations in Forest Soils in Relation to Parent Material and Soil Depth in South-Eastern Nigeria. *American Journal of Climate Change*, 09(04), 400–409. <https://doi.org/10.4236/ajcc.2020.94025>
- Coto Pérez, O., Marrero Coto, J., & Schippers, A. (2013). Quantification of the Microbial Community in Lateritic Deposits. *Advanced Materials Research*, 825, 33–36. <https://doi.org/10.4028/www.scientific.net/AMR.825.33>
- Elvenes, S., Bøe, R., Lepland, A., & Dolan, M. (2019). Seabed sediments of Søre Sunnmøre, Norway. *Journal of Maps*, 15(2), 686–696. <https://doi.org/10.1080/17445647.2019.1659865>
- Esri. (n.d.). *ArcGIS Pro* (Redlands, CA: Environmental Systems Research Institute.; 3.1.0) [Computer software].
- Gasparini, A. S., Fontes, M. P. F., Pacheco, A. A., & Ker, J. C. (2022). Gibbsite Crystallinity and Morphology in Ferralsols and Bauxites. *Minerals*, 12(11), 1441. <https://doi.org/10.3390/min12111441>

Geonorge. (n.d.). Retrieved 14 February 2024, from <https://www.geonorge.no/en/>

Ghosh, S., & Guchhait, S. K. (2020). Geochemical Properties and Lateritization Processes. In S. Ghosh & S. K. Guchhait, *Laterites of the Bengal Basin* (pp. 83–94). Springer International Publishing. https://doi.org/10.1007/978-3-030-22937-5_6

Hall, A. M., & Phillips, W. M. (2006). Weathering pits as indicators of the relative age of granite surfaces in the cairngorm mountains, scotland. *Geografiska Annaler: Series A, Physical Geography*, 88(2), 135–150. <https://doi.org/10.1111/j.0435-3676.2006.00290.x>

Holly A. Ewing & Edward A. Nater. (2003). Use of scanning electron microscopy to investigate records of soil weathering preserved in lake sediment. *The Holocene*, 13(1), Article 1. <https://doi.org/10.1191/0959683603hl594rp>

Hughes, A. L. C., Gyllencreutz, R., Lohne, Ø. S., Mangerud, J., & Svendsen, J. I. (2016). The last Eurasian ice sheets – a chronological database and time-slice reconstruction, DATED-1. *Boreas*, 45(1), Article 1. <https://doi.org/10.1111/bor.12142>

Iizumi, T., Luo, J.-J., Challinor, A. J., Sakurai, G., Yokozawa, M., Sakuma, H., Brown, M. E., & Yamagata, T. (2014). Impacts of El Niño Southern Oscillation on the global yields of major crops. *Nature Communications*, 5(1), 3712. <https://doi.org/10.1038/ncomms4712>

Jenkins, R., & Snyder, R. L. (1996). *Introduction to X-ray Powder Diffractometry* (1st ed.). Wiley. <https://doi.org/10.1002/9781118520994>

Jia, H., Ji, H., Yu, J., & Meng, X. (2020). Sediment supply control on the delivery of sediments to deep-lacustrine environment: A case study from Luanping Basin, northern China. *Geological Journal*, 55(5), 3679–3693. <https://doi.org/10.1002/gj.3608>

Jordsmonnkart. (n.d.). Nibio. Retrieved 14 February 2024, from <https://www.nibio.no/tema/jord/jordkartlegging/jordsmonnkart>

Kartverket.no. (2024, May 14). Kartverket.no. <https://kartverket.no/>

Kavya, S. R., Rani, B., Banu, M. R. F., & Jabin, P. P. N. (2023). Carbon Sequestration and Stabilisation Mechanisms in the Agricultural Soils: A Review. *International Journal of Plant & Soil Science*, 35(13), 79–94. <https://doi.org/10.9734/ijpss/2023/v35i132991>

Kerfahi, D., Tripathi, B. M., Dong, K., Kim, M., Kim, H., Ferry Slik, J. W., Go, R., & Adams, J. M. (2019). From the High Arctic to the Equator: Do Soil Metagenomes Differ According to Our Expectations? *Microbial Ecology*, 77(1), 168–185. <https://doi.org/10.1007/s00248-018-1215-z>

Krinsley, D. H., Krinsley, D. H., & Doornkamp, J. C. (2011). *Atlas of quartz sand surface textures* (1. paperb. ed). Cambridge Univ. Press.

Kumar Maity, S., & Maiti, R. (2018). Environment of Sediment Deposition. In S. Kumar Maity & R. Maiti, *Sedimentation in the Rupnarayan River* (pp. 39–55). Springer International Publishing. https://doi.org/10.1007/978-3-319-71315-1_3

Lin, J., Zhou, X., Lu, X., Xu, Y., Wei, Z., & Ruan, A. (2023). Grain size distribution drives microbial communities vertically assemble in nascent lake sediments. *Environmental Research*, 227, 115828. <https://doi.org/10.1016/j.envres.2023.115828>

Liu, P., & Massonne, H. (2019). An anticlockwise P – T – t path at high-pressure, high-temperature conditions for a migmatitic gneiss from the island of Fjortoft, Western Gneiss Region, Norway, indicates two burial events during the Caledonian orogeny. *Journal of Metamorphic Geology*, 37(4), 567–588. <https://doi.org/10.1111/jmg.12476>

Lo, F.-L., Chen, H.-F., & Fang, J.-N. (2017). Discussion of Suitable Chemical Weathering Proxies in Sediments by Comparing the Dissolution Rates of Minerals in Different Rocks. *The Journal of Geology*, 125(1), 83–99. <https://doi.org/10.1086/689184>

McKinney, W., & others. (2010). *Data structures for statistical computing in python*. In *Proceedings of the 9th Python in Science Conference* (Vol. 445, pp. 51–56) [Computer software]. <https://conference.scipy.org/proceedings/scipy2010/mckinney.html>

Miranda-Vélez, J. F., Leuther, F., Köhne, J. M., Munkholm, L. J., & Vogeler, I. (2023). Effects of freeze-thaw cycles on soil structure under different tillage and plant cover management practices. *Soil and Tillage Research*, 225, 105540. <https://doi.org/10.1016/j.still.2022.105540>

Mohammed, A., & Abdullah, A. (n.d.). *SCANNING ELECTRON MICROSCOPY (SEM): A REVIEW*.

Moore, J. A., Kimsey, M. J., Garrison-Johnston, M., Shaw, T. M., Mika, P., & Poolakkal, J. (2022). Geologic Soil Parent Material Influence on Forest Surface Soil Chemical Characteristics in the Inland Northwest, USA. *Forests*, 13(9), 1363. <https://doi.org/10.3390/f13091363>

Moura, E., Gehring, C., Braun, H., Ferraz Junior, A., Reis, F., & Aguiar, A. (2016). Improving Farming Practices for Sustainable Soil Use in the Humid Tropics and Rainforest Ecosystem Health. *Sustainability*, 8(9), 841. <https://doi.org/10.3390/su8090841>

Nandkumar N. Sawant. (2022). *Goa's Landscape Through Maps* (First Edition). Dnyanmangal Publication Distribution.

Norges geologiske undersøkelse. (n.d.). [Map]. <https://www.ngu.no/node/239>

Noronha, L., Siqueira, A., Sreekesh, S., Qureshy, L., & Kazi, S. (2002). Goa: Tourism, Migrations, and Ecosystem Transformations. *AMBIO: A Journal of the Human Environment*, 31(4), 295–302. <https://doi.org/10.1579/0044-7447-31.4.295>

Observasjoner og værstatistikk—Seklima. (n.d.). Retrieved 11 May 2024, from <https://seklima.met.no/>

Ohta, A., Imai, N., Terashima, S., Tachibana, Y., Ikehara, K., & Katayama, H. (2015). Elemental distribution of surface sediments around Oki Trough including adjacent terrestrial area: Strong impact of Japan Sea Proper Water on silty and clayey sediments. *BULLETIN OF THE GEOLOGICAL SURVEY OF JAPAN*, 66(3–4), 81–101. <https://doi.org/10.9795/bullgsj.66.81>

Okon, O. G., & Antia, U. E. (2022). Pedogenesis and Soil Biota Interactions in the Pedosphere. In B. Giri, R. Kapoor, Q.-S. Wu, & A. Varma (Eds.), *Structure and Functions of Pedosphere* (pp. 1–21). Springer Nature Singapore. https://doi.org/10.1007/978-981-16-8770-9_1

OpenTopography. (2021). *Copernicus GLO-90 Digital Surface Model* [dataset]. [object Object]. <https://doi.org/10.5069/G9028PQB>

Ouattara, B., Sermé, I., Ouattara, K., Sédogo, M. P., & Bismark Nacro, H. (2017). Cropping System Effects on Soil Monosaccharides in Western Burkina Faso. *Journal of Agricultural Studies*, 5(4), 97. <https://doi.org/10.5296/jas.v5i4.11985>

Pal, D., Dasog, G. S., & Bhattacharyya, T. (2009). Pedogenetic Processes in Cracking Clay Soils (Vertisols) in Tropical Environments of India: A Critique. *Journal of the Indian Society of Soil Science*, 57, 422–432.

Patel, A., Patel, R., & Maitrey, B. (2022). A REVIEW - IMPORTANCE OF PHYSICO-CHEMICAL PROPERTIES IN SOIL QUALITY. *VIDYA - A JOURNAL OF GUJARAT UNIVERSITY*, 1(2), 51–54. <https://doi.org/10.47413/vidya.v1i2.60>

Pombo, P. (2019). Water Cartographies of Goa: *Khazans*, Sedimentation and Dissolution of Coastal Cultural Landscapes. *Journal of Heritage Management*, 4(2), 192–207.
<https://doi.org/10.1177/2455929619877477>

Quaternary geology of Norway. (2013). Norges geologiske undersøkelse.

Ramberg, I. B. (2008). *The making of a land: Geology of Norway*. Norsk geologisk forening.

Regjeringen.no. (2017, May 16). [Portalforside]. Regjeringen.no; regjeringen.no.
<https://www.regjeringen.no/no/id4/>

Riveros Gavilanes, John Michael (2019): Low sample size and regression: A Monte Carlo approach. Published in: *Journal of Applied Economic Sciences*, Vol. XV, No. 1(67) (30 March 2020): pp. 22-44.

Roberts, R. J., Corfu, F., Torsvik, T. H., Ashwal, L. D., & Ramsay, D. M. (2006). Short-lived mafic magmatism at 560–570 Ma in the northern Norwegian Caledonides: U–Pb zircon ages from the Seiland Igneous Province. *Geological Magazine*, 143(6), 887–903.
<https://doi.org/10.1017/S0016756806002512>

Roshan, M. J., Hezmi, M. A., Rashid, A. S. A., Ullah, R., & Ullah, A. (2022). *Characterization of lateritic soil based on literature and lab testing*. <https://doi.org/10.21203/rs.3.rs-1977542/v1>

Ruiz-Martínez, G., Rivillas-Ospina, G. D., Mariño-Tapia, I., & Posada-Vanegas, G. (2016). SANDY: A Matlab tool to estimate the sediment size distribution from a sieve analysis. *Computers & Geosciences*, 92, 104–116. <https://doi.org/10.1016/j.cageo.2016.04.010>

Sarkar, S., Kuttippurath, J., & Patel, V. K. (2023). Long-term changes in precipitable water vapour over India derived from satellite and reanalysis data for the past four decades (1980–2020). *Environmental Science: Atmospheres*, 3(4), 749–759. <https://doi.org/10.1039/D2EA00139J>

Sawaiker, R. U., Gaude, S., Naik, S., Chari, S., Gaude, A., & Padwalkar, N. (2022). A Study of Traditionally Managed Khazan Ecosystems of Ponda Taluka, Goa. *International Journal of Ecology and Environmental Sciences*, 49(3), 247–252. <https://doi.org/10.55863/ijeec.2023.2734>

Schüllli-Maurer, I., Sauer, D., Stahr, K., Sperstad, R., & Sørensen, R. (n.d.). *Soil formation in marine sediments and beach deposits of southern Norway: Investigations of soil chronosequences in the Oslofjord region*.

Sharma, R. C., Saxena, R. K., & Verma, K. S. (2000). Reconnaissance mapping and management of salt-affected soils using satellite images. *International Journal of Remote Sensing*, 21(17), 3209–3218. <https://doi.org/10.1080/014311600750019831>

Singh, Y. (2023). X-Ray Diffraction in Mineralogical Research. *Journal of ISAS*, 1–11. <https://doi.org/10.59143/isas.jisas.1.4.WCJB9374>

Solbakken, E. (n.d.). *Viten fra Skog og landskap 1/06*.

Sonak, S. M. (2014a). An Introduction to Goa and Khazan Ecosystems. In S. M. Sonak, *Khazan Ecosystems of Goa* (pp. 15–31). Springer Netherlands. https://doi.org/10.1007/978-94-007-7202-1_2

Sonak, S. M. (2014b). *Environment and Development, Goa at Crossroads* (First Edition). Centre for Environment and Natural Resource Management, Srujan and Broadway Publishing House.

Stranden, I. L. (2024, February 13). *Tonnevis med matjord havner på søppelfyllinga hvert år*. NRK. <https://www.nrk.no/trondelag/tonnevis-med-matjord-havner-pa-soppelfyllinga-hvert-ar-1.16665336>

Stratford, W., Thybo, H., Faleide, J. I., Olesen, O., & Tryggvason, A. (2008). New Insights Into the Lithospheric Structure of Southern Norway. *Eos, Transactions American Geophysical Union*, 89(53), 554–555. <https://doi.org/10.1029/2008EO530002>

Sun, B., Ren, F., Ding, W., Zhang, G., Huang, J., Li, J., & Zhang, L. (2021). Effects of freeze-thaw on soil properties and water erosion. *Soil and Water Research*, 16(4), 205–216. <https://doi.org/10.17221/143/2020-SWR>

Thorwat, V. (n.d.). *Loutolim study area base rock map* [dataset].

T.M., K. K., Pal, S., Chand, P., & Kandpal, A. (2023). Carbon sequestration potential of sustainable agricultural practices to mitigate climate change in Indian agriculture: A meta-analysis. *Sustainable Production and Consumption*, 35, 697–708. <https://doi.org/10.1016/j.spc.2022.12.015>

Tripathi, A., Pandey, V., & Ranjan, M. R. (2021). Climate Change and Its Impact on Soil Properties. In D. K. Choudhary, A. Mishra, & A. Varma (Eds.), *Climate Change and the Microbiome* (Vol. 63, pp. 139–153). Springer International Publishing. https://doi.org/10.1007/978-3-030-76863-8_7

Tsanis, I., & Tapoglou, E. (2019). Winter North Atlantic Oscillation impact on European precipitation and drought under climate change. *Theoretical and Applied Climatology*, 135(1–2), 323–330. <https://doi.org/10.1007/s00704-018-2379-7>

Valdiya, K. S. (2016). *The Making of India*. Springer International Publishing. <https://doi.org/10.1007/978-3-319-25029-8>

Van Hinsbergen, D. J. J., Lippert, P. C., Dupont-Nivet, G., McQuarrie, N., Doubrovine, P. V., Spakman, W., & Torsvik, T. H. (2012). Greater India Basin hypothesis and a two-stage Cenozoic collision between India and Asia. *Proceedings of the National Academy of Sciences*, 109(20), 7659–7664. <https://doi.org/10.1073/pnas.1117262109>

Van Roermund & Drury. (1998). Ultra-high pressure ($P > 6$ GPa) garnet peridotites in Western Norway: Exhumation of mantle rocks from > 185 km depth. *Terra Nova*, 10(6), 295–301. <https://doi.org/10.1046/j.1365-3121.1998.00213.x>

Velbel, M. A., & Losiak, A. I. (2010). Denticles on Chain Silicate Grain Surfaces and Their Utility as Indicators of Weathering Conditions on Earth and Mars. *Journal of Sedimentary Research*, 80(9), 771–780. <https://doi.org/10.2110/jsr.2010.074>

Wendy Guiry in Guiry, M.D. & Guiry, G.M. (n.d.). *Navicula Bory, 1822: AlgaeBase*. AlgaeBase. World-Wide Electronic Publication, National University of Ireland, Galway. Retrieved 8 April 2024, from https://www.algaebase.org/search/genus/detail/?genus_id=43698

Wraa, P. (2020). *Skogbruket i Vestfold og Telemark*. 28.

Isabelle, Schüllli-Maurer., Daniela, Sauer., Karl, Stahr., Ragnhild, Sperstad., Rolf, Sørensen. (2007). Soil formation in marine sediments and beach deposits of southern Norway: investigations of soil chronosequences in the Oslofjord region. *Revista Mexicana De Ciencias Geologicas*,

Błażejczyk, K. and Skrynyk, O. (2019). Principal features of chornohora climate (ukrainian carpathians). *Bulletin of Geography. Physical Geography Series*, 17(1), 61-76. <https://doi.org/10.2478/bgeo-2019-0015>

Carlson, D. (2021). Comment on *essd-2021-53*.. <https://doi.org/10.5194/essd-2021-53-ec1>

Navarro, A., Merino, A., Sánchez, J., García-Ortega, E., Martín, R., & Tapiador, F. (2022). Towards better characterization of global warming impacts in the environment through climate classifications with improved global models. *International Journal of Climatology*, 42(10), 5197-5217. <https://doi.org/10.1002/joc.7527>

Robstad, C., Lodberg-Holm, H., Mayer, M., & Rosell, F. (2021). The impact of bio-logging on body weight change of the eurasian beaver. *Plos One*, 16(12), e0261453. <https://doi.org/10.1371/journal.pone.0261453>

Straumfors, A., Mundra, S., Foss, O., Mollerup, S., & Havard, K. (2021). The airborne mycobiome and associations with mycotoxins and inflammatory markers in the norwegian grain industry. *Scientific Reports*, 11(1). <https://doi.org/10.1038/s41598-021-88252-1>

Wang, T., Zhou, D., & Shen, X. (2021). Spatial-temporal variations of köppen climate types in china. *Terrestrial Atmospheric and Oceanic Sciences*, 32(4), 483. <https://doi.org/10.3319/tao.2021.10.18.01>


Wang, T., Zhou, D., & Shen, X. (2021). Spatial-temporal variations of köppen climate types in china. *Terrestrial Atmospheric and Oceanic Sciences*, 32(4), 483. <https://doi.org/10.3319/tao.2021.10.18.01>

Wu, B., Lang, X., & Jiang, D. (2021). Köppen climate zones in china over the last 21,000 years. *Journal of Geophysical Research Atmospheres*, 126(6). <https://doi.org/10.1029/2020jd034310>


Yılmaz, E. and Çiçek, İ. (2018). Detailed köppen-geiger climate regions of turkey<p>türkiye'nin detaylandırılmış köppen-geiger iklim bölgeleri. *Journal of Human Sciences*, 15(1), 225. <https://doi.org/10.14687/jhs.v15i1.5040>

List of tables and charts

Table 5. Sampling sites



Site number	Coordinates	Comments	Picture
NS-1	Latitude 59° 24' 30.06" N Longitude 9° 10' 23.592" E	Sampling location is next to a road path	


<p>NS-2</p>	<p>Latitude 59° 23' 49.416" N</p> <p>Longitude 9° 10' 55.92" E</p>	<p>This sample is the control sample</p>	
		<p>In red it is highlighted the specific spot where the sample was collected</p>	


EV-1	Latitude 59° 23' 34.704" N Longitude 9° 09' 54" E	This sample site is located in an oxbow lake, surrounded by wetland typical vegetation such as reeds, the sediments are located in the organic origin and are rich in sand and silt. In red it is highlighted the specific spot where the sample was collected	
------	--	--	--

In the left shows the moment the sampling was collected



EV-2A	Latitude 59° 24' 14.868" N Longitude 9° 10' 05.45" E	This sample consist of river sediments, taken at the river bed in shallow waters, right next to the shore.	
		For sampling in these conditions, once we are inside the water, we wait until the water calms so there is no mud or other sediments contaminating our sample. The sample tube was	

		<p>introduced into the river sediment all the way through, after that the tube is carefully pulled back to allow the air in the tube to escape and then the tap was put on top when still inside the water.</p>	
EV-2B	<p>Latitude 59° 24' 15.732" N</p> <p>Longitude 9° 10' 5.664" E</p>	<p>Sample taken in wetlands with aquatic vegetation such as reeds</p>	

			
EV-3	<p>Latitude 59° 24' 14.4" N</p> <p>Longitude 9° 09' 48.816" E</p>	<p>This sample site is in an ancient preserved fluvial flood terrace formation with dense grass and around pine trees.</p>	

The soil from this sample presents more air, more roots, a darker brown colour, and less humidity content, since it not embedded in water.




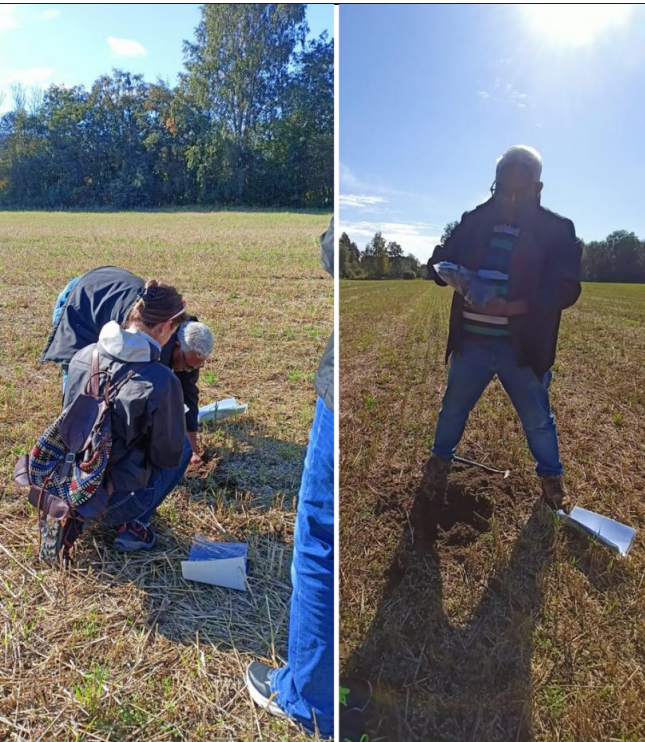
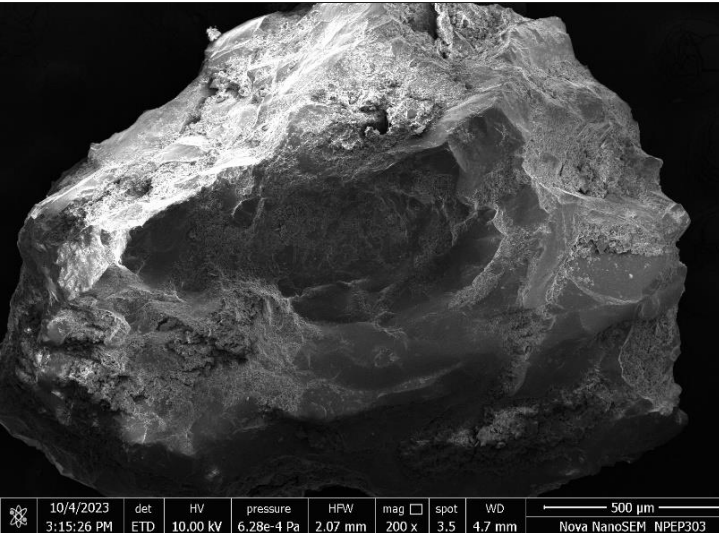
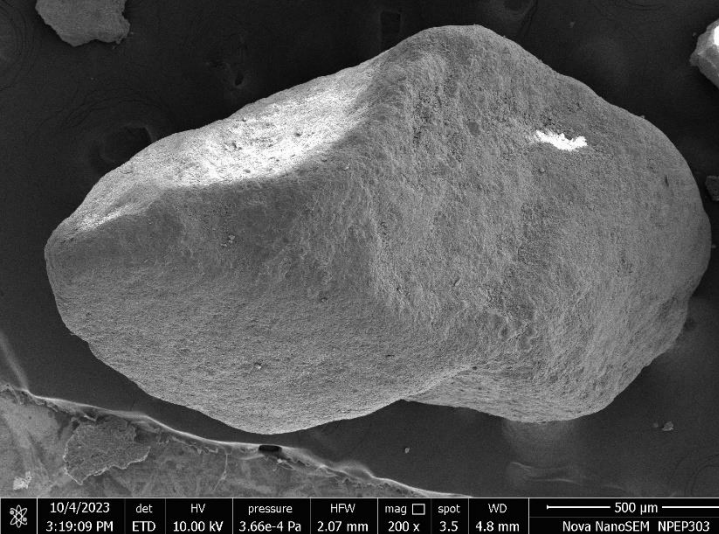
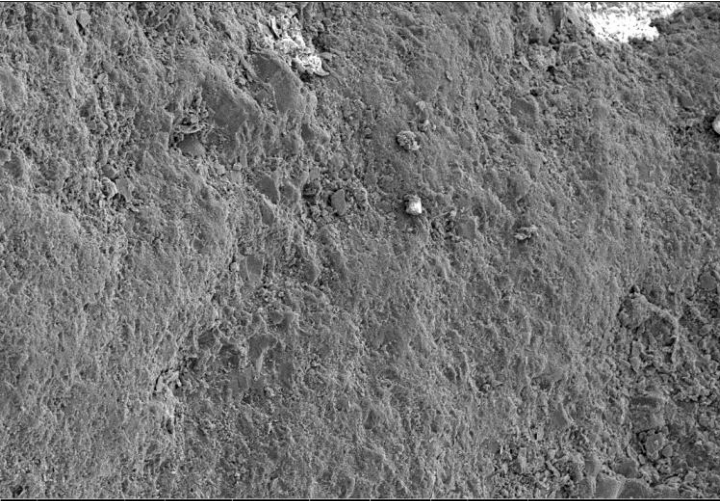
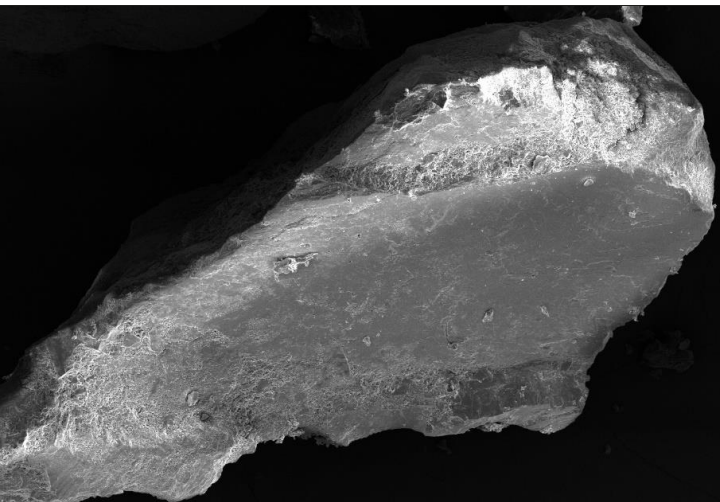
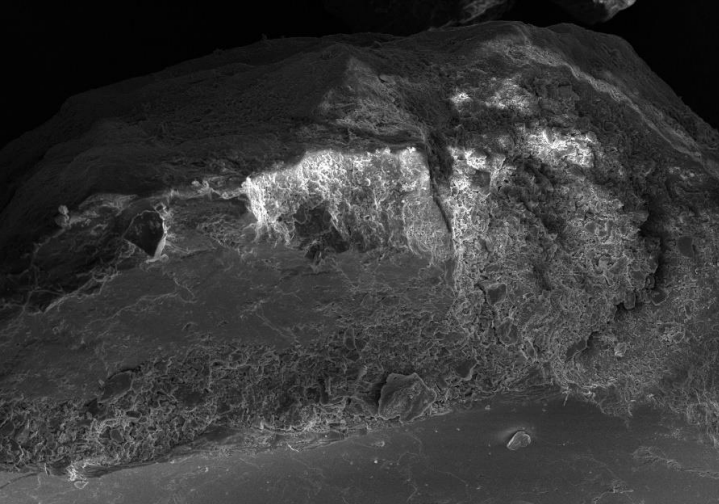
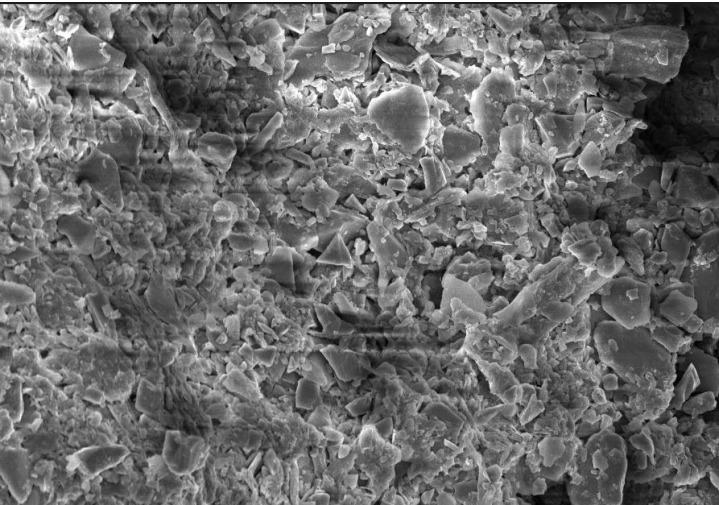
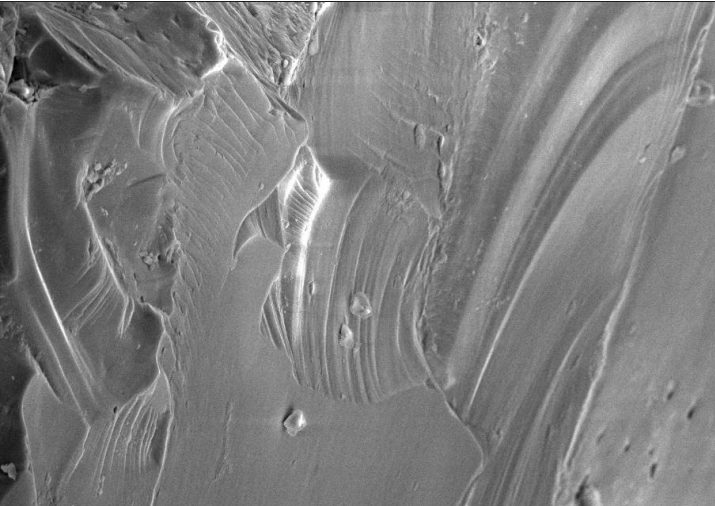
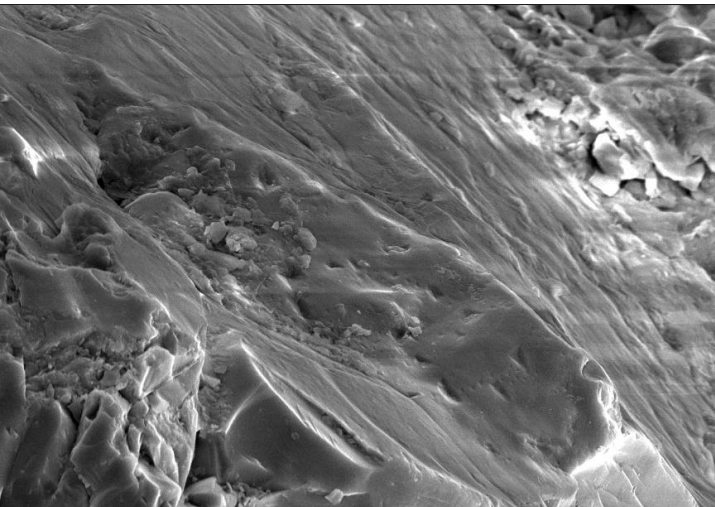
EV-4	<p>Latitude 59° 24' 21.348" N</p> <p>Longitude 9° 09' 56.808" E</p>	<p>This sample was taken in a centric location inside a wheat crop field.</p>	
		<p>The methodology used to get representative sample is called Coning and quartering sampling.</p>	

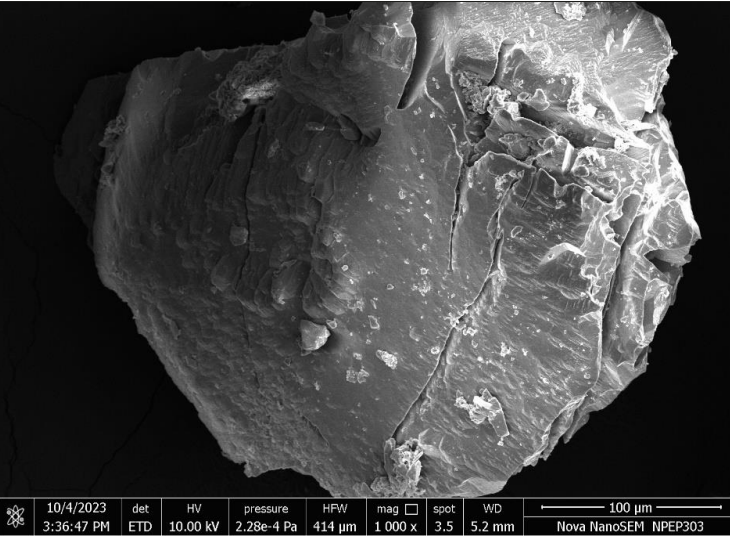
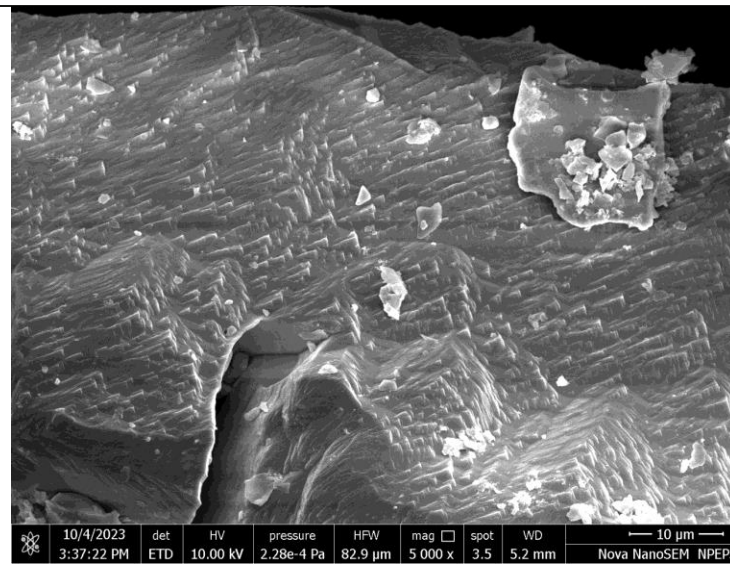
Table 6. Scanning electron microscope descriptions of Norwegian samples.

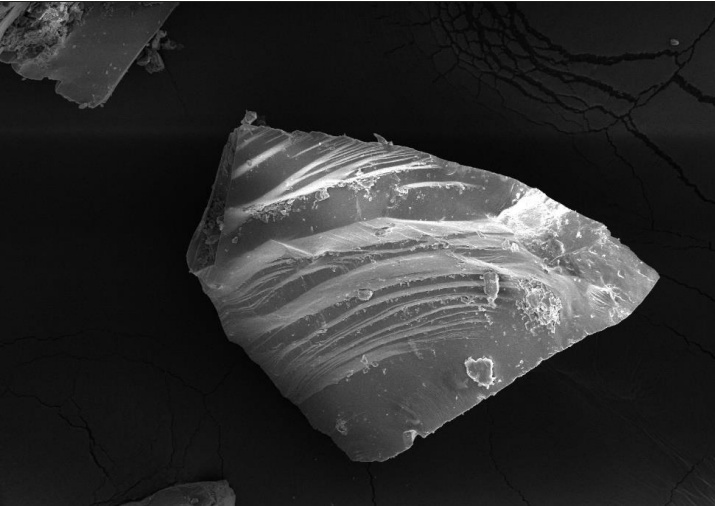
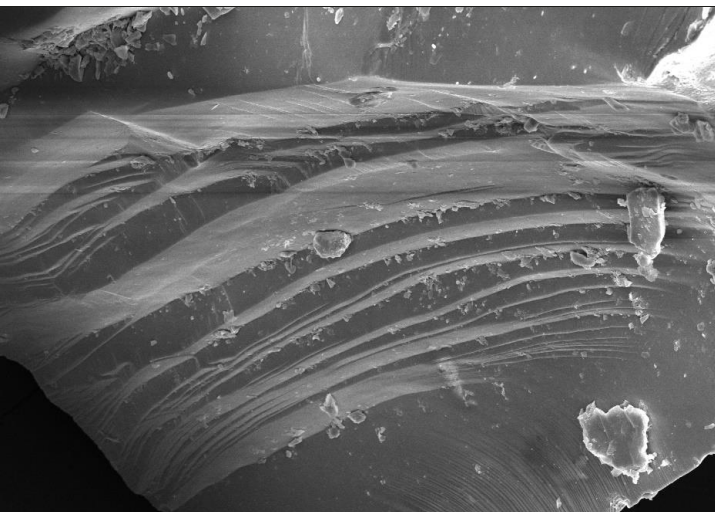
NS-2			
Serial no	Grain no	Description	Inference
1	G1_1_001	Sub-angular grain with subconchoidal fractures and adhering clay particles around its surface	 <p>10/4/2023 3:15:26 PM det ETD HV 10.00 kV pressure 6.28e-4 Pa HPW 2.07 mm mag 200 x spot 3.5 WD 4.7 mm 500 μm Nova NanoSEM NPEP303</p>
2	G2_1_003	Sub-rounded fluvial grain with rounded edges	 <p>10/4/2023 3:19:09 PM det ETD HV 10.00 kV pressure 3.66e-4 Pa HPW 2.07 mm mag 200 x spot 3.5 WD 4.8 mm 500 μm Nova NanoSEM NPEP303</p>

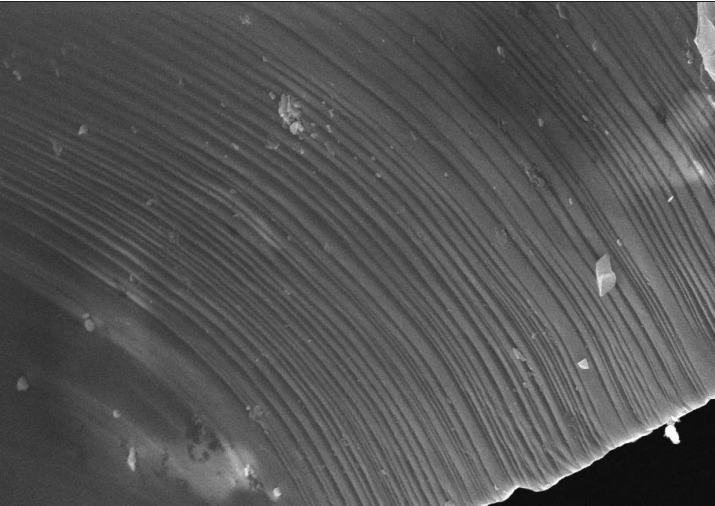
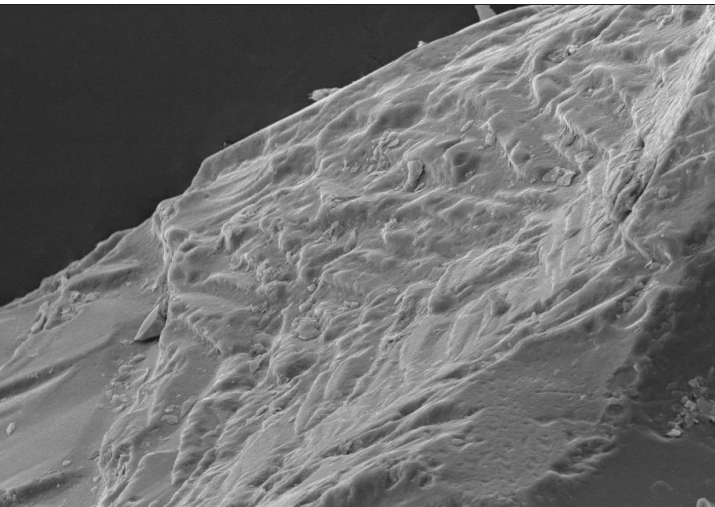
3	G2_1_004	<p><i>Detail of the chemical weathering probably from acid dissolution leaving irregular depressions around the surface of Grain 2</i></p>	 <p>10/4/2023 3:19:50 PM det ETD HV 10.00 kV pressure 3.42e-4 Pa HFW 414 μm mag 1 000 x spot 3.5 WD 4.7 mm 100 μm Nova NanoSEM NPEP303</p>
4	G3_1_005	<p><i>Very angular grain</i></p>	 <p>10/4/2023 3:20:57 PM det ETD HV 10.00 kV pressure 3.20e-4 Pa HFW 1.04 mm mag 400 x spot 3.5 WD 5.3 mm 200 μm Nova NanoSEM NPEP303</p>

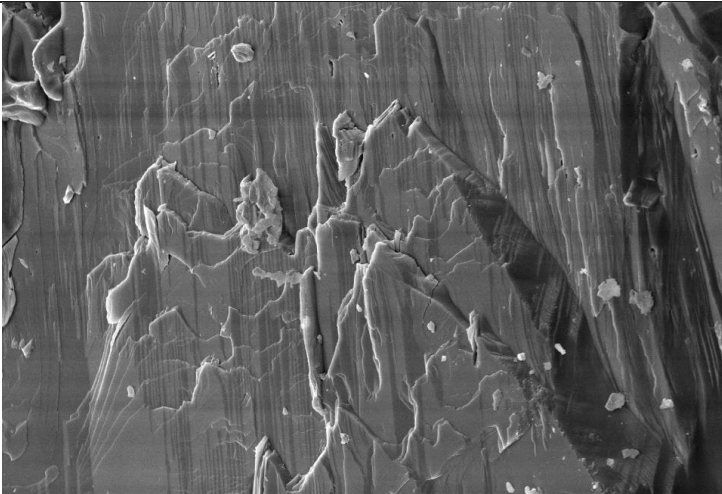
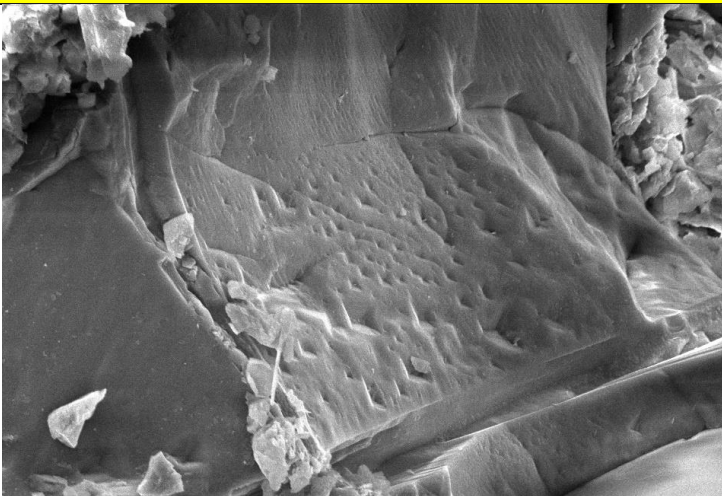
5	G3_1_006	<i>Detail of weathering</i>	 <table border="1" data-bbox="678 672 1401 712"> <tr> <td>10/4/2023</td> <td>det</td> <td>HV</td> <td>pressure</td> <td>HFW</td> <td>mag</td> <td>spot</td> <td>WD</td> <td>100 µm</td> </tr> <tr> <td>3:21:40 PM</td> <td>ETD</td> <td>10.00 kV</td> <td>2.99e-4 Pa</td> <td>414 µm</td> <td>1 000 x</td> <td>3.5</td> <td>5.3 mm</td> <td>Nova NanoSEM NPEP303</td> </tr> </table>	10/4/2023	det	HV	pressure	HFW	mag	spot	WD	100 µm	3:21:40 PM	ETD	10.00 kV	2.99e-4 Pa	414 µm	1 000 x	3.5	5.3 mm	Nova NanoSEM NPEP303
10/4/2023	det	HV	pressure	HFW	mag	spot	WD	100 µm													
3:21:40 PM	ETD	10.00 kV	2.99e-4 Pa	414 µm	1 000 x	3.5	5.3 mm	Nova NanoSEM NPEP303													
6	G3_1_007	<i>Solution</i>	 <table border="1" data-bbox="678 1281 1401 1321"> <tr> <td>10/4/2023</td> <td>det</td> <td>HV</td> <td>pressure</td> <td>HFW</td> <td>mag</td> <td>spot</td> <td>WD</td> <td>10 µm</td> </tr> <tr> <td>3:22:23 PM</td> <td>ETD</td> <td>10.00 kV</td> <td>2.99e-4 Pa</td> <td>82.9 µm</td> <td>5 000 x</td> <td>3.5</td> <td>5.3 mm</td> <td>Nova NanoSEM NPEP303</td> </tr> </table>	10/4/2023	det	HV	pressure	HFW	mag	spot	WD	10 µm	3:22:23 PM	ETD	10.00 kV	2.99e-4 Pa	82.9 µm	5 000 x	3.5	5.3 mm	Nova NanoSEM NPEP303
10/4/2023	det	HV	pressure	HFW	mag	spot	WD	10 µm													
3:22:23 PM	ETD	10.00 kV	2.99e-4 Pa	82.9 µm	5 000 x	3.5	5.3 mm	Nova NanoSEM NPEP303													

7	G5_1_015	<i>Conchoidal breakage pattern with arc-shaped semirapallel shapes</i>	 <table border="1" data-bbox="678 672 1396 716"> <tr> <td>10/4/2023</td> <td>det</td> <td>HV</td> <td>pressure</td> <td>HFW</td> <td>mag</td> <td>spot</td> <td>WD</td> <td>10 µm</td> </tr> <tr> <td>3:28:14 PM</td> <td>ETD</td> <td>10.00 kV</td> <td>2.61e-4 Pa</td> <td>82.9 µm</td> <td>5 000 x</td> <td>3.5</td> <td>5.0 mm</td> <td>Nova NanoSEM NPEP30</td> </tr> </table>	10/4/2023	det	HV	pressure	HFW	mag	spot	WD	10 µm	3:28:14 PM	ETD	10.00 kV	2.61e-4 Pa	82.9 µm	5 000 x	3.5	5.0 mm	Nova NanoSEM NPEP30
10/4/2023	det	HV	pressure	HFW	mag	spot	WD	10 µm													
3:28:14 PM	ETD	10.00 kV	2.61e-4 Pa	82.9 µm	5 000 x	3.5	5.0 mm	Nova NanoSEM NPEP30													
8	G5_1_016	<i>Striations with V-shaped indentations</i>	 <table border="1" data-bbox="678 1288 1396 1332"> <tr> <td>10/4/2023</td> <td>det</td> <td>HV</td> <td>pressure</td> <td>HFW</td> <td>mag</td> <td>spot</td> <td>WD</td> <td>5 µm</td> </tr> <tr> <td>3:28:58 PM</td> <td>ETD</td> <td>10.00 kV</td> <td>2.44e-4 Pa</td> <td>41.4 µm</td> <td>10 000 x</td> <td>3.5</td> <td>5.0 mm</td> <td>Nova NanoSEM NPEP30</td> </tr> </table>	10/4/2023	det	HV	pressure	HFW	mag	spot	WD	5 µm	3:28:58 PM	ETD	10.00 kV	2.44e-4 Pa	41.4 µm	10 000 x	3.5	5.0 mm	Nova NanoSEM NPEP30
10/4/2023	det	HV	pressure	HFW	mag	spot	WD	5 µm													
3:28:58 PM	ETD	10.00 kV	2.44e-4 Pa	41.4 µm	10 000 x	3.5	5.0 mm	Nova NanoSEM NPEP30													

9	G8_1_023	<i>Semiparallel groove marks</i>	 <table border="1" data-bbox="667 660 1401 705"> <tr> <td>10/4/2023 3:36:47 PM</td> <td>det ETD</td> <td>HV 10.00 kV</td> <td>pressure 2.28e-4 Pa</td> <td>HFW 414 µm</td> <td>mag 1 000 x</td> <td>spot 3.5</td> <td>WD 5.2 mm</td> <td>100 µm Nova NanoSEM NPEP303</td> </tr> </table>	10/4/2023 3:36:47 PM	det ETD	HV 10.00 kV	pressure 2.28e-4 Pa	HFW 414 µm	mag 1 000 x	spot 3.5	WD 5.2 mm	100 µm Nova NanoSEM NPEP303
10/4/2023 3:36:47 PM	det ETD	HV 10.00 kV	pressure 2.28e-4 Pa	HFW 414 µm	mag 1 000 x	spot 3.5	WD 5.2 mm	100 µm Nova NanoSEM NPEP303				
10	G8_1_024	<i>Hacksaw terminations, as indicators of weathering conditions</i>	 <table border="1" data-bbox="667 1332 1401 1377"> <tr> <td>10/4/2023 3:37:22 PM</td> <td>det ETD</td> <td>HV 10.00 kV</td> <td>pressure 2.28e-4 Pa</td> <td>HFW 82.9 µm</td> <td>mag 5 000 x</td> <td>spot 3.5</td> <td>WD 5.2 mm</td> <td>10 µm Nova NanoSEM NPEP303</td> </tr> </table>	10/4/2023 3:37:22 PM	det ETD	HV 10.00 kV	pressure 2.28e-4 Pa	HFW 82.9 µm	mag 5 000 x	spot 3.5	WD 5.2 mm	10 µm Nova NanoSEM NPEP303
10/4/2023 3:37:22 PM	det ETD	HV 10.00 kV	pressure 2.28e-4 Pa	HFW 82.9 µm	mag 5 000 x	spot 3.5	WD 5.2 mm	10 µm Nova NanoSEM NPEP303				

11	G11_2_01	Arc-shaped semiparallel shapes	 <table border="1" data-bbox="678 672 1396 716"> <tr> <td>10/4/2023</td> <td>det</td> <td>HV</td> <td>pressure</td> <td>HPW</td> <td>mag</td> <td>spot</td> <td>WD</td> <td>100 μm</td> </tr> <tr> <td>3:46:44 PM</td> <td>ETD</td> <td>10.00 kV</td> <td>7.69e-4 Pa</td> <td>414 μm</td> <td>1 000 x</td> <td>3.5</td> <td>5.3 mm</td> <td>Nova NanoSEM NPEP303</td> </tr> </table>	10/4/2023	det	HV	pressure	HPW	mag	spot	WD	100 μ m	3:46:44 PM	ETD	10.00 kV	7.69e-4 Pa	414 μ m	1 000 x	3.5	5.3 mm	Nova NanoSEM NPEP303
10/4/2023	det	HV	pressure	HPW	mag	spot	WD	100 μ m													
3:46:44 PM	ETD	10.00 kV	7.69e-4 Pa	414 μ m	1 000 x	3.5	5.3 mm	Nova NanoSEM NPEP303													
12	G11_2_03	Arc-shaped semiparallel shapes	 <table border="1" data-bbox="678 1288 1396 1332"> <tr> <td>10/4/2023</td> <td>det</td> <td>HV</td> <td>pressure</td> <td>HPW</td> <td>mag</td> <td>spot</td> <td>WD</td> <td>40 μm</td> </tr> <tr> <td>3:48:01 PM</td> <td>ETD</td> <td>10.00 kV</td> <td>5.13e-4 Pa</td> <td>166 μm</td> <td>2 500 x</td> <td>3.5</td> <td>5.3 mm</td> <td>Nova NanoSEM NPEP303</td> </tr> </table>	10/4/2023	det	HV	pressure	HPW	mag	spot	WD	40 μ m	3:48:01 PM	ETD	10.00 kV	5.13e-4 Pa	166 μ m	2 500 x	3.5	5.3 mm	Nova NanoSEM NPEP303
10/4/2023	det	HV	pressure	HPW	mag	spot	WD	40 μ m													
3:48:01 PM	ETD	10.00 kV	5.13e-4 Pa	166 μ m	2 500 x	3.5	5.3 mm	Nova NanoSEM NPEP303													

13	G11_2_05	<i>Deformed cleavage</i>	 <p>10/4/2023 3:49:05 PM det ETD HV 10.00 kV pressure 4.48e-4 Pa HPW 41.4 μm mag 10 000 x spot 3.5 WD 5.3 mm 5 μm Nova NanoSEM NPEP30</p>
14	G15_2_01 7	<i>V-shaped indentations</i>	 <p>10/4/2023 3:58:53 PM det ETD HV 10.00 kV pressure 2.61e-4 Pa HPW 82.9 μm mag 5 000 x spot 3.5 WD 5.3 mm 10 μm Nova NanoSEM NPEP30</p>

15	G16_2_02 0	<i>Parallel striations</i>	 <p>10/4/2023 4:01:42 PM det ETD HV 10.00 kV pressure 2.44e-4 Pa HRW 82.9 μm mag 5 000 x spot 3.5 WD 5.1 mm 10 μm Nova NanoSEM NPEP303</p>
NS-1			
16	G23_3_00 3	<i>V-shaped indentations</i>	 <p>10/4/2023 4:11:07 PM det ETD HV 10.00 kV pressure 5.37e-4 Pa HRW 41.4 μm mag 10 000 x spot 3.5 WD 5.2 mm 5 μm Nova NanoSEM NPEP303</p>

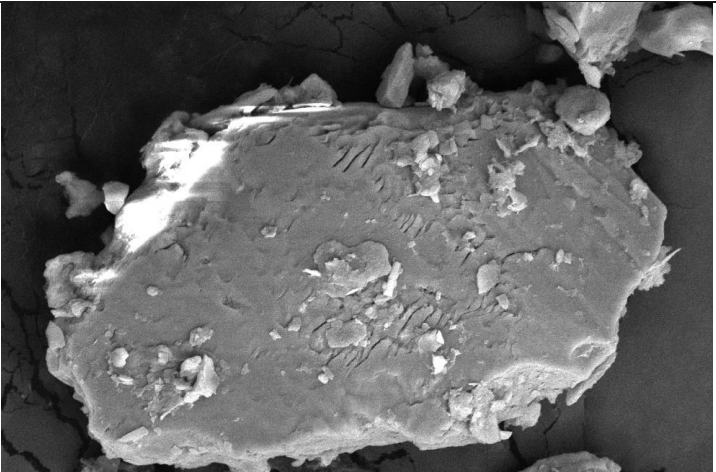
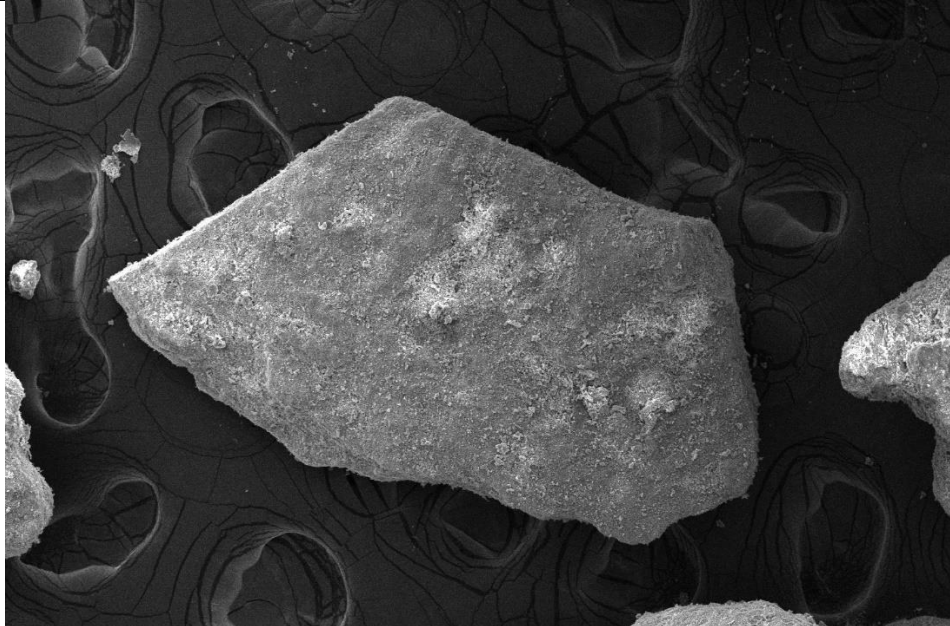



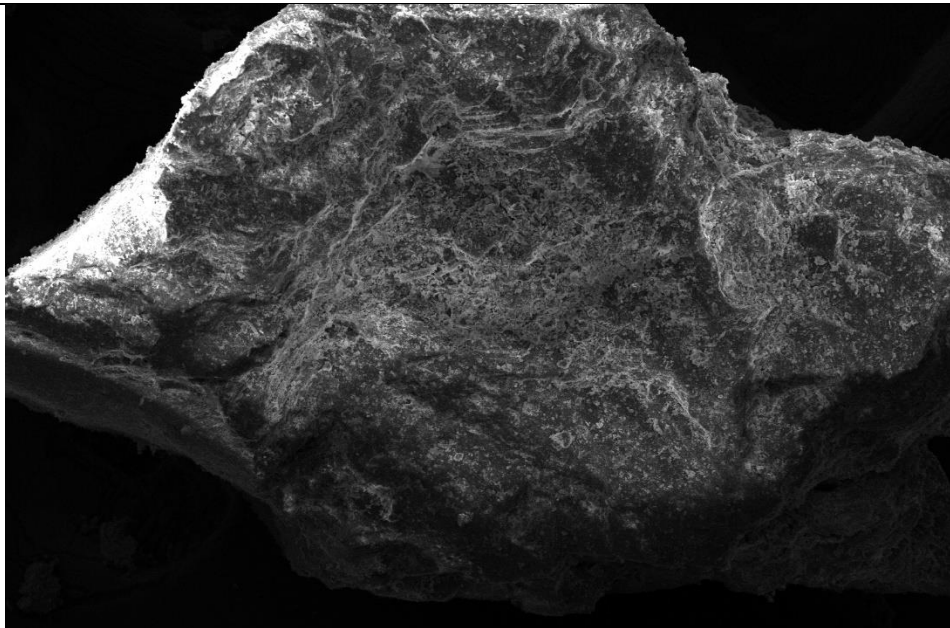



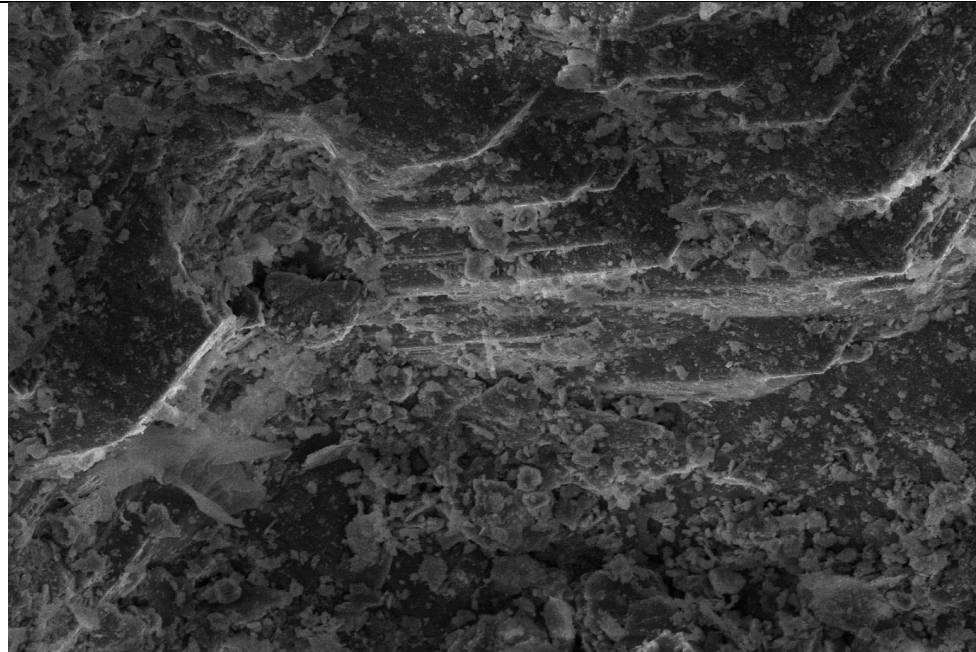
17	G39_4_01 2	Groove marks	 <p data-bbox="678 638 1396 683"> <small> 10/4/2023 4:32:24 PM det ETD HV 10.00 kV pressure 3.27e-4 Pa HPW 41.4 μm mag 10 000 x spot 3.5 WD 5.4 mm Nova NanoSEM NPEP303 </small> </p> <p data-bbox="1244 638 1340 660">← 5 μm →</p>
----	---------------	-----------------	---

Table 7. Scanning electron microscope descriptions of Goan samples.

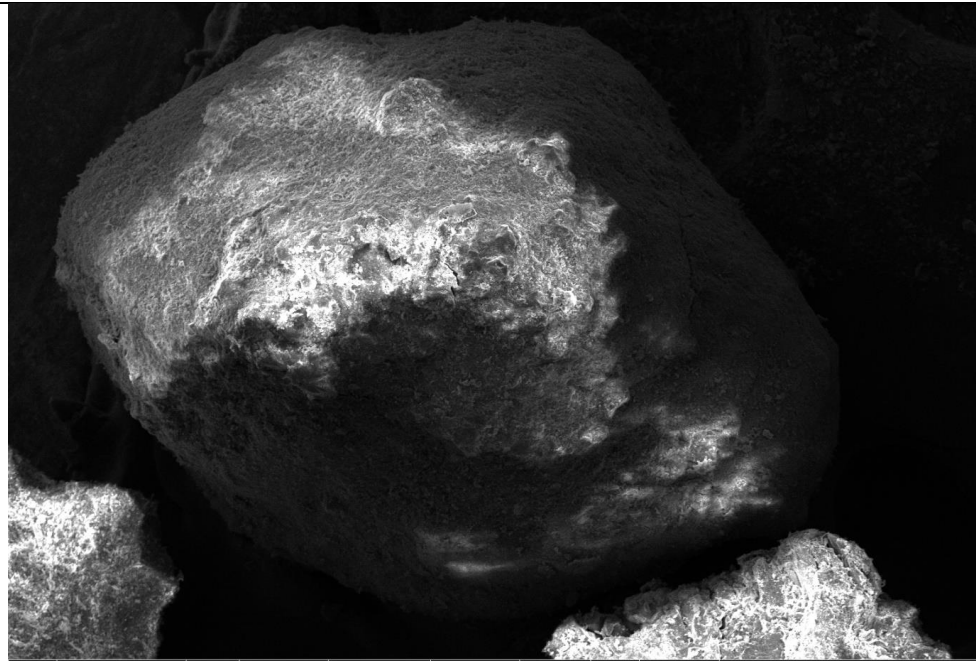
<p>GO_001, Highly porous, angular to subangular laterite that was redeposited. Grain size from silt to fine sand.</p>	 <table border="1" data-bbox="427 840 1380 896"> <tr> <td></td> <td>3/15/2024 11:39:18 AM</td> <td>det ETD</td> <td>HV 15.00 kV</td> <td>pressure 1.15e-3 Pa</td> <td>HFW 1.66 mm</td> <td>mag <input type="checkbox"/> 250 x</td> <td>spot 3.0</td> <td>WD 5.2 mm</td> <td>300 μm Nova NanoSEM NPEP303</td> </tr> </table>		3/15/2024 11:39:18 AM	det ETD	HV 15.00 kV	pressure 1.15e-3 Pa	HFW 1.66 mm	mag <input type="checkbox"/> 250 x	spot 3.0	WD 5.2 mm	300 μm Nova NanoSEM NPEP303
	3/15/2024 11:39:18 AM	det ETD	HV 15.00 kV	pressure 1.15e-3 Pa	HFW 1.66 mm	mag <input type="checkbox"/> 250 x	spot 3.0	WD 5.2 mm	300 μm Nova NanoSEM NPEP303		
<p>GO_004, Subangular laterite.</p>	 <table border="1" data-bbox="427 1545 1380 1601"> <tr> <td></td> <td>3/15/2024 11:43:51 AM</td> <td>det ETD</td> <td>HV 15.00 kV</td> <td>pressure 4.19e-4 Pa</td> <td>HFW 829 μm</td> <td>mag <input type="checkbox"/> 500 x</td> <td>spot 3.0</td> <td>WD 5.1 mm</td> <td>100 μm Nova NanoSEM NPEP303</td> </tr> </table>		3/15/2024 11:43:51 AM	det ETD	HV 15.00 kV	pressure 4.19e-4 Pa	HFW 829 μm	mag <input type="checkbox"/> 500 x	spot 3.0	WD 5.1 mm	100 μm Nova NanoSEM NPEP303
	3/15/2024 11:43:51 AM	det ETD	HV 15.00 kV	pressure 4.19e-4 Pa	HFW 829 μm	mag <input type="checkbox"/> 500 x	spot 3.0	WD 5.1 mm	100 μm Nova NanoSEM NPEP303		

GO_005,
Step-like
cleavage of
highly
weathered
quartz.



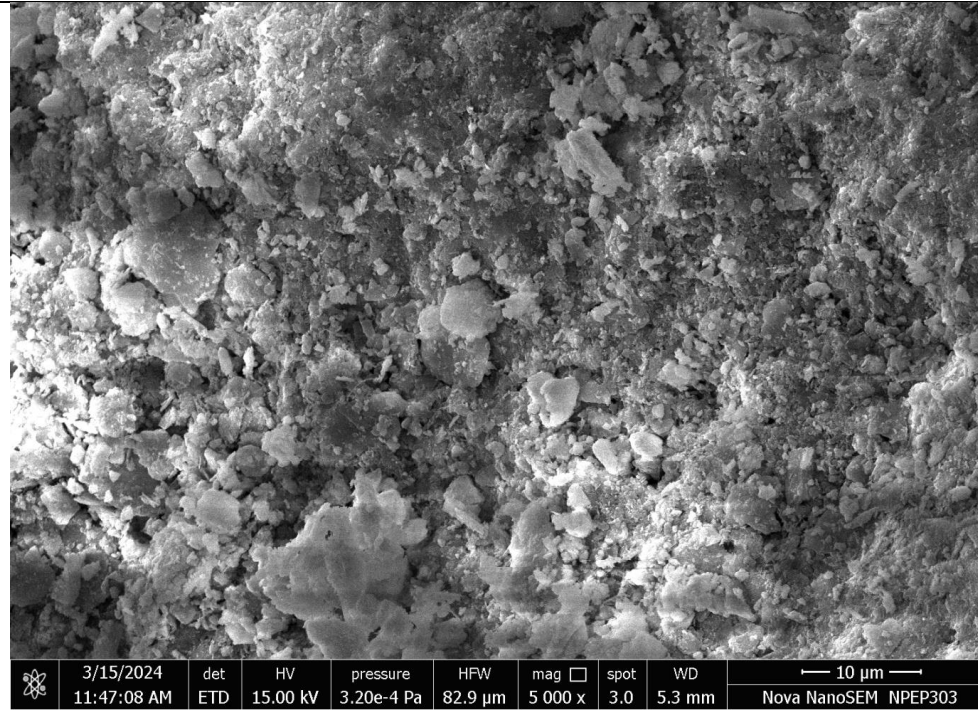
	3/15/2024 11:44:27 AM	det ETD	HV 15.00 kV	pressure 3.92e-4 Pa	HPW 166 µm	mag <input type="checkbox"/> 2 500 x	spot 3.0	WD 5.0 mm	← 30 µm → Nova NanoSEM NPEP303
---	--------------------------	------------	----------------	------------------------	---------------	---	-------------	--------------	-----------------------------------

GO_006, Sub-
rounded
Gibbsite with
hametite
coating.



	3/15/2024 11:45:10 AM	det ETD	HV 15.00 kV	pressure 3.66e-4 Pa	HPW 1.04 mm	mag <input type="checkbox"/> 400 x	spot 3.0	WD 5.0 mm	← 200 µm → Nova NanoSEM NPEP303
---	--------------------------	------------	----------------	------------------------	----------------	---------------------------------------	-------------	--------------	------------------------------------

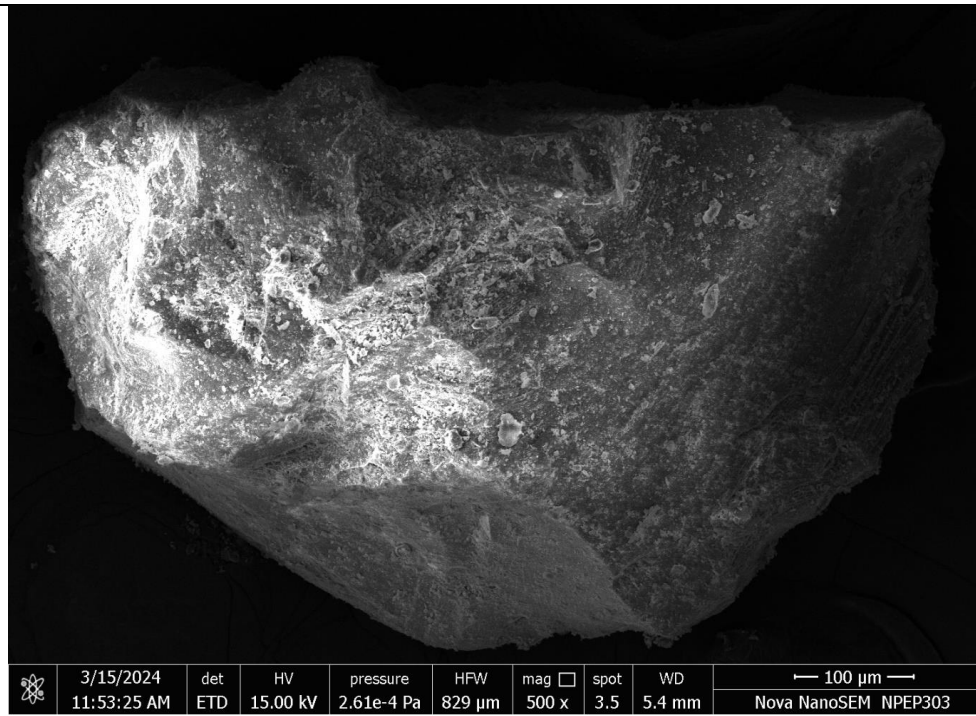
GO_009,
Gibbsite
crystals
deposited,
showing a
flaky aspect.



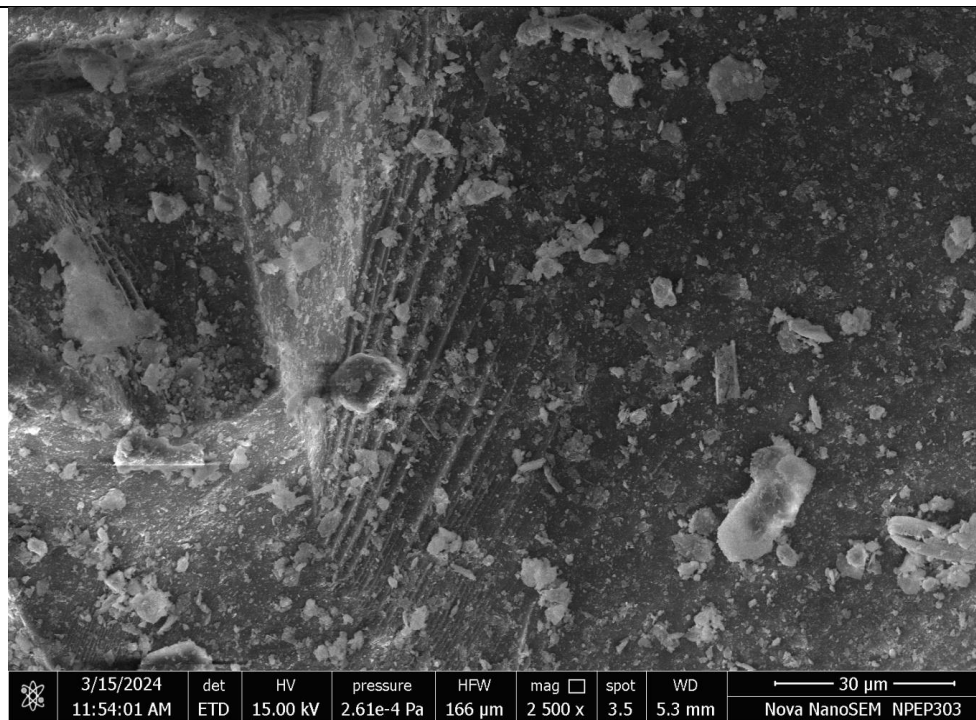
GO_011,
Fiber
minerals.
Gibbsite with
flaky and
platy aspect.



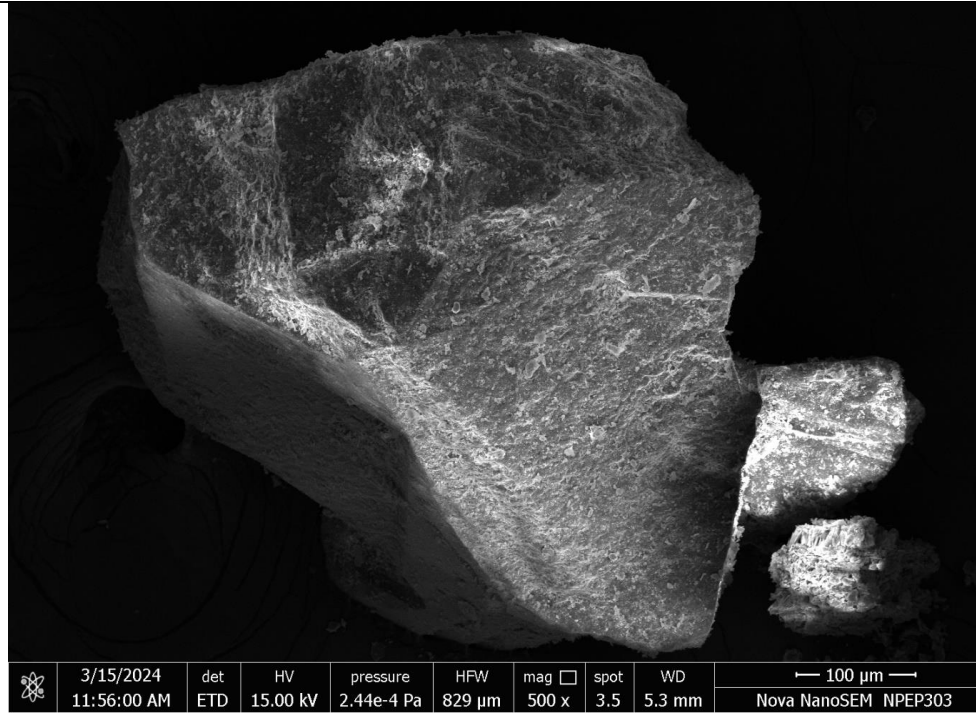
GO_014,
Subconcoidal
fracture on
the right
corner.



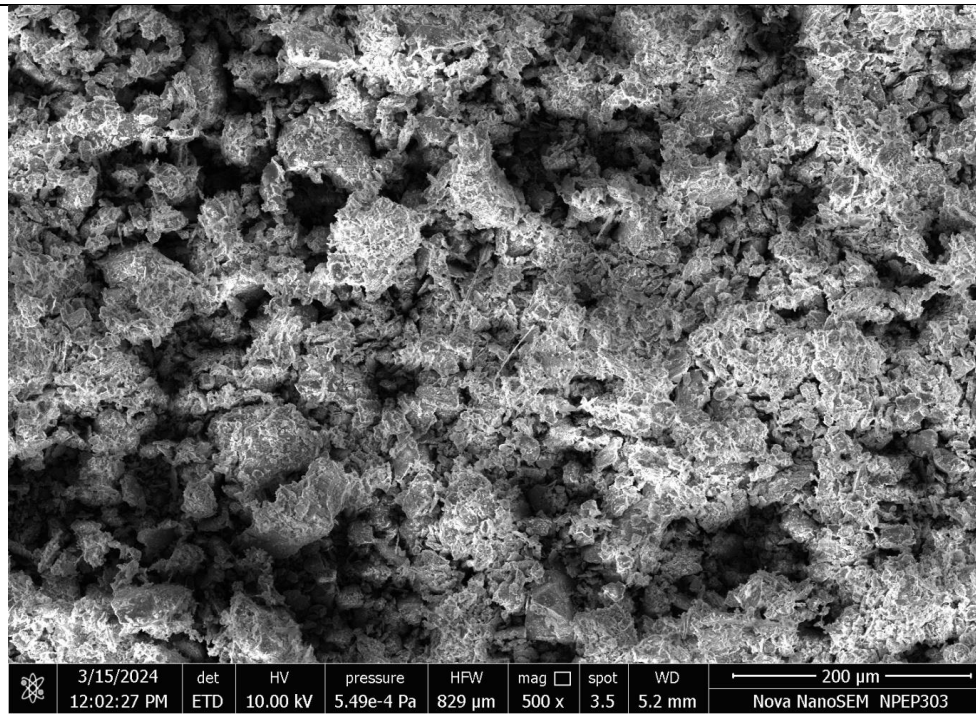
GO_015,
Cleavage
plane with
gibbsite
precipitation



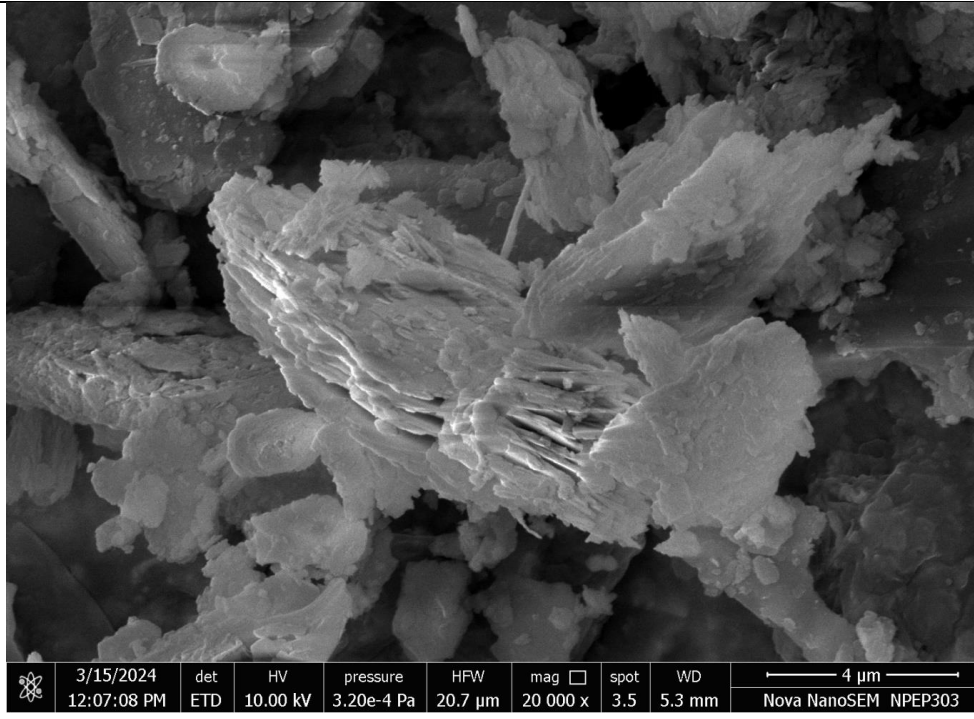
GO_017,
Angular grain
with
precipitation
on the
surface.
Darker areas
show location
of the
fractures.



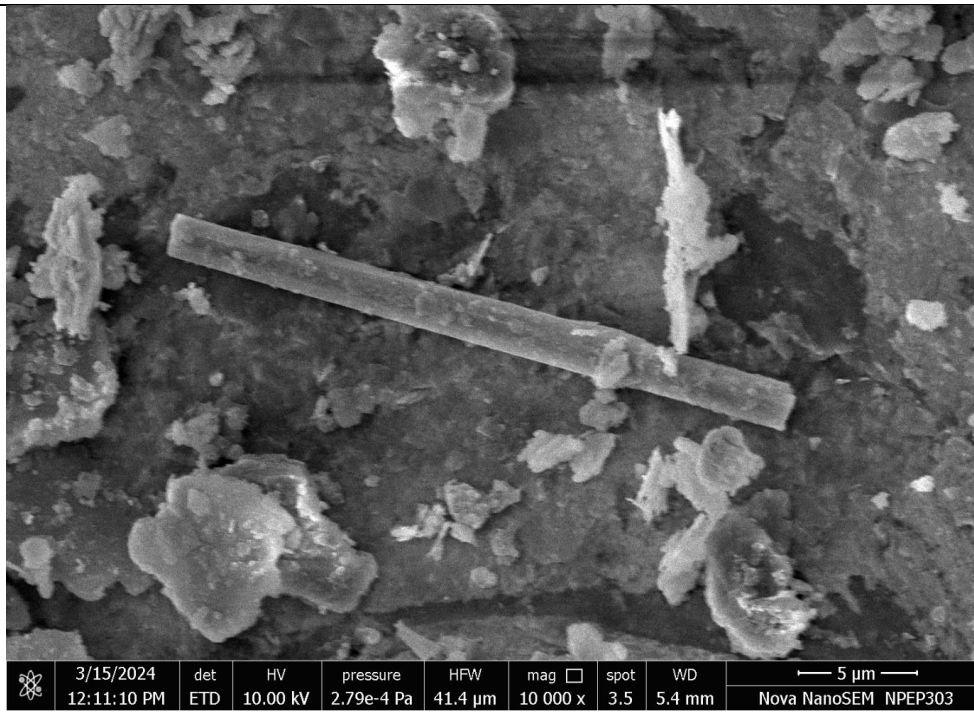
GO-
POWDER_001
, Highly
porous clay.



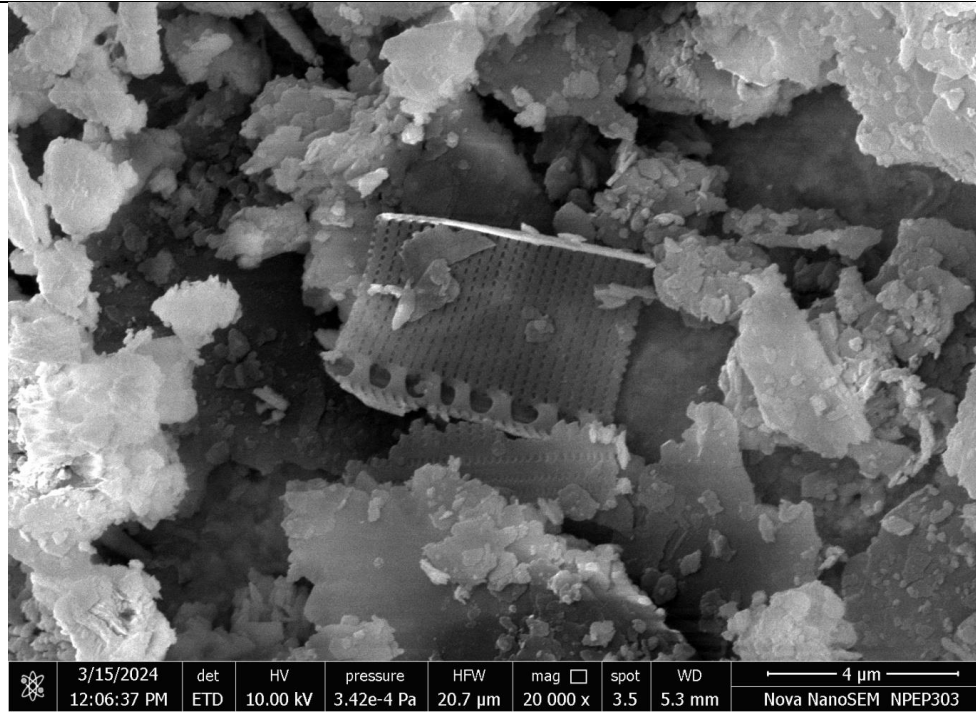
GO-
POWDER_007
, Gibbsite.



GO-
POWDER_008
, unknown
fibrous
mineral.



GO-
POWDER_006
, Diatom
frustule.



GO-
POWDER_012
, Diatom
frustule.

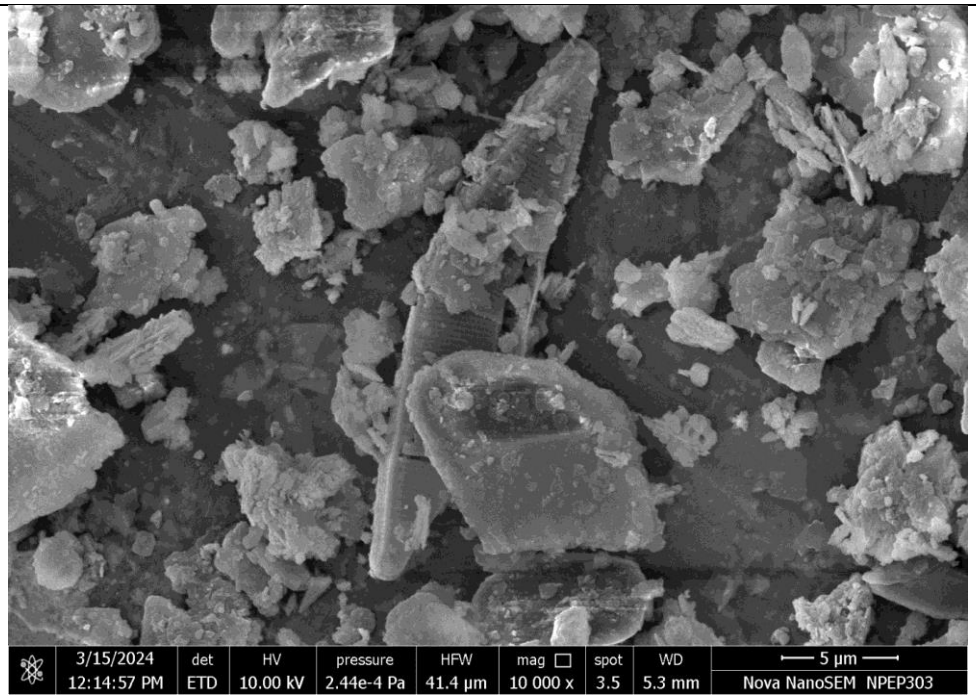
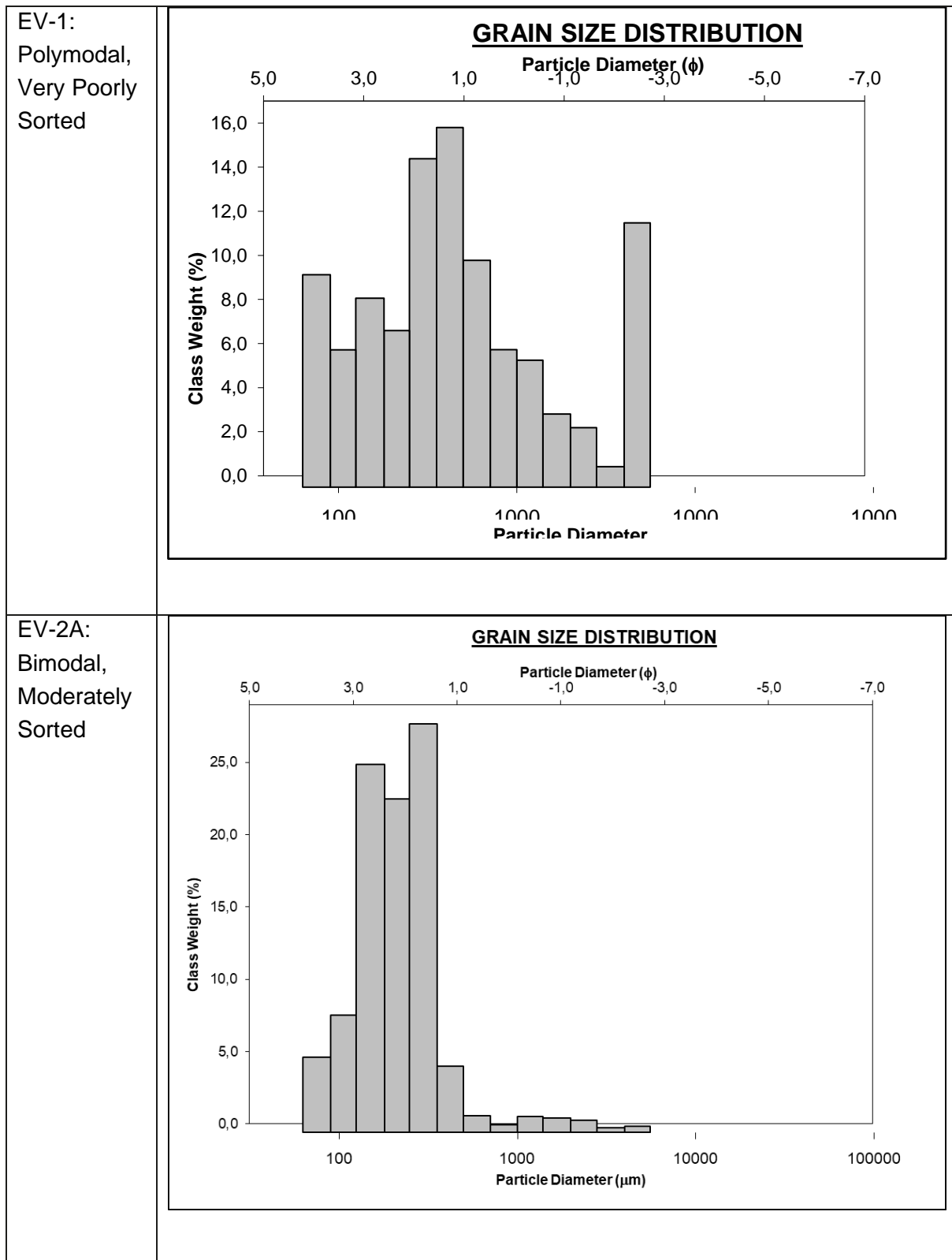
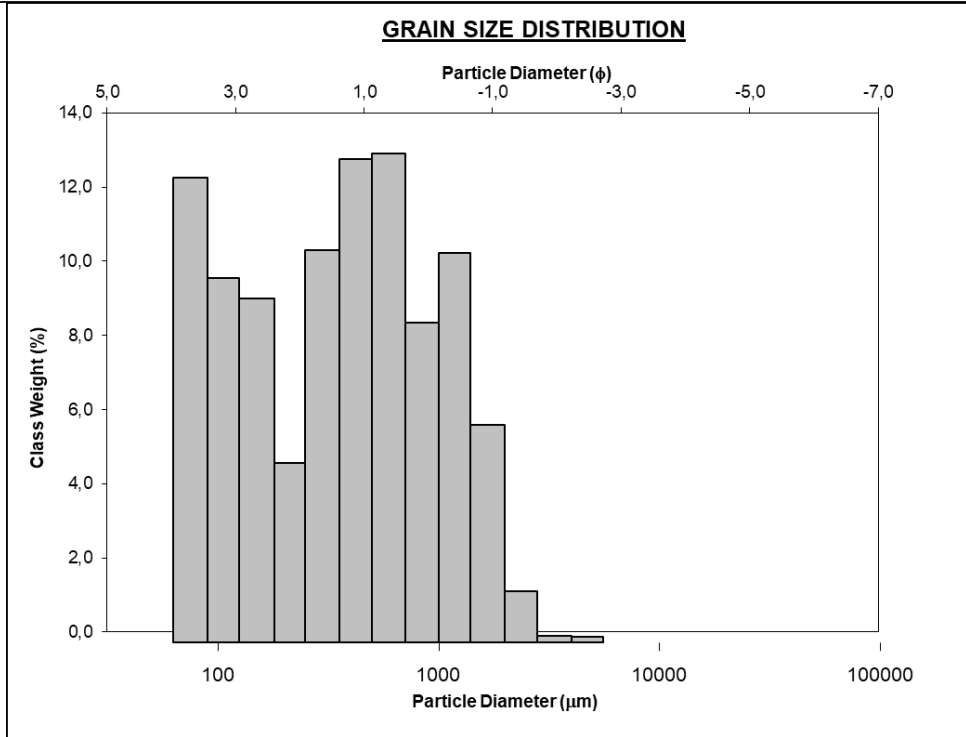


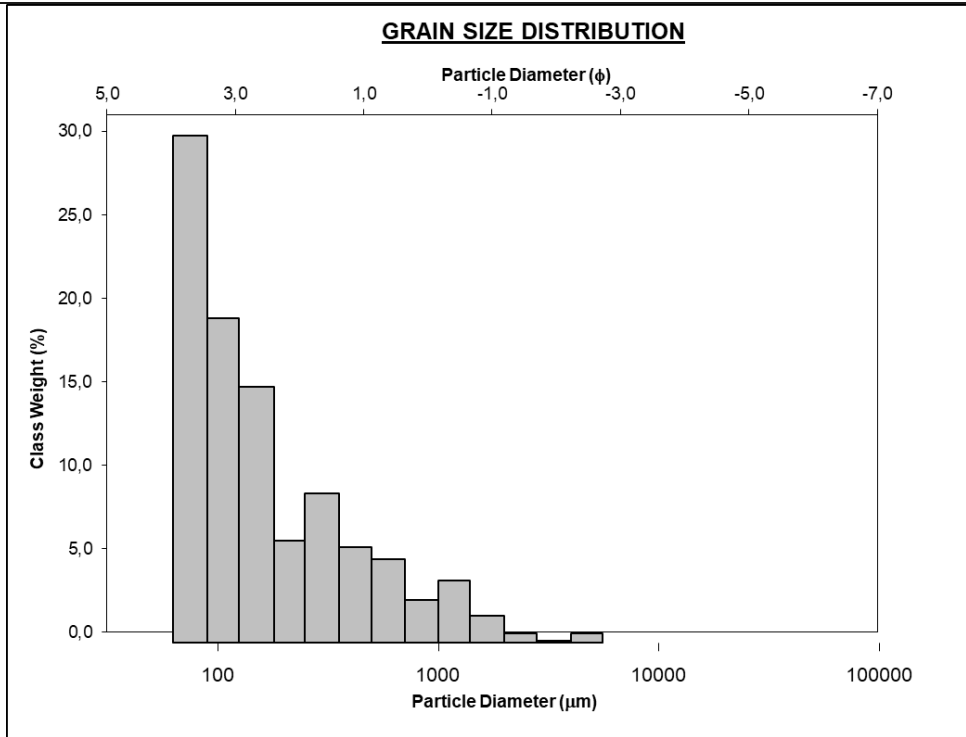
Table 8. Grain size distribution of Norwegian sample sites.



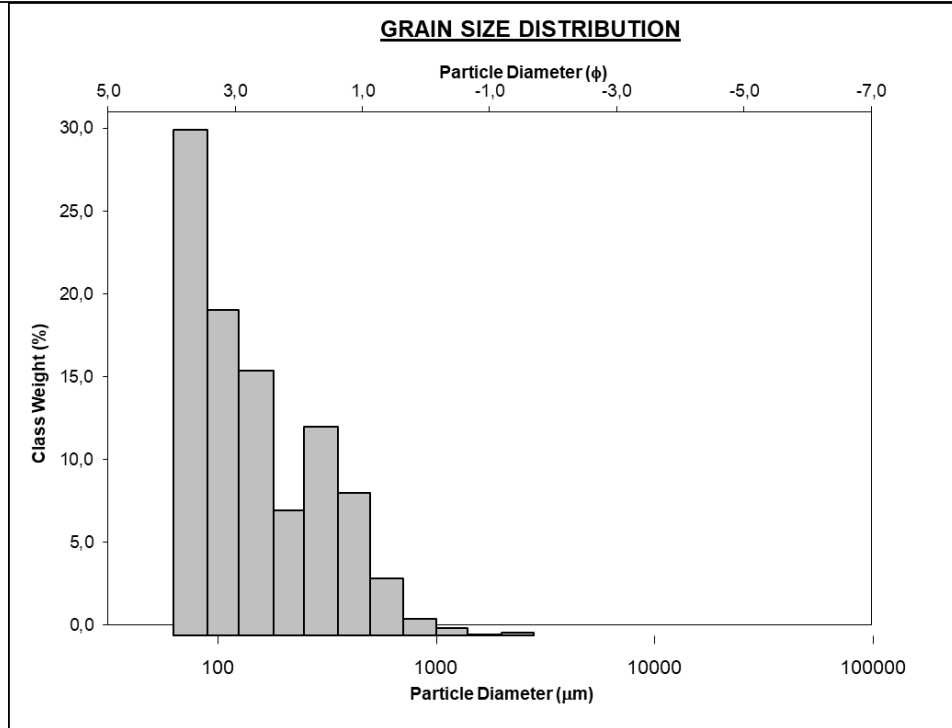
EV-2B:
Trimodal,
Very Poorly
Sorted



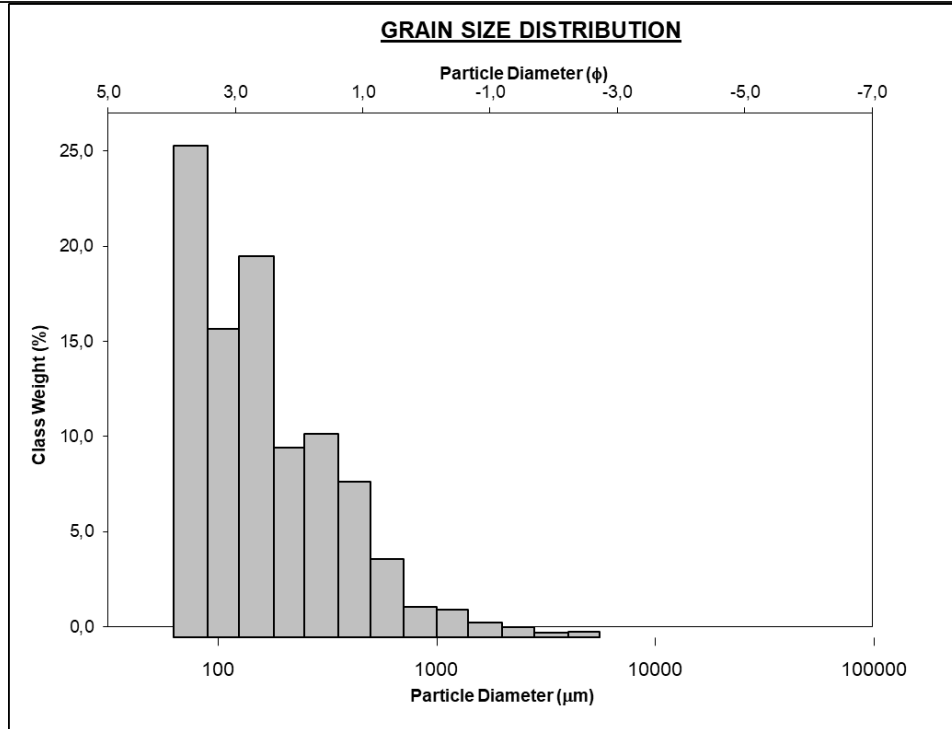
EV-3:
Bimodal,
Very Poorly
Sorted



EV-4:
Bimodal,
Very Poorly
Sorted



NS-1:
Trimodal,
Poorly
Sorted



NS-2: Very
Coarse Silty
Sandy Fine
Gravel

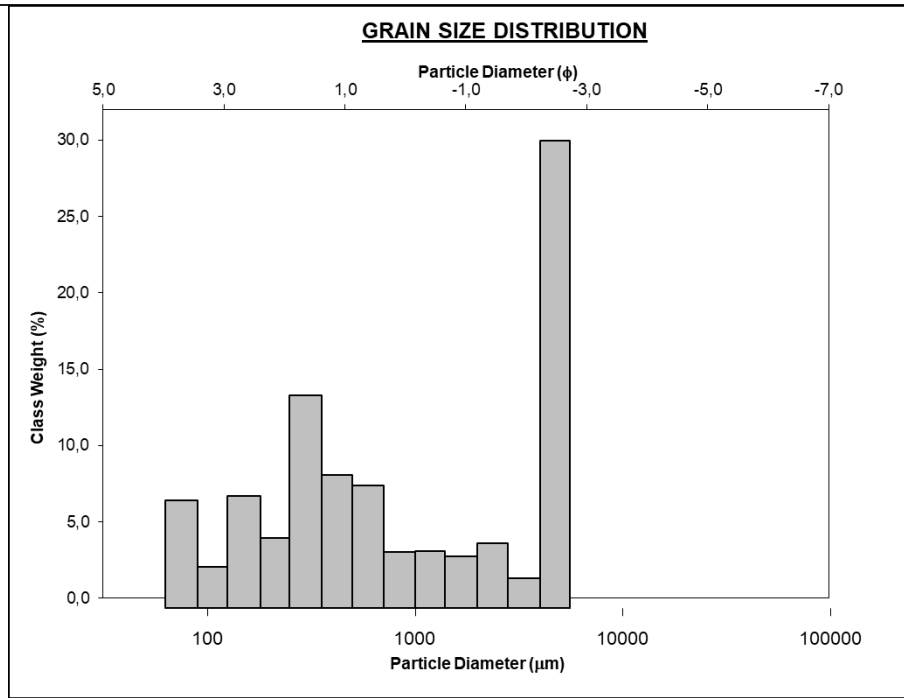
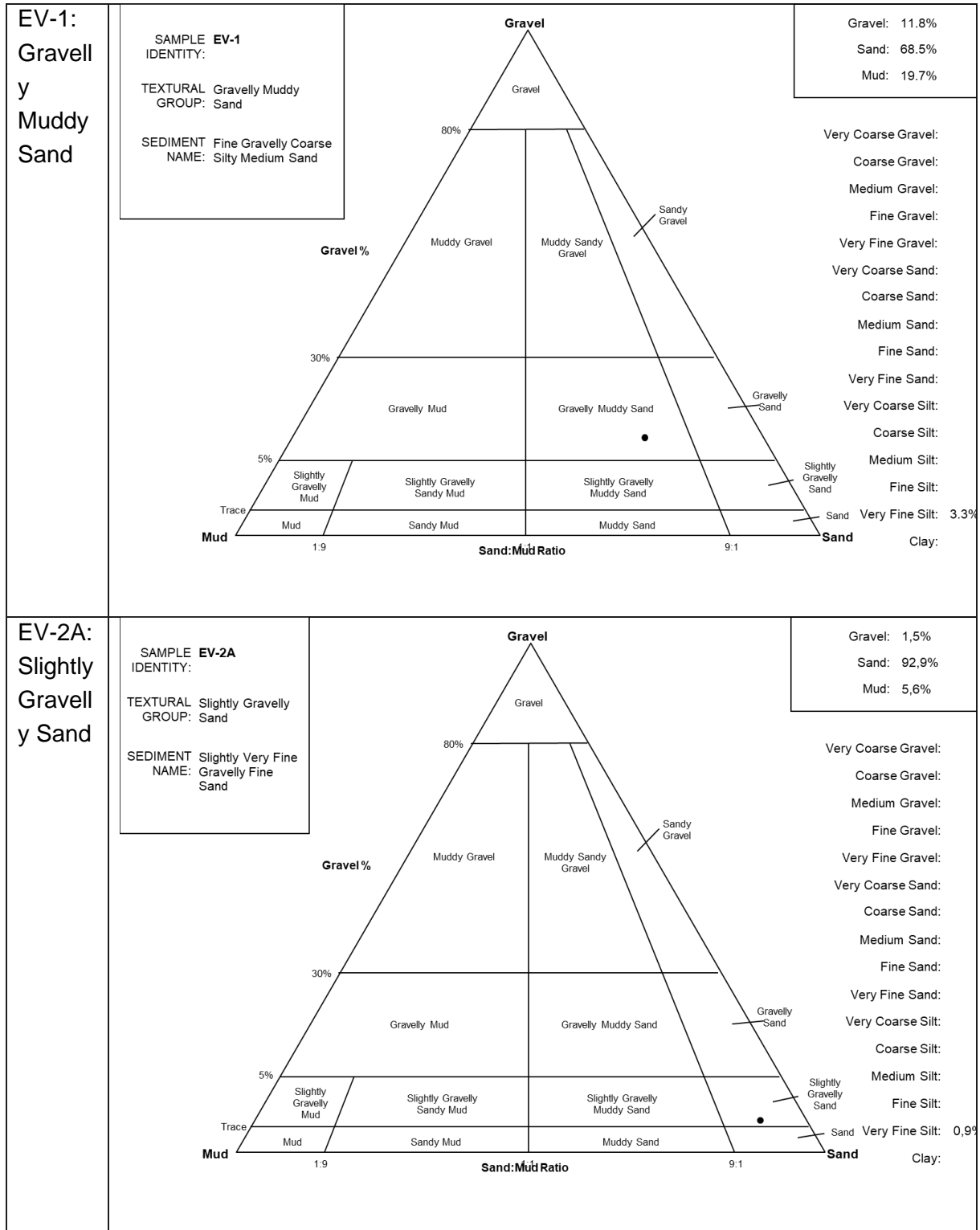
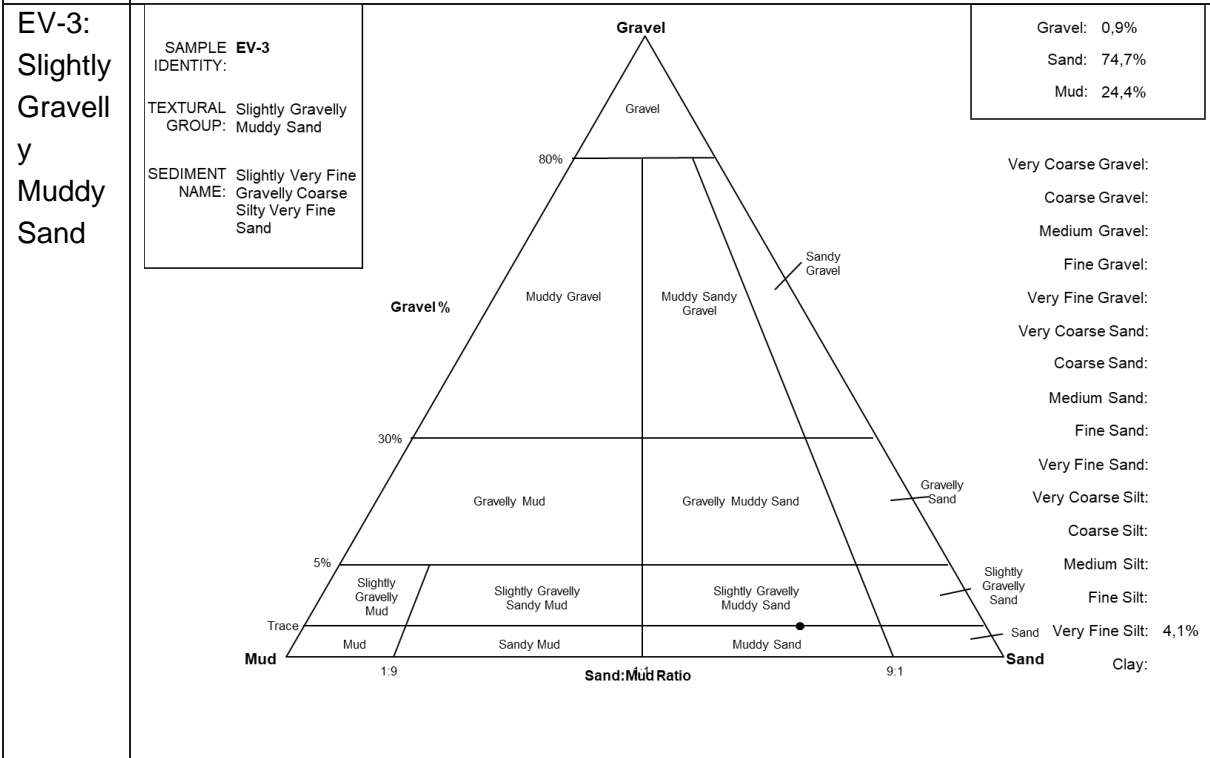
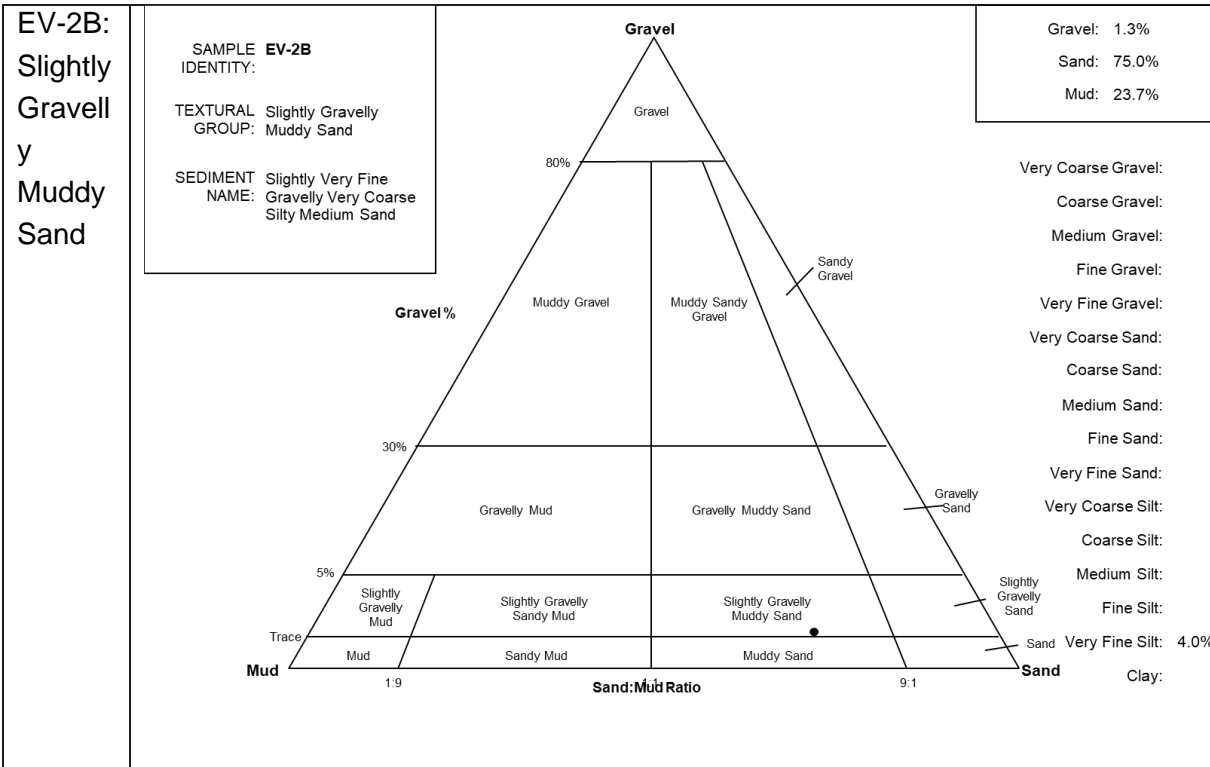
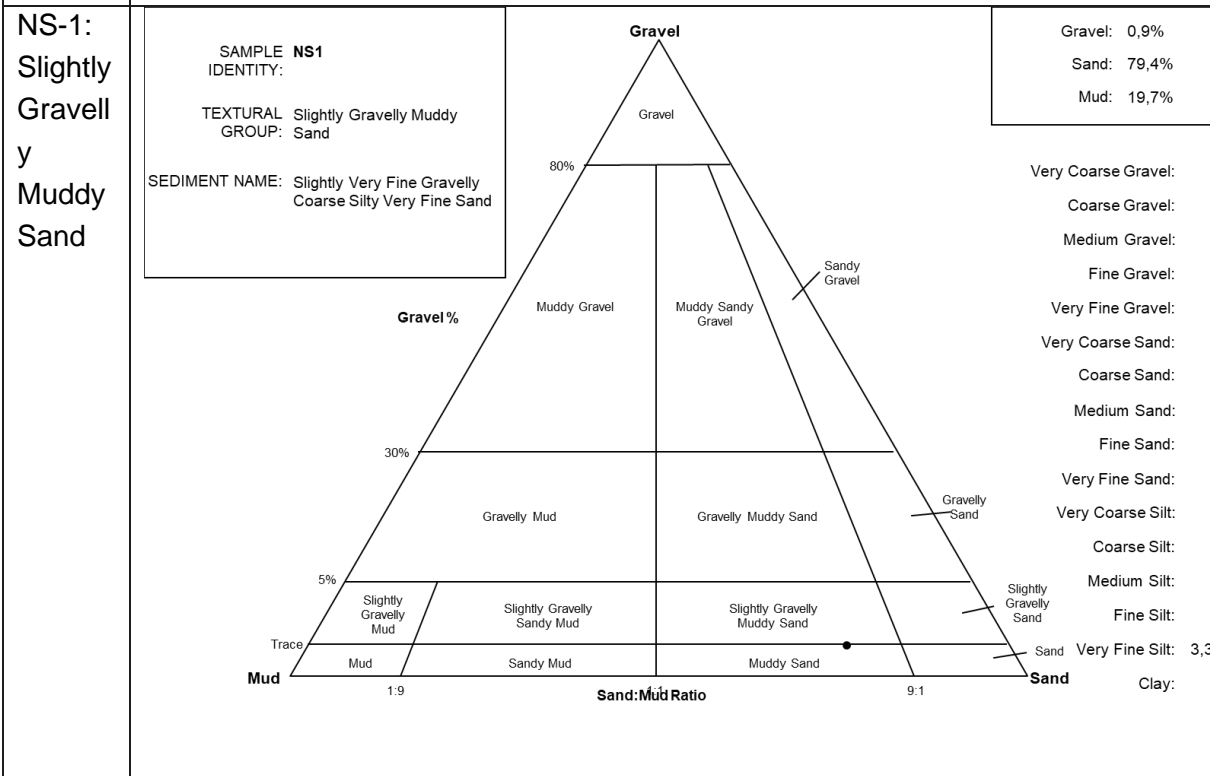
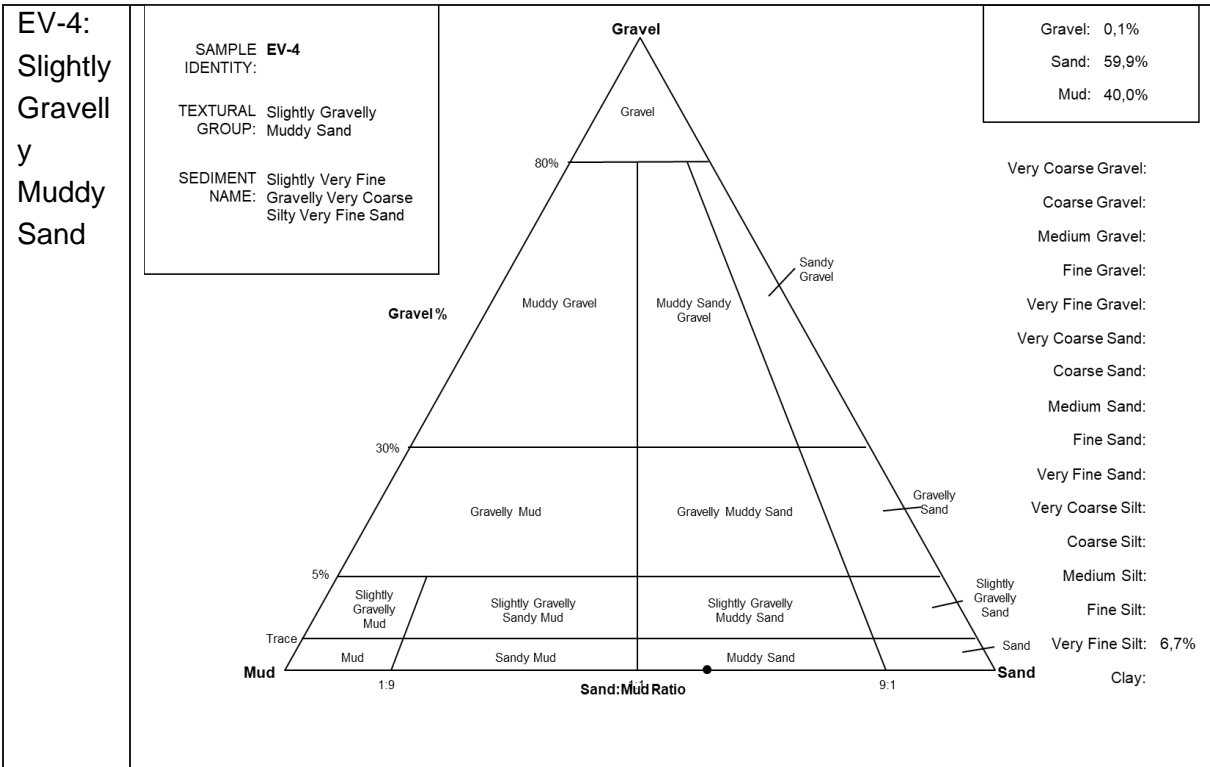


Table 9. Ternary diagram of the soil textural groups for the Norwegian samples.







**NS-2:
Muddy
Sandy
Gravel**

SAMPLE **NS2**
IDENTITY:
TEXTURAL Muddy Sandy
GROUP: Gravel
SEDIMENT Very Coarse Silty
NAME: Sandy Fine Gravel

Gravel: 32,9%
Sand: 58,4%
Mud: 8,7%

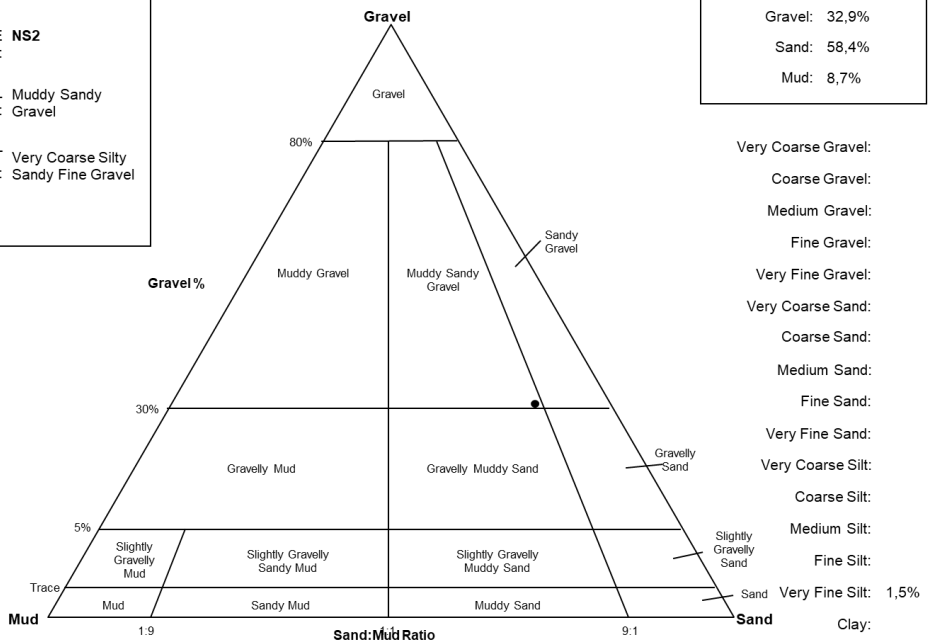
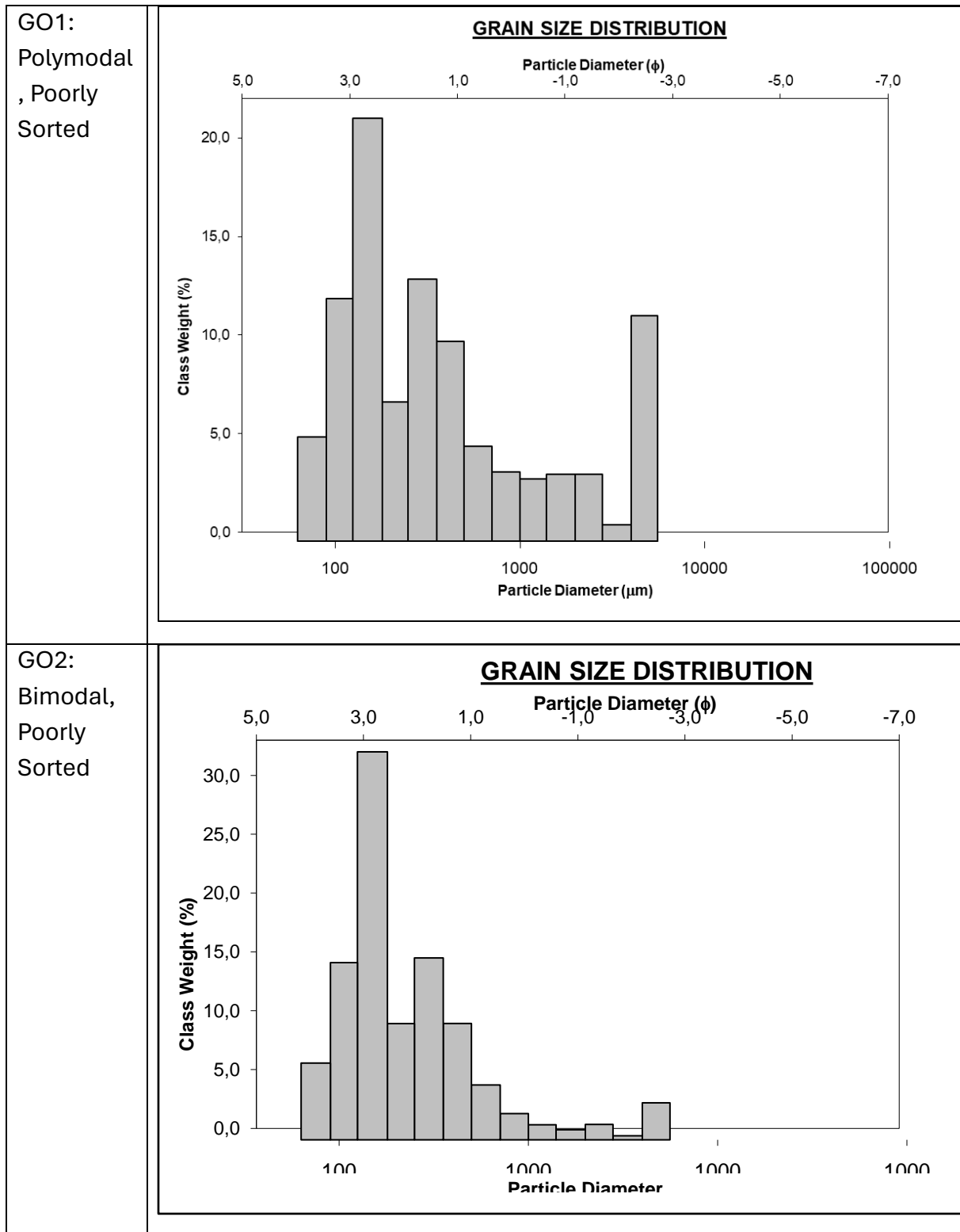
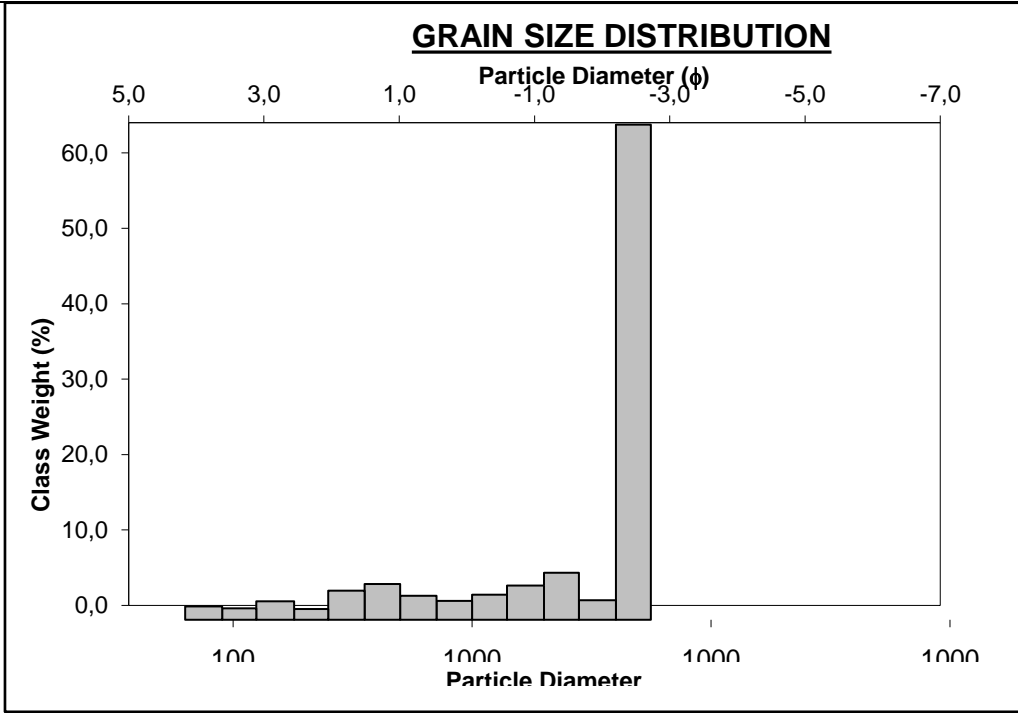


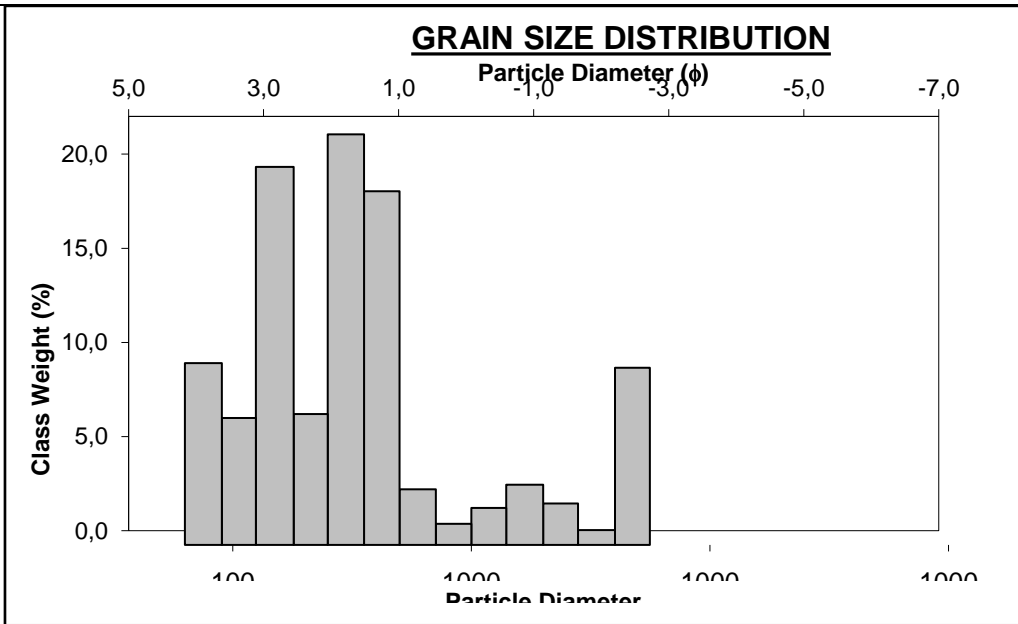
Table 10. Grain size distribution of Goan sample sites.



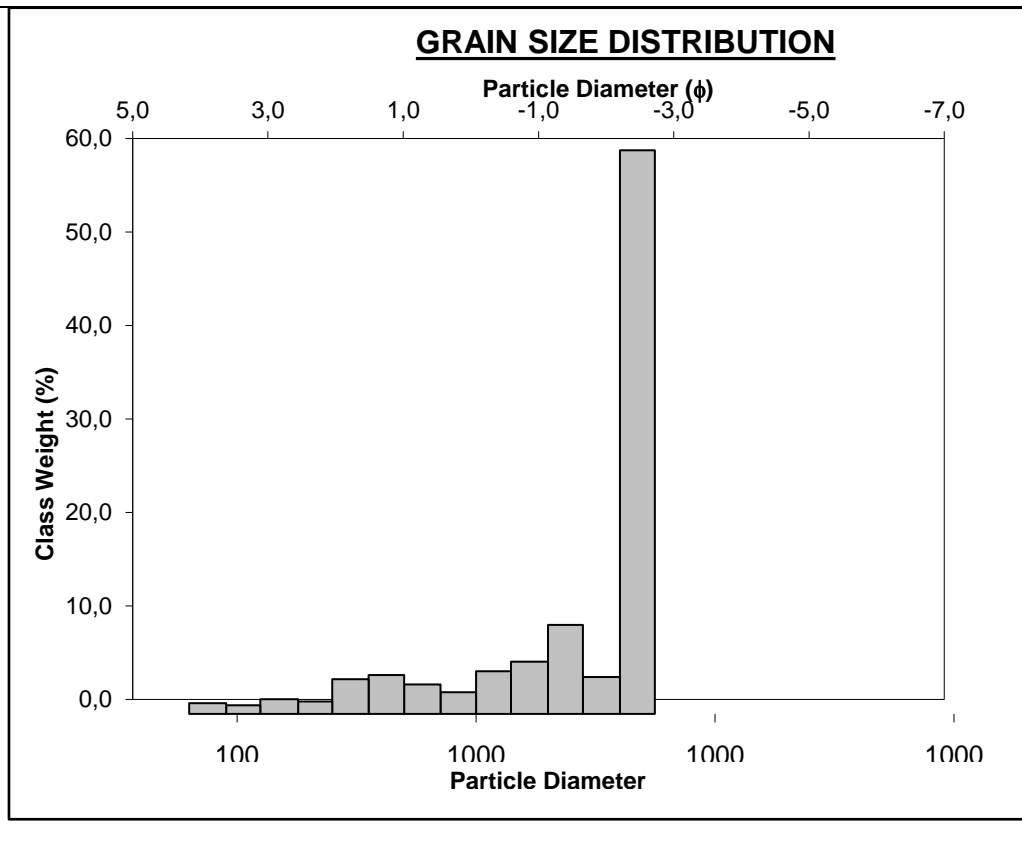
GO3:
Unimodal,
Poorly
Sorted



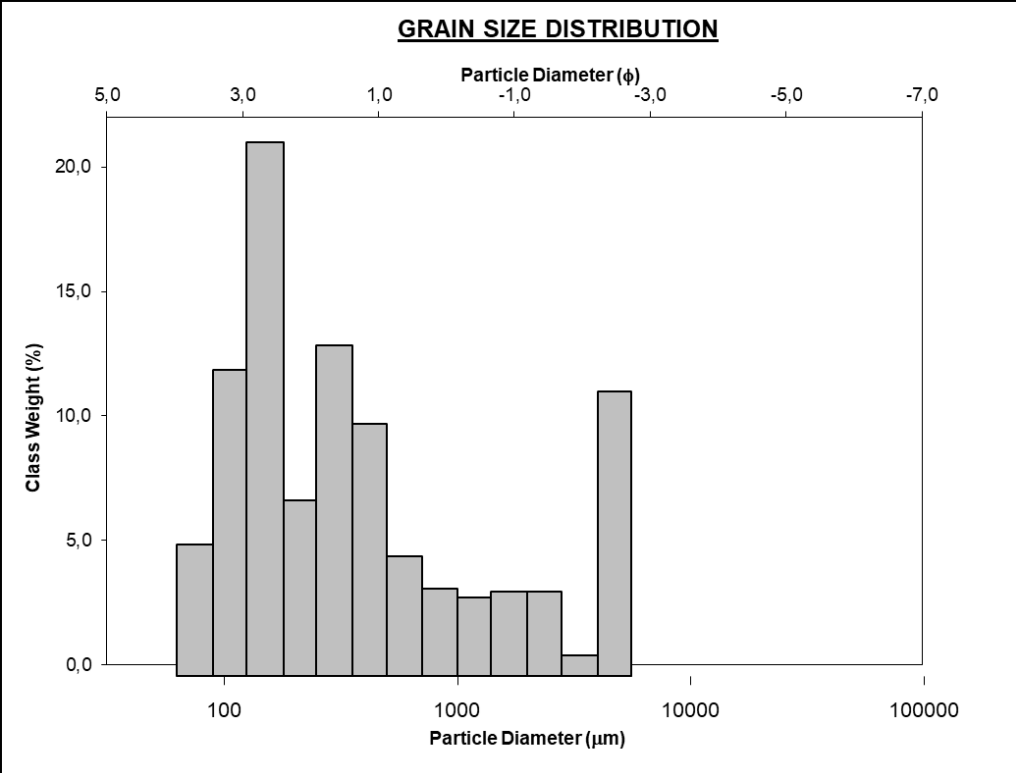
GO4:
Polymodal
, Poorly
Sorted



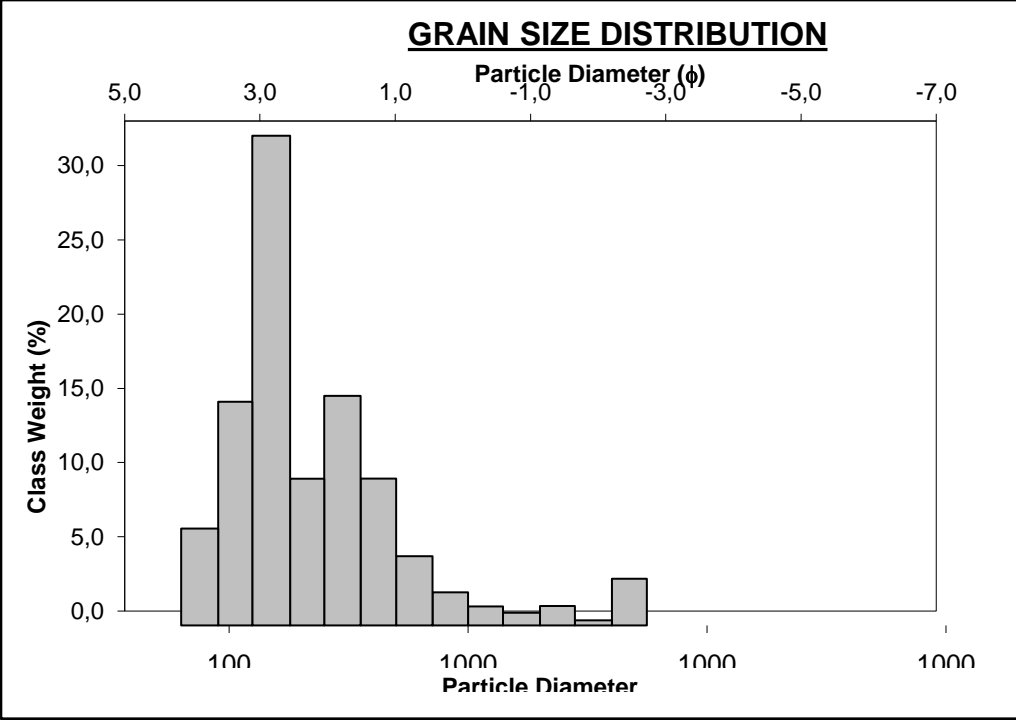
GO5:
Bimodal,
Poorly
Sorted



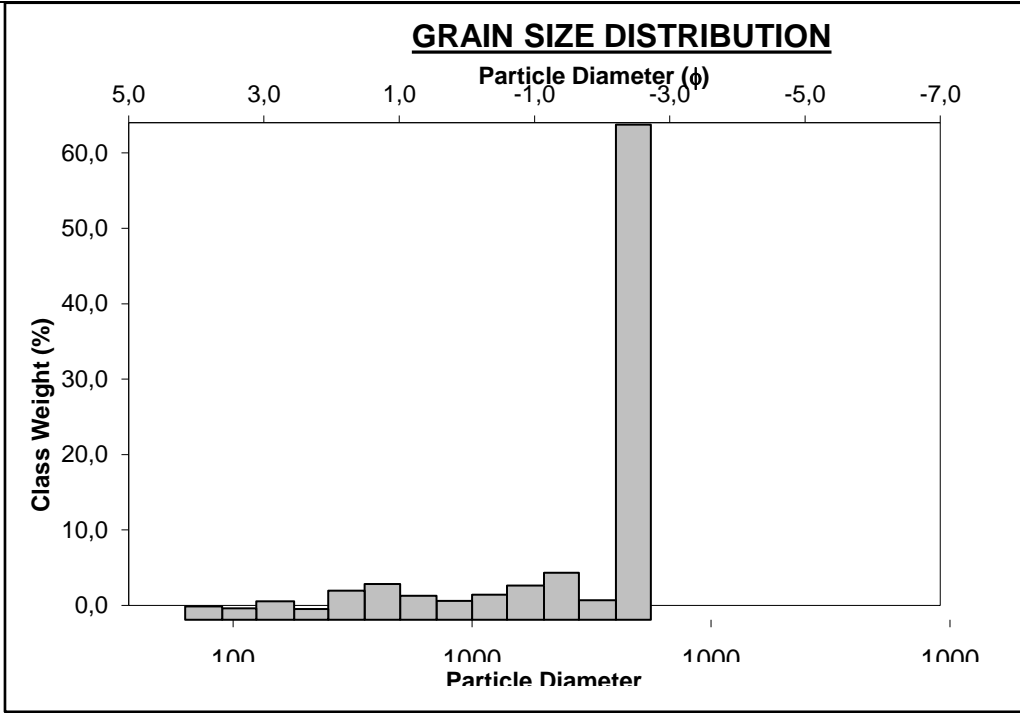
GO1:
Polymodal
, Poorly
Sorted



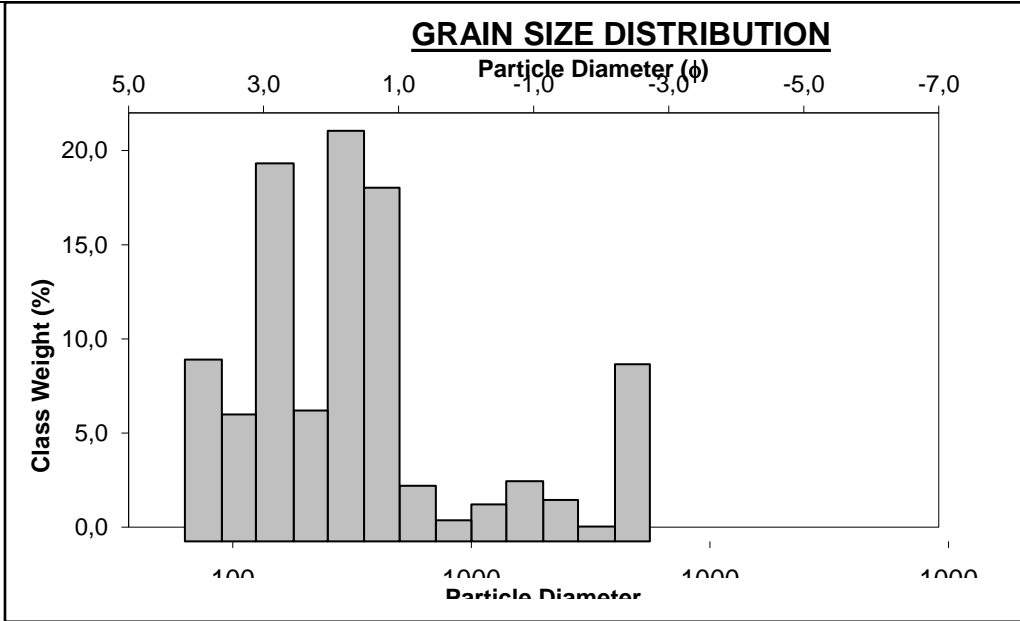
GO2:
Bimodal,
Poorly
Sorted



GO3:
Unimodal,
Poorly
Sorted



GO4:
Polymodal
, Poorly
Sorted



GO5:
Bimodal,
Poorly
Sorted

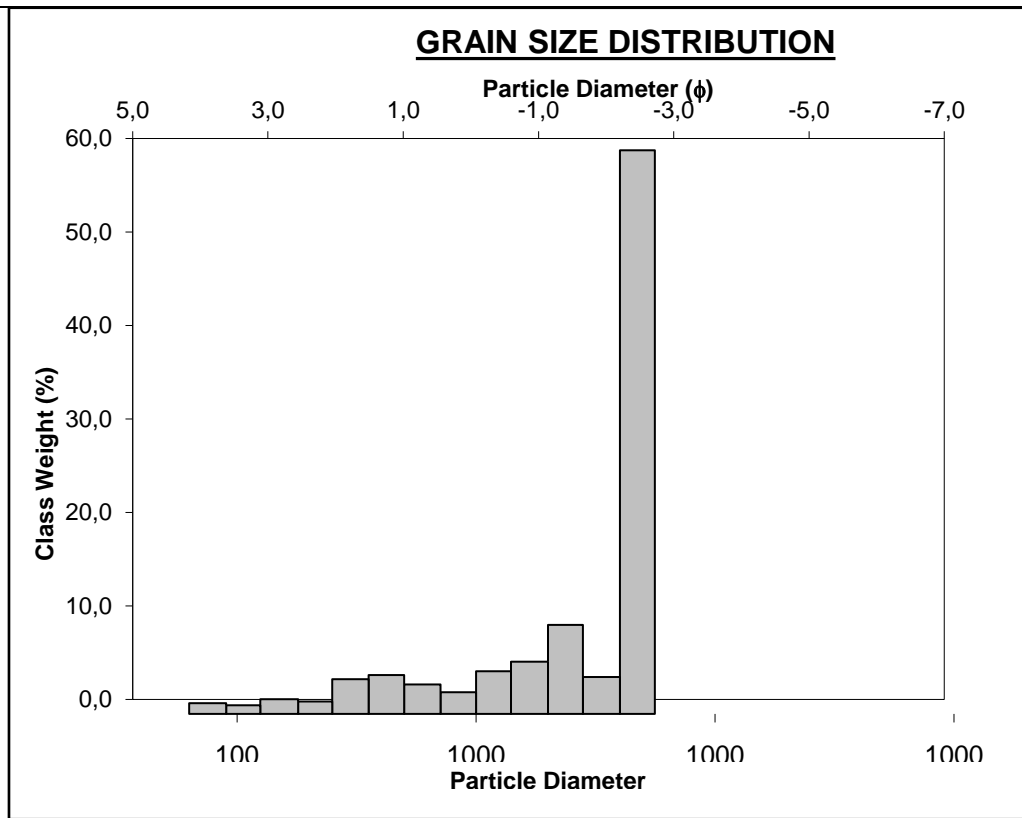
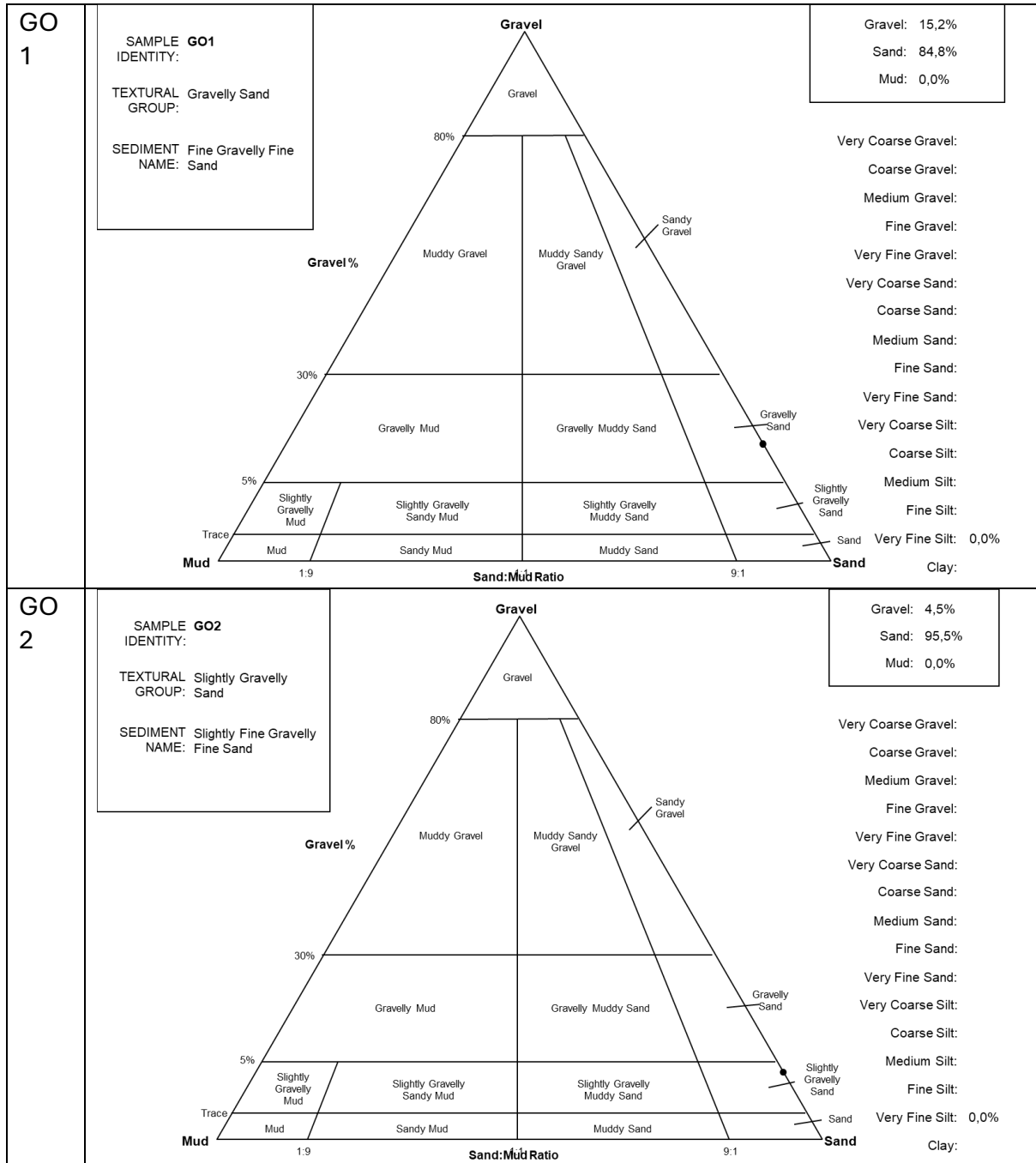
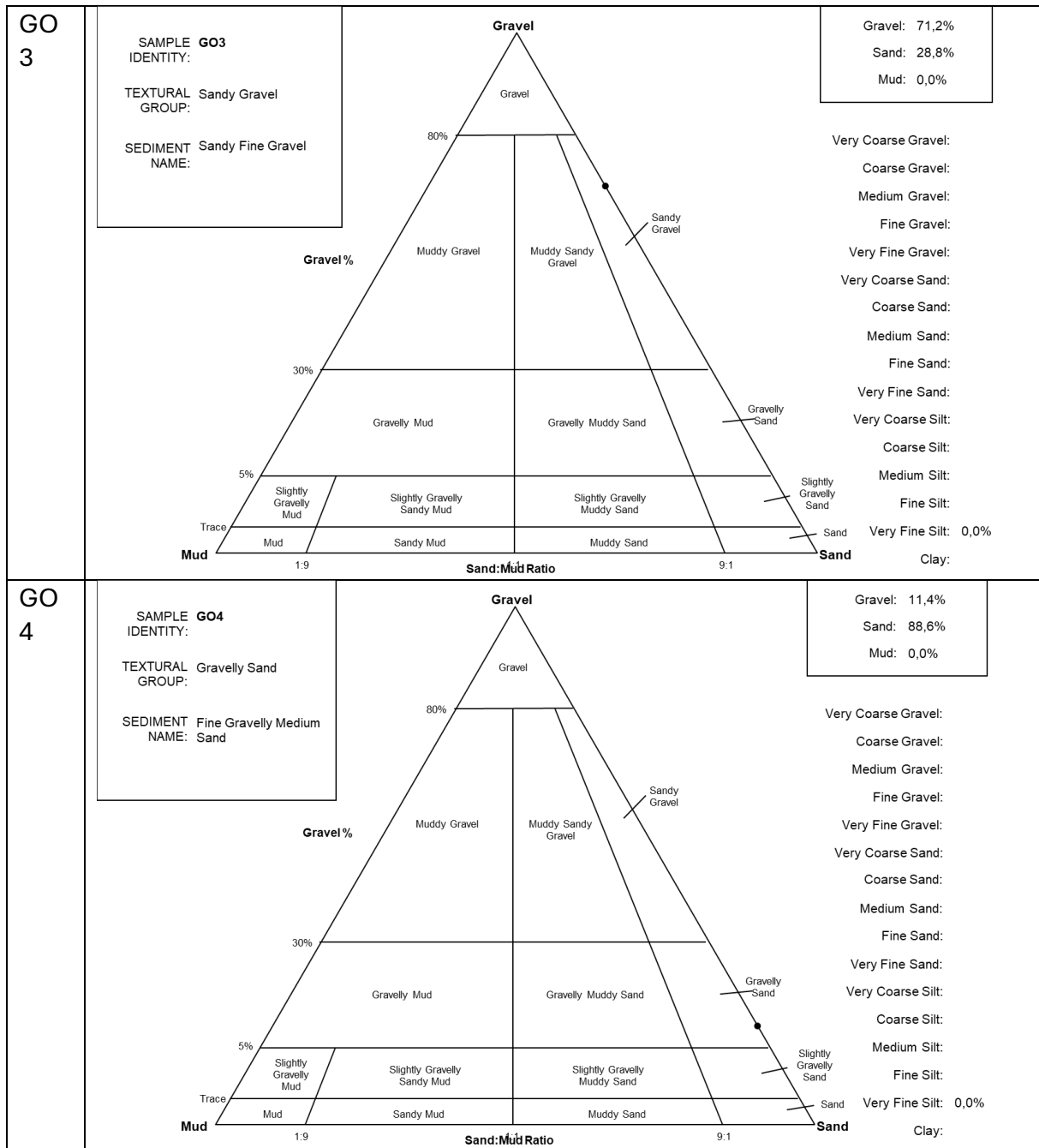


Table 11. Ternary diagram of the soil textural groups for the Goan samples.

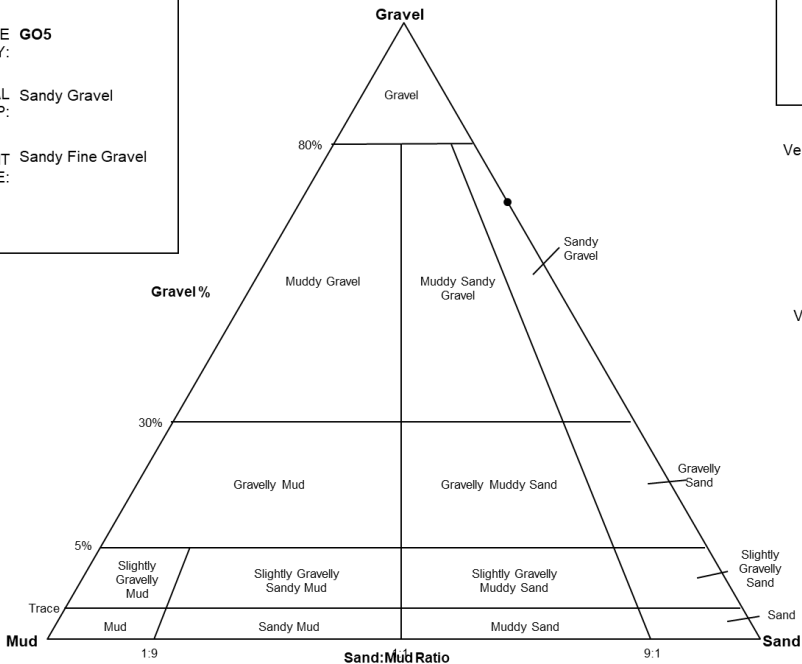




**GO
5**

SAMPLE IDENTITY: **GO5**
 TEXTURAL GROUP: **Sandy Gravel**
 SEDIMENT NAME: **Sandy Fine Gravel**

Gravel: 71,6%
 Sand: 28,4%
 Mud: 0,0%



- Very Coarse Gravel:
- Coarse Gravel:
- Medium Gravel:
- Fine Gravel:
- Very Fine Gravel:
- Very Coarse Sand:
- Coarse Sand:
- Medium Sand:
- Fine Sand:
- Very Fine Sand:
- Very Coarse Silt:
- Coarse Silt:
- Medium Silt:
- Fine Silt:
- Very Fine Silt: 0,0%
- Clay: